

# **Isolation, Characterization and Bioactivity Screening of Cyclic Imines**

Dissertation zur Erlangung des Doktorgrades

Dr. rer. nat.

der Mathematisch-Naturwissenschaftlichen Fakultät  
der Christian-Albrechts-Universität zu Kiel

vorgelegt von

Joyce A. Nieva

Kiel, 2021

Faculty Dean:

Prof. Dr. Frank Kempken

First Examiner:

Prof. Dr. Maarten Boersma

Second Examiner:

Prof. Dr. Deniz Tasdemir

Date of Oral Examination:

28 April 2021

## DECLARATION

I hereby declare that the content and form presented in this thesis entitled "Isolation, Characterization and Bioactivity Screening of Cyclic Imines" was completed by me under the supervision of my PhD Committee, with no other help than the cited sources.

This thesis was prepared in accordance to the rules of good scientific practice of the German Research Foundation (DFG) and has not been published in its entirety to any other institution as part of an examination procedure. Parts of this work have already been published in a journal.

No academic degree has been withdrawn.

Bremerhaven, 23. 02. 2021

A handwritten signature in black ink, appearing to read "Nieva". The signature is written in a cursive style with a large initial letter.

Joyce A. Nieva

*“Being precedes doing.”*

# TABLE OF CONTENTS

<b>Table of Contents</b>		v
<b>Abstract</b>		vii
<b>Zusammenfassung</b>		ix
<b>Abbreviations</b>		xi
<b>List of Figures</b>		xiii
<b>List of Tables</b>		xv
Chapter 1	<b>General Introduction</b>	16
Chapter 2	<b>Aims and Outline of the Study</b>	29
Chapter 3	<b>Mass Cultivation of <i>Alexandrium ostenfeldii</i> and Isolation of Gymnodimine A and 13-desMethyl Spirolide C</b>	31
	Introduction	32
	Materials and Methods	33
	Results and Discussion	37
Chapter 4	<b>Mass Spectrometry-Based Characterization of New Spirolides from <i>Alexandrium ostenfeldii</i> (Dinophyceae)</b>	44
	Introduction	45
	Materials and Methods	48
	Results and Discussion	52
	Conclusion	67
Chapter 5	<b>Gymnodimine A and 13-desMethyl Spirolide C Alter Intracellular Calcium Levels via Acetylcholine Receptors</b>	68
	Introduction	69
	Materials and Methods	71
	Results	72
	Discussion	76

Chapter 6	<b>Activation of Oxidative Stress and Inflammation Response Pathways by Gymnodimine A and 13-desMethyl Spirolide C</b>	80
	Introduction	81
	Materials and Methods	83
	Results and Discussion	89
Chapter 7	<b>General Discussion</b>	96
	<b>References</b>	104
	<b>Supplementary Information</b>	114
	<b>Afterword</b>	129

## ABSTRACT

The harmful algal bloom(HAB)-forming species *Alexandrium ostenfeldii* produces paralytic shellfish poisoning (PSP) toxins and the lesser known spiroimine shellfish poisoning (SSP) toxins. These toxins primarily belong to macrocyclic imine class, with cyclic imine moiety and macrocyclic nature as their distinct characteristics. By far, *A. ostenfeldii* is the only species identified to produce two types of cyclic imines—gymnodimines and spiroolides. Studies on these toxins produced by different *A. ostenfeldii* strains revealed high structural diversity. The presence of highly varied structural types of cyclic imines that requires elaborate synthesis pathways implies its underlying function for the producing organism. However, known roles and mode of action (MOA) of cyclic imines are rather limited. That is, other than its “fasting-acting” toxicity and antagonistic activity against of nicotinic acetylcholine receptors, no other MOA of cyclic imines have been identified. Considering the increasing occurrence of HABs and the socio-economic impacts of toxins associated in *A. ostenfeldii*, it is crucial to elucidate not only the structural diversity of cyclic imines but also their respective modes of action and biological significance of their production. As such, this study aimed to isolate, characterize, and screen the bioactivity of the two types of cyclic imines (i.e., gymnodimines and spiroolides) produced by *A. ostenfeldii*. Two strains of *A. ostenfeldii* (OKNL 48 and X-LF-19-F10) were mass cultivated to directly obtain purified samples of structurally known gymnodimines (i.e., gymnodimine A (GYM A)) and spiroolides (i.e., 13-desmethyl spiroolide C (SPX 1)). A total of 345 µg of GYM A and 559 µg of SPX 1 were purified (>95% purity) from the large-scale microalgal culture. Three other *A. ostenfeldii* strains (AON 24, NX-56-10 and MX-S-B11) were identified to produce both structurally unknown spiroolides. Isolation of the pure novel spiroolides were not possible in quantities necessary for NMR structure elucidation work. Thus, mass-spectrometric (MS)-based techniques was sought as an alternative approach for the structural characterization of unknown compounds. Using the technique, this study revealed the presence of nine novel spiroolides, eight of which have either a 5:5:6 (C-type spiroolides) or 5:6:6 (G-type spiroolides) triketal ring configuration. Another novel spiroolide putatively belongs to a new spiroolide subclass, which has a 6:5:6 triketal ring configuration that is only observed in pinnatoxins, another class of cyclic imines. The initial structural insights by mass spectral techniques demonstrate that structural variability of spiroolides is not only limited to the presence or absence of certain functional groups (as observed in other eight novel spiroolides) but also the triketal ring system. Moreover, the proposed 6:5:6 triketal ring system in one of the novel spiroolides suggests that similar biosynthetic steps are involved in the synthesis of spiroolides and pinnatoxins. To gain a better understanding on the potential role of cyclic imines, purified GYM A and SPX 1 were subjected into cell line-based bioassays to identify other MOA of

the toxins. Intracellular calcium levels ( $[Ca]_i$ ) measured in rat pheochromocytoma (PC12) cells suggested that both toxins elicited differential effect on acetylcholine receptor (AChRs) subtypes. GYM A and SPX 1 activates nicotinic AChRs (nAChRs) while only GYM A activate muscarinic AChRs (mAChRs). The activation of AChRs and the subsequent influx of calcium ions into the cell illustrates the putative capacity of the toxins to mimic acetylcholine. These observations were possible as a result of determining the response of GYM A or SPX 1 on  $[Ca]_i$  signaling in PC12 cells. Moreover, preliminary investigations on the effects of GYM A and SPX 1 to AREc32 and Nf- $\kappa$ B- $\beta$ -THP-1 cell lines indicated that toxins potentially induce adaptive stress response pathways. SPX 1 likely activates both oxidative stress response and inflammation response pathways. GYM A, on the other hand, possibly initiates inflammation response pathways but lacks the capacity to induce oxidative stress response pathway. The ability of the toxins to potentially activate adaptive response pathways indicated that GYM A or SPX 1 might initiate cellular processes that will restore homeostasis suggesting possible medicinal applications of the toxins. Studies on the response of GYM A and SPX 1 to  $[Ca]_i$  and adaptive stress response pathways provided more understanding on the potential MOA of the toxins. Further knowledge on structural diversity and MOA of cyclic imines could hopefully direct us to determine structure-activity relationship and, to some extent, purpose of the toxins to the producing organism.



## ZUSAMMENFASSUNG

Die schädliche Algenblüten (HAB) bildende Art *Alexandrium ostenfeldii* produziert Toxine, die zur paralytischen Schalentiervergiftung (PSP) führen sowie weitere, weniger bekannte Toxine die Spiroimin-Schalentiervergiftung (SSP) verursachen. Diese Toxine gehören zur Klasse der makrozyklischen Imine, wobei der zyklische Iminanteil und die makrozyklische Natur ihre charakteristischen Merkmale sind. Soweit bekannt ist, ist *A. ostenfeldii* die einzige Spezies, die zwei Arten von zyklischen Iminen produziert - Gymnodimine und Spirolide. Untersuchungen dieser von verschiedenen *A. ostenfeldii*-Stämmen produzierten Toxine ergaben eine hohe strukturelle Diversität. Das Vorhandensein höchst unterschiedlicher Strukturtypen zyklischer Imine, die aufwendige Synthesewege erfordern, lässt auf eine zugrundeliegende Funktion für den produzierenden Organismus schließen. Allerdings sind die bekannten Funktionen und Wirkungsweisen (MOA) der zyklischen Imine sehr begrenzt. Das heißt, abgesehen von der "schnellen" Toxizität und der antagonistischen Aktivität gegen nikotinische Acetylcholinrezeptoren wurden keine weiteren MOAs von zyklischen Iminen identifiziert. In Anbetracht des zunehmenden Auftretens von HABs und der sozio-ökonomischen Auswirkungen der mit *A. ostenfeldii* assoziierten Toxine ist es von entscheidender Bedeutung, nicht nur die strukturelle Vielfalt der zyklischen Imine aufzuklären, sondern auch ihre jeweiligen Wirkungsweisen und die biologische Bedeutung ihrer Produktion. Ziel dieser Studie war zum einen die Erforschung der Toxinvariabilität von drei *A. ostenfeldii* Stämmen (AON 24, NX-56-10 und MX-S-B11), zum anderen die Isolierung, Charakterisierung und das Screening der Bioaktivität von zwei Arten zyklischer Imine (Gymnodimine und Spirolide), die von *A. ostenfeldii* produziert werden. Dazu wurden die beiden *A. ostenfeldii* Stämme OKNL 48 und X-LF-19-F10 massenkultiviert, um die strukturell bekannten Verbindungen Gymnodimin A (GYM A) 13-Desmethylspirolid C (SPX 1) als Reinsubstanzen zu erhalten. Insgesamt wurden 345 µg GYM A und 559 µg SPX 1 aus der Mikroalgen-Großkultur aufgereinigt (>95% Reinheit). Aus den *A. ostenfeldii*-Stämmen AON 24, NX-56-10 und MX-S-B11 wurden mehrere strukturell unbekannte Spirolide identifiziert. Die Isolierung der neuen Spirolide war nicht in den für die NMR-Strukturaufklärung notwendigen Mengen möglich. Daher wurde nach massenspektrometrischen (MS)-basierten Techniken als alternativer Ansatz für die strukturelle Charakterisierung unbekannter Verbindungen gesucht. Mit Hilfe dieser Technik wurden in dieser Studie neun neue Spirolide entdeckt, von denen acht entweder eine 5:5:6 (C-Typ-Spirolide) oder 5:6:6 (G-Typ-Spirolide) Triketal-Ringkonfiguration aufweisen. Ein weiteres neuartiges Spirolid gehört vermutlich zu einer neuen Spirolid-Subklasse, die eine 6:5:6-Triketal-Ringkonfiguration aufweist, die nur in Pinnatoxinen, einer anderen Klasse von zyklischen Iminen,

beobachtet wird. Die ersten strukturellen Erkenntnisse durch massenspektrometrische Techniken zeigen, dass die strukturelle Variabilität der Spirolide nicht nur auf das Vorhandensein oder Fehlen bestimmter funktioneller Gruppen beschränkt ist (wie bei den anderen acht neuen Spiroliden beobachtet), sondern auch auf das Triketalringsystem. Darüber hinaus legt das vorgeschlagene 6:5:6-Triketalringsystem eines der neuen Spirolide nahe, dass ähnliche biosynthetische Schritte an der Synthese von Spiroliden und Pinnatoxinen beteiligt sind. Um ein besseres Verständnis für die potenzielle Rolle der zyklischen Imine zu erlangen, wurden gereinigtes GYM A und SPX 1 in zelllinienbasierten Bioassays untersucht, um weitere MOA der Toxine zu identifizieren. Intrazelluläre Kalziumspiegel ( $[Ca]_i$ ), die in Phäochromozytoma-Zellen (PC12) der Ratte gemessen wurden, deuteten darauf hin, dass beide Toxine eine unterschiedliche Wirkung auf Acetylcholinrezeptor (AChR)-Subtypen auslösen. GYM A und SPX 1 aktivieren nikotinische AChRs (nAChRs), während nur GYM A muskarinische AChRs (mAChRs) aktiviert. Die Aktivierung der AChRs und der anschließende Einstrom von Kalziumionen in die Zelle verdeutlicht die mutmaßliche Fähigkeit der Toxine, Acetylcholin zu imitieren. Diese Beobachtungen waren über die Messung durch GYM A oder SPX 1 veränderte intrazelluläre  $[Ca]_i$ -Signale in PC12-Zellen möglich. Darüber hinaus deuteten Voruntersuchungen zu den Effekten von GYM A und SPX 1 auf AREC32- und Nf- $\kappa$ B- $\beta$ -THP-1-Zelllinien darauf hin, dass die Toxine potenziell adaptive Stressantwortwege induzieren. SPX 1 aktiviert wahrscheinlich sowohl die oxidative Stressreaktion als auch die Entzündungsreaktionswege. GYM A hingegen initiiert möglicherweise Entzündungsreaktionswege, hat aber nicht die Fähigkeit, den oxidativen Stressreaktionsweg zu induzieren. Die Fähigkeit der Toxine, potentiell adaptive Reaktionswege zu aktivieren, deutet darauf hin, dass GYM A oder SPX 1 zelluläre Prozesse initiieren könnten, die die Homöostase wiederherstellen, was mögliche medizinische Anwendungen der Toxine nahelegt. Studien zur Reaktion von GYM A und SPX 1 auf  $[Ca]_i$  und adaptive Stressreaktionswege lieferten weitere Erkenntnisse über die potenzielle MOA der Toxine. Weiteres Wissen über die strukturelle Vielfalt und die MOA der zyklischen Imine könnte uns hoffentlich dazu bringen, die Struktur-Aktivitäts-Beziehung und in gewissem Maße auch die biologische Rolle der Toxine für den produzierenden Organismus zu bestimmen.

## ABBREVIATIONS

[Ca] <sub>i</sub>	Intracellular calcium concentrations
[M + H] <sup>+</sup>	Pseudo-molecular ion
20-Me SPX G	20-methyl spirolide G
βlac	β-lactamase
<i>t</i> BHQ	<i>tert</i> -Butylhydroquinone
ACh	Acetylcholine
AChRs	Acetylcholine receptors
ACN	Acetonitrile
ARE	Antioxidant response element
ASP	Amnesic shellfish poisoning
AZP	Azaspiracid shellfish poisoning
CAD	Collision activated dissociation
CFP	Ciguatera shellfish poisoning
CI	Cyclic Imine
CID	Collision induced dissociation
CRCs	Concentration response curves
DMEM	Dulbecco's modified eagle's medium,
DSP	Diarrhetic shellfish poisoning
EC <sub>IR1.5</sub>	Effective concentration needed for the induction of adaptive response pathway
EPI	Enhanced product ion
FI	Fluorescence intensity
FBS	Fetal Bovine Serum
FRET	Fluorescence resonance energy transfer
GST	Glutathione S-transferase
GYM A	Gymnodimine A
HABs	Harmful algal blooms
HEPES	4-(2-hydroxyethyl)-1-piperazineethanesulfonic acid
HR-MS	High-resolution mass spectrometry
IC <sub>10</sub>	Cytotoxicity of the cell
Ip	intraperitoneal (injection)
IR	Induction ratio
LAS AF	<i>Leica</i> Application Suite Advanced Fluorescence
LC-HRMS/MS	LC-tandem high-resolution mass spectrometry
LC-MS/MS	Tandem mass spectroscopy coupled to liquid chromatography
LOD	Limit of detection

LSU	Large-subunit
mAChRs	Muscarinic acetylcholine receptors
MeOH	Methanol
nAChRs	Nicotinic acetylcholine receptors
Nd	Not detected
NEAA	Non-essential amino acid
NfκB	Nuclear Factor kappa-light-chain-enhancer of activated B cells
NL	Neutral loss
NMR	Nuclear magnetic resonance
NRPSs	Non-ribosomal peptide synthases
NSP	Neurotoxic shellfish poisoning
OA	Okadaic acid
PC 12	Rat pheochromocytoma (cells)
PKSs	Polyketide synthases
PnTX	Pinnatoxin
PnTX A	Pinnatoxin A
PSP	Paralytic shellfish poisoning
Q1	First quadrupole
Q2	Second quadrupole
Q3	Third quadrupole
QSARS	Quantitative structure–activity relationships
RDA	Retro-Diels-Alder
ROI	Region of interest
ROS	Reactive oxygen species
RPMI	Roswell Park Memorial Institute
SAR	Structure-activity-relationship
SPX	Spirolides
SPX 1	13-desmethyl spirolide C
SPE	Solide-phase extraction
SPX G	Spirolide G
SR	Specificity Ratio
SRM	Selected reaction monitoring
SSP	Spiroimine Shellfish Poisoning
TF	Transcription factor
TNFα	Tumor necrosis factor alpha

## LIST OF FIGURES

Figure 1.1. Chemical structure of the most common gymnodimine and spirolide.	22
Figure 1.2. Schematic diagram of the toxin detection using LC-MS/MS.	23
Figure 1.3 Worldwide distribution of gymnodimines and spirolides.	25
Figure 1.4 Images of <i>Alexandrium ostenfeldii</i> .	26
Figure 3.1. Schematic diagram of the SPE methods tested in this study.	38
Figure 3.2 Schematic diagram of fractions obtained from using HP-20 resin.	39
Figure 3.3 Schematic diagram of the extraction and purification procedure performed in this study.	41
Figure 3.4 Ion chromatograms of gymnodimine A (GYM A) and 13-desmethyl spirolide C (SPX 1) from the standard reference material and from <i>A. ostenfeldii</i> strains OKNL 48 and X-LF-19-F10.	42
Figure 4.1 Mass spectrometry-based structural characterization of unknown compounds.	47
Figure 4.2 Sampling locations of <i>A. ostenfeldii</i> strains AON 24, NX-5610 and MX-S-B11.	49
Figure 4.3. Triple quadruple set-ups under single reaction monitoring mode.	50
Figure 4.4. Triple quadruple set-ups under precursor ion scan mode.	50
Figure 4.5. Triple quadruple set-ups under product ion mode.	51
Figure 4.6. Collision-induced (CID) spectra of SPX 1 and novel spirolides detected in <i>A. ostenfeldii</i> strains related to C-type spirolides.	52
Figure 4.7. Chemical structure and fragmentation pattern of SPX 1.	53
Figure 4.8. CID spectra of 20-methyl spirolide G and novel SPX detected in <i>A. ostenfeldii</i> strains related to G-type spirolides.	54
Figure 4.9. Chemical structure and fragmentation pattern of spirolide G and 20-methyl spirolide G.	55
Figure 4.10. Proposed structures of compounds 1 from AON 24 and compounds 2 and 3 from NX-56-10.	57
Figure 4.11. Proposed structures of compounds 4, 6, 7 and 8 from MX-S-B11.	60
Figure 4.12. Triketal ring system of C- and G-type spirolides and Pinnatoxin E/F.	61
Figure 4.13. Proposed structure of compound 5 from MX-S-B11.	62
Figure 4.14. Proposed structures of compounds 9 from MX-S-B11.	64
Figure 5.1. Transmission image of PC12 cells and fluorescence images of flou-3 acetoxymethylester (Flou-3 AM)-stained PC 12 cells before and during depolarization.	72
Figure 5.2. Intracellular calcium ( $[Ca]_i$ ) level changes induced by activation of voltage-gated calcium channels.	73
Figure 5.3. $[Ca]_i$ changes induced by ACh, GYM A and SPX 1.	73
Figure 5.4. $[Ca]_i$ changes induced by ACh, GYM A and SPX 1 through pharmacologically isolated nAChRs or mAChRs.	75

Figure 5.5. [Ca] <sub>i</sub> level changes in cells pretreated with mAChR-blocker atropine and nAChR-blocker tubocurarine with GYM A or SPX 1.	76
Figure 6.1. Activation of an adaptive stress response pathway.	81
Figure 6.2. Difference between native and recombinant cell that uses reporter gene.	83
Figure 6.3. Measurement of βlac induction in NfκB- <i>bla</i> THP-1 using fluorescence resonance energy transfer (FRET).	86
Figure 6.4. Activation experiments of <i>t</i> BHQ, methanol blank, medium blank, GYM A and SPX 1 using AREc32 cell lines.	91
Figure 6.5 Activation experiments of TNFα, methanol blank, medium blank, GYM A and SPX 1 using NfκB- <i>bla</i> THP-1 cell lines.	93
Figure 7.1. Structural configuration of GYM A, SPX 1 and Pinnatoxin A (PnTX A)	99

## LIST OF TABLES

Table 1.1. Harmful algal bloom associated phycotoxins.	18
Table 3.1 Growth rates and toxin cell quota from <i>A. ostenfeldii</i> strains.	37
Table 3.2. Recovery and purity of toxins from the SPE fractions.	39
Table 3.3. Toxin recovery and purity using HP-20 eluted with 90% ACN (F2) and 100% ACN (F4).	39
Table 3.4. Total amount of toxin recovered from the extraction and purification procedure conducted in this study.	41
Table 4.1 Structurally elucidated spirolides from <i>Alexandrium ostenfeldii</i> and their corresponding mass transition.	46
Table 4.2. Measured and calculated accurate masses of the key product ions of compounds 1 from AON 24 and NX-56-10 obtained by HR-MS.	56
Table 4.3. Measured and calculated accurate masses of the key product ions of compounds 4–6 from MX-S-B11 obtained by HR-MS.	59
Table 4.4. Measured and calculated accurate masses of the key product ions of compounds 7–9 from MX-S-B11 obtained by HR-MS.	63
Table 4.5. Cell quota and relative SPX content of <i>A. ostenfeldii</i> strains from the Netherlands (AON 24), Norway (NX-56-10) and Greenland (MX-S-B11).	66
Table 6.1 Transcription factor-sensor complex in adaptive stress response pathways.	82
Table 6.2 Amount of GYM A and SPX 1 used in adaptive stress response assay.	83
Table 6.3 Experimental parameters for the induction of oxidative stress and inflammation response.	84
Table 6.4. Inhibition concentrations ( $IC_{10}$ ) and effective concentrations ( $EC_{IR1.5}$ ) for the AREc32 assay.	90
Table 6.5. Effective concentrations ( $EC_{IR1.5}$ ) for the NfκB assay.	92
Table 7.1. Examples of unknown SPX used in this study that have identical nominal masses with known SPX described in previous studies.	97

# CHAPTER 1

## General Introduction

### 1.1 Harmful algal blooms and phycotoxins

#### 1.1.1 Harmful algal blooms (HABs)

Algal blooms or the seasonal succession of plankton are natural phenomena. Recurrent community assemblies, which are driven by biotic and abiotic factors, are of great significance for food webs and energy and matter distribution among organism of higher trophic levels (Sommer *et al.*, 2012). Plankton community assemblages are generally composed of various species of distant phylogenetic groups such as diatoms, dinoflagellates, haptophytes and cyanobacteria (Assmy *et al.*, 2009). Apart from fueling the food chain and ecosystem (i.e., through biogeochemical element cycling), algal blooms can also have adverse effects. Complications arise when a single species rapidly increases in number and when supported by eutrophication, blooms proliferate above normal abundances. In cases where the most dominant species possesses traits that induce unfavorable changes to the marine community, they are referred to as harmful algal blooms (HABs). HAB events adversely impact marine communities but their consequences are not yet fully understood. Such blooms can produce harmless water discolorations and when there is high biomass in blooms, especially in sheltered bays, it may cause noxious or nuisance effects on the environment such as oxygen depletion or foam formation (Glibert *et al.*, 2005). In more severe circumstances, HABs are formed by or include significant levels of microalgal species that produce toxins. A significant fraction of the phytoplankton species known to cause blooms are capable of producing toxins (Visciano *et al.*, 2016). Bioaccumulation of these toxins poses a threat to other organism in the food web such as fishes, marine mammals and in extreme cases, humans. Shellfish acquire these toxins by direct filter feeding of the toxin-producing microalgal species. As a result, mortality follows or the toxin accumulates in these organisms. The effects of the toxins to humans are primarily due to consumption of the contaminated fisheries products (Hallegraeff, 1993).

As with other plankton blooms, HAB formation are mediated by ocean circulation, physical (e.g., currents, stratification, and upwelling) and chemical factors (e.g., salinity and nutrients), among others. Along with these, the life cycle and behaviors of the microalgal species contribute to bloom formation (Sellner *et al.*, 2003). Formation of HABs has also been linked to eutrophication (Anderson *et al.*, 2002; Smayda, 2008; Glibert *et al.*, 2010) and to climate change (Peperzak, 2005; Moore *et al.*, 2008). Anthropogenic activities particularly the increasing presence of aquaculture and



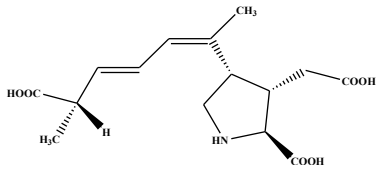
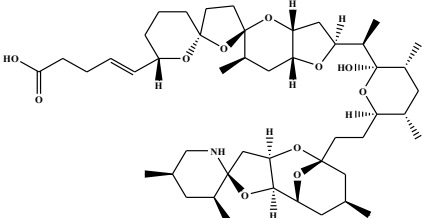
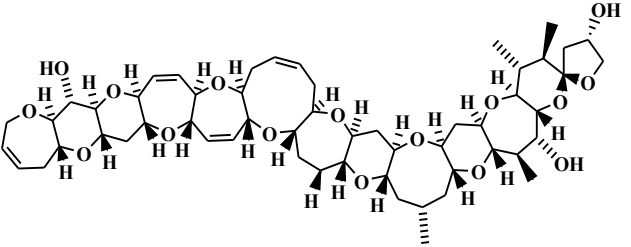
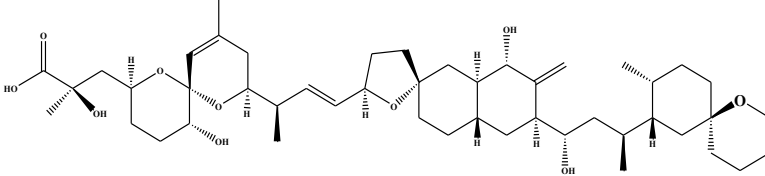
mariculture sites, have been also attributed to the potential development in HAB formation (Sellner *et al.*, 2003).

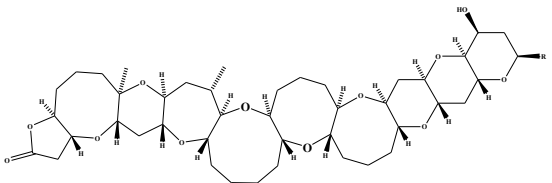
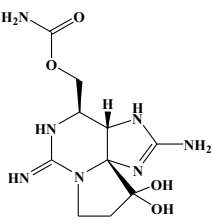
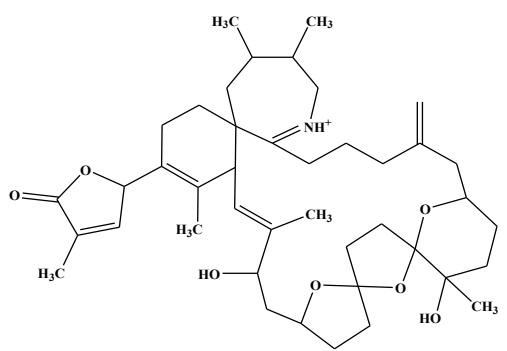
Incidence of HABs in terms of frequency, intensity and distribution have continuously increased over the past decades (Gobler, 2020). The increasing occurrence of HABs worldwide has caused direct negative impacts to the economic and public health sectors. Effects of HABs on tourism have contributed to economic losses in this industry (Hoagland and Scatasta, 2006). Other economic sectors are likewise affected as aquaculture sites experience massive fish kills and shellfish contamination, thereby, considerably reducing economic benefits derived from cultured seafood products (Anderson *et al.*, 2000). Consequently, food safety and security are also affected particularly those from shellfish industry due to HAB-related illnesses caused by consumption of contaminated seafood products (Grattan *et al.*, 2016). While consumption of contaminated fish and shellfish are the main route of exposure for HAB-related health concerns, toxic effects on humans are also caused by skin contact with contaminated water or inhalation of aerosols from the toxins (Berdalet *et al.*, 2016).

#### 1.1.2 Phycotoxins

Phycotoxins are toxic secondary metabolites of algal origin. In the plankton there are a rather high number of different phycotoxins that highly differ in structure, toxicity, and biological activity (Van Dolah *et al.*, 2000). Several approaches on toxin classification have been attempted and the classifications are based on taxonomic and phylogenetic ground, chemical properties (e.g., polarity and lipophilicity), or shared structural elements and enzymes of biosynthetic pathways (Cembella, 2003). A widely used toxin classification refers to the human toxic syndromes they cause in human; each phycotoxin is associated with a specific type of poisoning. Phycotoxin-associated syndromes include Amnesic, Diarrhetic, Neurotoxic, Paralytic shellfish poisoning and Ciguatera fish poisoning (Hallegraef *et al.*, 2014). Briefly, amnesic shellfish poisoning (ASP) induces gastrointestinal symptoms as well as profound and potentially permanent memory loss as a result of domoic acid exposure. Diarrhetic shellfish poisoning (DSP) is mainly characterized by gastrointestinal distress upon ingestion of shellfish contaminated with okadaic acid and its derivatives. The symptoms elicited by consumption of clams, oysters and mussels containing neurotoxic shellfish poisoning (NSP)-toxins (i.e., brevetoxins) include neurological and gastrointestinal problems, among others.

**Table 1.1.** Harmful algal bloom associated phycotoxins (modified from Grattan *et al.*, 2016)

Syndrome	Causative Organism	Major Toxin	Structural Unit	Sample Structure
Amnesic shellfish poisoning (ASP)	<i>Pseudo-nitzschia</i> spp.	Domoic Acid	Amino acid	 <p>Domoic Acid</p>
Azspiracid shellfish poisoning (AZP)	<i>Azadinium</i> spp. <i>Amphidoma languida</i>	Azspiracid	Secondary amine	 <p>Azspiracid-1</p>
Ciguatera fish poisoning (CFP)	<i>Gambierdiscus</i> spp.	Ciguatoxin	Ladder-frame polyether	 <p>Ciguatoxin 1</p>
Diarrhetic shellfish poisoning (DSP)	<i>Dinophysis</i> spp. <i>Prorocentrum</i> spp.	Okadaic Acid	Linear polyethers	 <p>Okadaic Acid</p>

Neurotoxic shellfish poisoning (NSP)	<i>Karenia brevis</i>	Brevetoxins	Ladder-frame polyether	 <p>R = CH<sub>2</sub>C(=CH<sub>2</sub>)CHO Brevetoxin-1</p>
Paralytic shellfish poisoning (PSP)	<i>Alexandrium</i> spp. <i>Gymnodinium catenatum</i> <i>Pyrodinium bahamense</i> var. <i>compressum</i>	Saxitoxin	Tetrahydro-purines	 <p>Saxitoxin</p>
Spiroimine shellfish poisoning (SSP)	<i>Prorocentrum lima</i> <i>P. maculosum</i> <i>Vulcanodinium rugosum</i> <i>Alexandrium ostenfeldii</i> <i>Karenia selliformis</i> <i>Alexandrium ostenfeldii</i>	Prorocentrolides Spiroprorocentrimine Pinnatoxins Gymnodimines Spirolides	Macrocyclic imines	 <p>13-desmethyl spirolide C</p>

Numbness of the neck and face, dizziness or 'floating' sensation and in severe cases, paralysis are mainly due to the paralytic shellfish poisoning (PSP) toxins such as saxitoxin. Ciguatera fish poisoning (CFP) induces the abovementioned symptoms such as gastrointestinal problems and neurological symptoms along with cardiovascular disorders (Grattan *et al.*, 2016).

In the context of chemical structures, phycotoxins, can also be classified according to the structural units that are distinct for each toxin group (Table 1.1) (Hallegraef *et al.*, 2014). Although there is a high diversity in size (i.e., small to high molecular weight molecules) and structural formula of phycotoxins, most of them share a unique structural feature that is the ether rings. These rings frequently occur as five- to nine-membered rings which can be condensed by common bonds forming a ladder-type structure (e.g., brevetoxins) or fused together by sharing a single carbon atom resulting in spiroketal formation (e.g., spirolides) (Van Wagoner *et al.*, 2014). The signature structural feature of phycotoxins, especially those that are produced by dinoflagellates, indicates that they may share a common building block or even elements of biosynthetic pathways (Wright and Cembella, 1998). Acetate, glycolate and glycine have been identified as precursor units of phycotoxins associated with dinoflagellates. Variations in the structural formation of these toxins could be a result of the different modifications that occur along the assembly process that includes but is not limited to functional group addition or deletion or both (Van Wagoner *et al.*, 2014). For this reason, there is a remarkable diversity not only among different toxin classes but also within toxins of the same class. The extent of structural diversity and the respective biosynthetic pathways of most phycotoxins remains unknown.

The presence of highly diverse phycotoxins may indicate their potential of diverse functionalities. However, it remains largely unknown what the function of such compounds could be, including the open question if there is a biological and ecological role of phycotoxins. Nevertheless, chemical defense, which details the antipredator, allelopathic and antibacterial properties of the toxins, have often been ascribed as one of the possible ecological function of phycotoxins (Ianora *et al.*, 2011). Intracellular signaling and storage have also been proposed as their probable biological role (Blanco *et al.*, 2020). With respect to biotechnological applications, phycotoxins have also been proposed useful for their putative role in therapeutics. For example, PSTs are known to block voltage-gated sodium channels (VGSC) in the cell membrane. This is of particular interest because of the potential applications in the neuromuscular system (Parker *et al.*, 2002). The close interaction between saxitoxin (STX), a type of PST, and VGSC may suggest the possible use of STX to induce anesthesia (Wiese *et al.*, 2010). Probable applications of brevetoxins

may be as post-stroke recovery drugs (Sequeira *et al.*, 2019). Other phycotoxins could be possibly used as analgesics, anesthetics, and antidepressant, anticancer and antiallergic drugs, among others (Cho *et al.*, 2020).

### 1.1.3 Macrocyclic imines

Macrocyclic imine toxins are considered as one of the newly discovered phycotoxins that could potentially affect the shellfish food industry. Characterized by the presence of 14–27 carbons atoms that form a macrocyclic ring system, it also includes the conserved units of 5–7 membered cyclic imine moiety and spiroketal ring system (Guéret and Brimble, 2010). Different types of macrocyclic imine toxins are produced by a wide array of microalgal species. Prorocentrolides and spiro-prorocentrimine have been shown to be produced by *Prorocentrum lima* and *P. maculosum*. Pinnatoxins and portimine, which is the smallest cyclic imine, have been linked to *Vulcanodinium rugosum*. Gymnodimines, initially identified from *Karenia selliformis* have also been recently reported to occur in *Alexandrium ostenfeldii*. Spirolides, on the other hand, were produced exclusively by *A. ostenfeldii* (Table 1.1).

## 1.2 Gymnodimines (GYM) and spirolides (SPX)

### 1.2.1 First reports of GYM and SPX

Gymnodimines (GYM) comprise of a cyclic imine ring, butenolide side chain and a 16-membered macrocycle (Figure 1.1A, Van Wagoner *et al.*, 2014). GYM was discovered in the 1990s following an anomaly observed in the mouse bioassay during a routine toxin profiling of shellfish (*Tiostrea chilensis*) collected from the South Island of New Zealand. Despite low levels of previously known toxins (i.e., DSP and PSP), an uncommon highly potent response was observed in mice after treatment with the lipophilic shellfish extract. The behavioral response included paralysis, neurological disturbances and rapid death of mice, which was different in the case of DSP or PSP intoxication. This clearly indicated that a fast-acting toxin with characteristic neurotoxic potential must be present in the shellfish samples (MacKenzie *et al.*, 1995). The newly discovered phycotoxin was later identified as gymnodimine (Seki *et al.*, 1995). *Karenia selliformis* (initially recorded as *Gymnodinium cf. mikimotoi*) was confirmed as the GYM-producer organism (Seki *et al.*, 1995; Miles *et al.*, 2000; 2003).

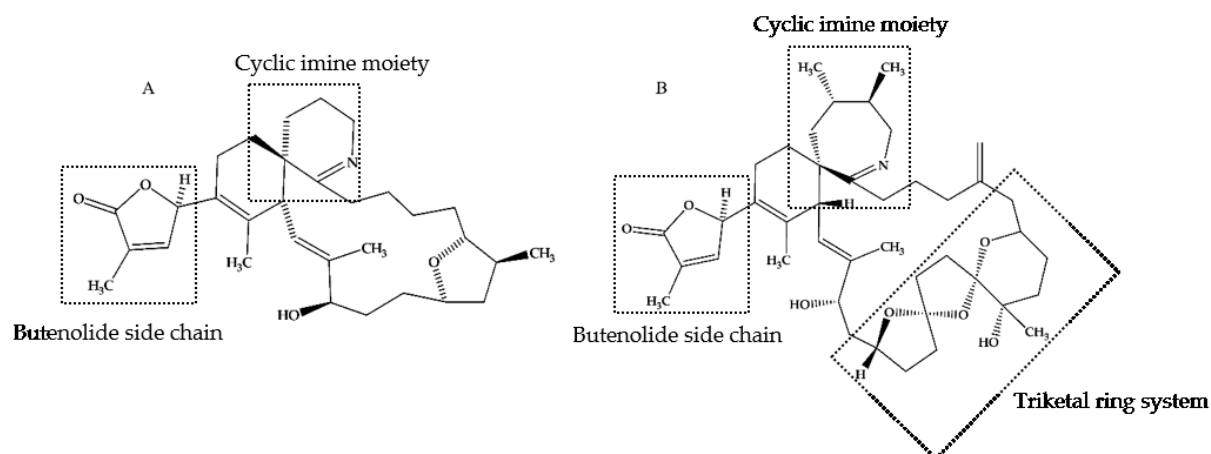


**Figure 1.1.** Chemical structure of the most common (A) gymnodimine (gymnodimine A) and (B) spirolide (13-desmethyl spirolide C) (modified from Bourne *et al.*, 2010).

Around the same time when GYM was identified in New Zealand, SPX was discovered in Nova Scotia, Canada. Similar to GYM, the discovery of SPX was also based on detecting inconsistency between the low DSP levels of the shellfish samples (*Mytilus edulis*) and severe and unusual symptoms in mouse bioassays. These inconsistencies thus indicated the presence of compounds other than DSP toxins, which were later identified as spiroptides (Hu *et al.*, 1995). A link between the occurrence of spiroptides in shellfish and plankton was established following the seasonal bloom of dinoflagellates in Nova Scotia, Canada. After detailed morphological investigation of the dominant dinoflagellate present in the microalgae assemblage, *Alexandrium ostenfeldii* was identified as the spiroptide-producing organism (Cembella *et al.*, 2000). SPX also share structural features with GYM but additionally have a triketal ring system, which is lacking in GYM (Figure 1.1B, Van Wagoner *et al.*, 2014).

### 1.2.2 Detection methods

GYM and SPX were initially detected and, as other marine phycotoxins, monitored for a long time using mouse bioassays (Yasumoto *et al.*, 1978; AOAC, 1990). In such assays, the onset of symptoms (i.e., shaking, stiffening or paralysis) after the intraperitoneal injection and death of the mice represents the methodical start- and endpoint, respectively. Mouse bioassays are difficult to be standardized as results may depend on the strain, gender and weight of mice. Because of these uncertainties, and most importantly, due to ethical reasons, this approach was abolished in many countries. In 2014, the European Commission established tandem mass spectroscopy coupled to liquid chromatography (LC-MS/MS) as the standard method for marine toxin detection and monitoring. This methodology was also applied to GYM and SPX detection. LC-MS/MS is widely

used for both its high selectivity and high sensitivity and it provides a faster and more reliable detection method that has been sought for these toxins (Quilliam, 1997). This technique is capable of detecting different types of toxins, including GYM and SPX, in a sample mixture. Toxins are identified based on their retention time (or the time at which the toxin is eluted from the separation column), exact molecular masses and fragmentation pattern (Figure 1.2).

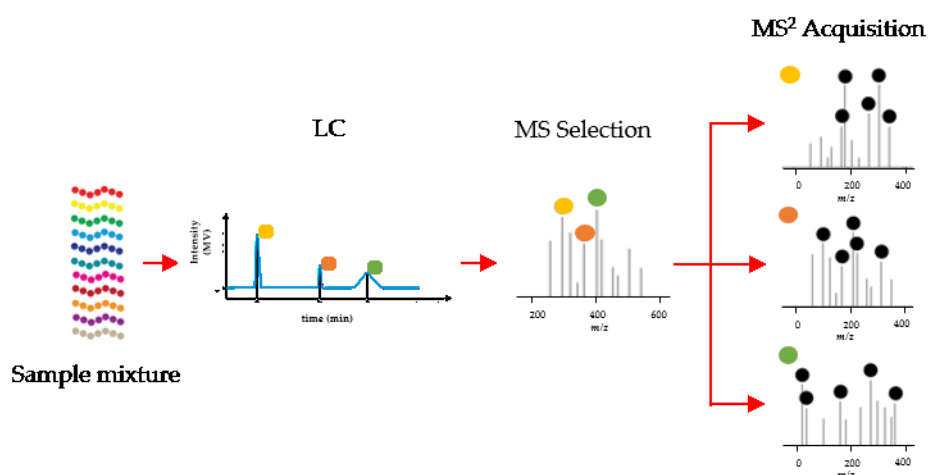


**Figure 1.2.** Schematic diagram of toxin detection using LC-MS/MS. Toxins are separated from the sample mixture through the LC. As the toxins enter into the first MS, toxins are ionized and are further selected according to their molecular masses (denoted as mass to charge ratio ( $m/z$ )). Toxins are fragmented in the second MS. Toxins are differentiated from one another according to their retention time, molecular weight and fragmentation pattern (modified from McLafferty and Tureček, 1993)

The detection of GYM and SPX makes use of specific mass fragment that distinguishes spiroimines from other compounds. These specific mass fragments have the mass to charge ratio ( $m/z$ ) of 121 for the six-membered cyclic imine ring in GYM (Figure 1.1A) and a  $m/z$  of 164 for the seven-membered cyclic imine ring in SPX (Figure 1.1B). LC-MS/MS also provides quantitative information for those toxins for which reference materials with known concentrations are available. Gymnodimine A and 13-desmethyl spiroolide C are the commonly used reference material for the quantification of GYM- and SPX-like compounds, respectively. Thus, quantification of the different structural types of GYM or SPX are expressed as equivalents of Gymnodimine A and 13-desmethyl spiroolide C.

The advancement of LC-MS/MS protocols allowed the detection of other structural analogues (compounds that derive from the same structural skeleton but with structural difference) of cyclic imines. In particular, real-time analysis of lipophilic toxins conducted in a cruise ship equipped with a LC-MS/MS system allowed the detection of two analogues of SPX, which are 13-desmethyl

spirolide C and 20-methyl spirolide G, in some microalgal samples from the North Sea (Krock *et al.*, 2008). The application of mass spectral methods in the detection of gymnodimine A is likewise demonstrated in the shellfish samples collected from the mariculture farms in Tunisia (Biré *et al.*, 2002) and China (Liu. *et al.*, 2011). To date, there are fifteen SPX and six GYM structural analogues or types that have been structurally elucidated from both shellfish and microalgal samples (Zurhelle *et al.*, 2018).

Aside from the abovementioned chemical methods, GYM and SPX were also detected through functional assays, which mainly includes receptor-based binding assays. The presence of gymnodimine A and 13-desmethyl spirolide C are ascribed to their ability to bind to the neuronal and muscle types of nicotinic acetylcholine receptor (Vilariño *et al.*, 2009; Rodríguez *et al.*, 2011). While these techniques offer a more sensitive approach than mass spectral methods, LC-MS/MS has been the most preferred approach because of the straightforward sample preparation methods and the robustness of the results.

### 1.2.3 Occurrence of GYM and SPX

After the first detection of GYM in New Zealand, GYM have also been reported from microalgal samples in many other coastal areas including the northeast waters of Australia (Takahashi *et al.*, 2007), northern (Harju *et al.*, 2016) and southern (Biré *et al.*, 2002; Naila *et al.*, 2012) parts of Europe, west coast of South Africa (Krock *et al.*, 2009) and the south eastern coast of the USA (Van Wagoner *et al.*, 2011). SPX, on the one hand, have been detected in European waters (Hummert *et al.*, 2002; Aasen *et al.*, 2005; MacKinnon *et al.*, 2006; Villar González *et al.*, 2006; Touzet *et al.*, 2008; Katikou *et al.*, 2010; Tillmann *et al.*, 2014; Van de Waal *et al.*, 2015; Martens *et al.*, 2017), the eastern coast of the USA (Gribble *et al.*, 2005) and in South American waters (Álvarez *et al.*, 2010; Almandoz *et al.*, 2014; Guinder *et al.*, 2018).

Another structural analogue of GYM was discovered in *A. ostensfeldii*, which was the first report of the specific toxin in any other dinoflagellate species aside from *K. selliformis* (Van Wagoner *et al.*, 2011). The co-occurrence of GYM and SPX in a single microalgal species was also demonstrated from the clonal isolates of *A. ostensfeldii* from the Netherlands (Van de Waal *et al.*, 2015; Martens *et al.*, 2017). Contrary to GYM, SPX have not yet been identified in any other dinoflagellate species besides *A. ostensfeldii*.



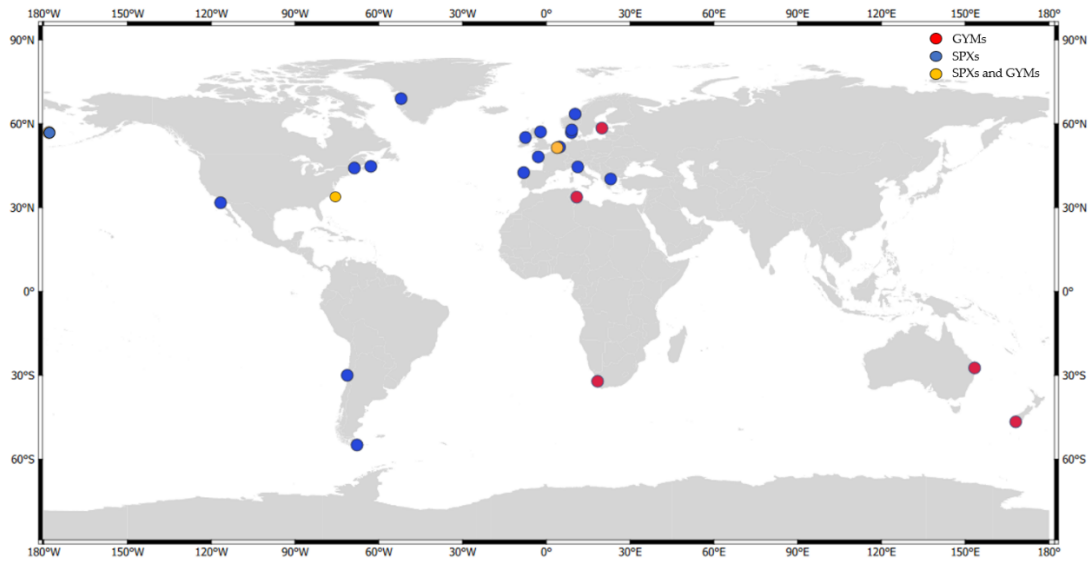


**Figure 1.3** Worldwide distribution of gymnodimines and spirolides from field and clonal microalgal samples (modified from Bacchiocchi *et al.*, 2020).

#### 1.2.4 *Alexandrium ostenfeldii*

*Alexandrium ostenfeldii* is a mixotrophic dinoflagellate first described in Iceland (Paulsen, 1904). This species was initially considered as an “Arctic-boreal” organism (Okolodkov and Dodge, 1996) but is currently known to occur in temperate waters around the world. After *A. ostenfeldii* was discovered in Iceland, the organism has also been reported to occur in the coastal waters of Europe, (Balech and Tangen, 1985; Fraga and Sanchez, 1985; Moestrup and Hansen, 1988; John *et al.*, 2003), northern and southern Pacific (Jacobson and Anderson, 1996; Levasseur *et al.*, 1997; Cembella *et al.*, 1999; Cembella *et al.*, 2001), as well as in northern and southern America (Jacobson and Anderson; 1996; Levasseur *et al.*, 1997; Cembella *et al.*, 1999; Cembella *et al.*, 2001). In terms of toxin production, *A. ostenfeldii* has been initially identified to produce PSP toxins (Hansen *et al.*, 1995; Mackenzie *et al.*, 1995). Later on, it was discovered that the microalgal species also produces spirolides (Cembella *et al.*, 2000) and gymnodimine (Van Wagoner *et al.*, 2011). To date, *A. ostenfeldii* is the only species that is capable of producing toxins of the three aforementioned toxin classes (Salgado *et al.*, 2015)

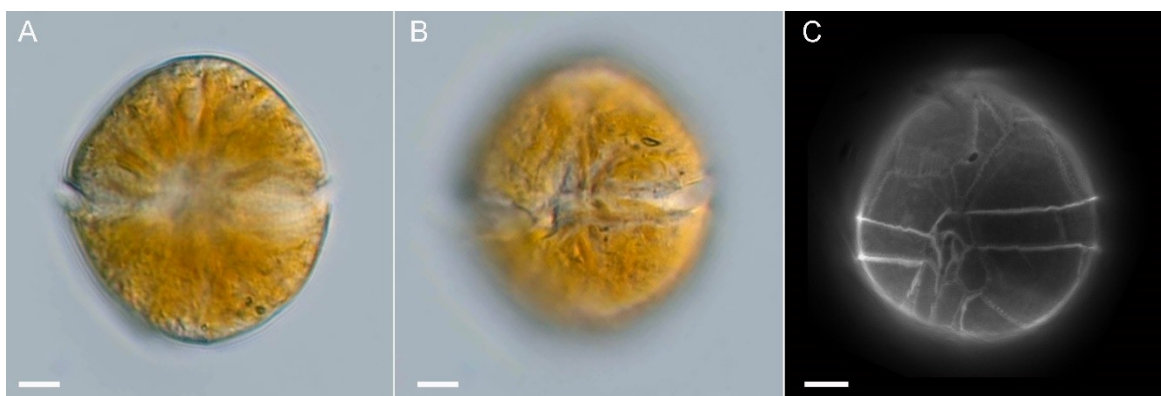


**Figure 1.4.** Images of *Alexandrium ostenfeldii*. (A) and (B) are bright field images of two focal planes of an *A. ostenfeldii* (MX-S-B11) cell in ventral view. (C) is an epifluorescence image of calcofluor-stained *A. ostenfeldii* (OKNL strain from the Netherlands) cell. White parts are the species-specific characteristic shape and arrangement of thecal plates of the species. Scale bars = 5 $\mu$ m (Images courtesy of Dr. Urban Tillmann)

### 1.2.5 Biosynthesis of GYM and SPX

The similarity of the structural features and the incidence in the same microalgal species indicate that GYM and SPX may have a common biosynthetic pathway. As with many other marine polyketide phycotoxins, the biosynthesis of GYM and SPX mainly involve the formation of the polyketide chain. It is suggested by Van Wagoner *et al.* (2014) that glycine is the building block needed for the polyketide backbone formation for spiroimines. Through the successive condensation reaction (a reaction in which the combination of two or more molecules forms a larger molecule) of extender units (i.e., carboxylic acids), a growing carbon chain is produced. These processes are initiated by various enzymes including polyketide synthases (PKSs) and acyl-coenzyme A (Van Wagoner *et al.*, 2014). Other enzymes of other biosynthetic pathway may also be linked to the polyketide chain synthesis. For example, non-ribosomal peptide synthases (NRPSs) have been identified to participate especially in the biosynthesis of dinoflagellate-associated toxins with an amino group (i.e., glycine) (Verma *et al.*, 2019). As the polyketide chain is formed, it further undergoes a cascade of cyclization reactions. Depending on the direction of the biosynthetic reaction, GYM or SPX are formed. Thus, the macrocyclic nature of GYM and SPX are carried out on a stepwise biosynthetic transformation that uses various enzymes (Van Wagoner *et al.*, 2014). However, the detailed biosynthetic reactions and the respective PKSs genes responsible for the GYM and SPX production remain to be determined.

### 1.2.6 Bioactivity of GYM and SPX

GYM and SPX are classified as fast-acting toxins since they induce a rapid response in mouse toxicity assays. Within minutes of intraperitoneal (i.p.) injection of the toxins, mice exhibited

neurological symptoms (e.g., decreased coordination, respiratory distress, convulsions, tremors, etc) in a manner that was not previously observed. The immediate response observed in mice indicates the rapid adsorption of the spiroimines to the peritoneum (Gill *et al.*, 2003; Hu *et al.*, 1996; Richard *et al.*, 2001). Notably, it was observed that treated mice could either die rapidly or fully recover with no signs of long-term effects, suggesting an “all or nothing”-effect of the toxins (Otero *et al.*, 2011).

Mouse toxicity studies further showed the different toxic effects of the toxins in relation to the route of administration. The time for symptoms to manifest extended and the onset of death slowed down when the toxins were orally administered (i.e., through forced feeding). The toxicity of GYM and SPX were even lower when administered by voluntary feeding. The order of toxicity for both toxins is i.p injection > oral administration > voluntary feeding (Otero *et al.*, 2011; Munday *et al.*, 2012). The lower toxicity of GYM and SPX (~four-fold decrease) when ingested compared to when injected may describe their reduced threat to humans (Otero *et al.*, 2011; Munday *et al.*, 2012). For this reason, it is still under debate to which extent GYM and SPX might pose a risk to human health, especially as so far no adverse effect on humans have been reported to be caused by these toxins (EFSA Panel on CONTAM, 2010).

Histological studies have revealed damages observed on the neuromuscular, sensory, digestive and respiratory systems of the mice treated with toxins (Otero *et al.*, 2011; Munday *et al.*, 2012). Visible damage was particularly observed in the brain tissues of mice, indicating that the toxin might have acted with high affinity to the mouse central nervous system. Pharmacological studies confirmed the effect of GYM and SPX towards the brain signaling pathways. The mode of action of the toxin using inhibition assays described GYM and SPX as anticholinergic to acetylcholine receptors (AChRs). This means that toxins inhibited the binding of the acetylcholine to AChRs. Furthermore, it was demonstrated that both toxins closely interact with nicotinic AChRs (nAChRs) (Kharrat *et al.*, 2008; Aráoz *et al.*, 2015; Bourne *et al.*, 2010; Hauser *et al.*, 2012) but have no strong interaction on muscarinic AChRs (mAChRs) (Aráoz *et al.*, 2015; Hauser *et al.*, 2012). No other than the above-mentioned bioassays have been conducted to GYM and SPX.

### **1.3 Research gaps in knowledge about cyclic imines**

Identification of the natural origin of cyclic imines and establishment of detection and monitoring methods have provided information on the global distribution of the toxins. GYM and SPX composition among microalgal stains varies considerably, indicating a high structural variability of both toxins (Hu *et al.*, 2001; Sleno *et al.*, 2004a; Ciminiello *et al.*, 2010; Aasen *et al.*, 2005;

Roach *et al.*, 2009; Tillmann *et al.*, 2014; Van de Waal *et al.*, 2015; Guinder *et al.*, 2018). The different types of spiroimines initially detected through mouse bioassays or mass spectral methods were confirmed through structural characterization techniques (i.e. nuclear magnetic resonance (NMR) spectroscopy) (Hu *et al.*, 1995; 2001; Sleno *et al.*, 2004a; Aasen *et al.*, 2005; MacKinnon *et al.*, 2006; Ciminiello *et al.*, 2007; 2010; Roach *et al.*, 2009; Zurhelle *et al.*, 2018). Current toxicity and mode of action assays identified GYM and SPX as “fasting-acting” toxins (Munday *et al.*, 2012; Otero *et al.*, 2012) and antagonists of nicotinic acetylcholine receptors (nAChRs) (Kharrat *et al.*, 2008; Aráoz *et al.*, 2015; Bourne *et al.*, 2010; Hauser *et al.*, 2012), respectively.

Taking into account the increased occurrence of toxin-associated algal blooms and the important advances of studies specifically focused on GYM and SPX, there is still a substantial knowledge gap that needs to be filled. In particular, the high structural variability of the toxins should be further investigated in order to determine to which extent toxins differ from their currently known structural configurations. As such, structural characterization studies could be performed on other GYM- or SPX-like compounds especially those that are present at low amounts. Determining the different types of toxins could provide insights in its potential role for the producing organism as well as effects on potential target organism, both of which up to now are not yet known. To provide additional understanding of the ecological function of GYM and SPX, more bioactivity studies on the toxins could still be performed in order to gain a better understanding on the MOA of the toxins and how the chemical structure of the toxin might be ascribed to its MOA. This is of interest considering that cyclic imines, in general, are not regulated in the European Union (EFSA Panel on CONTAM, 2010). Although no human intoxication has directly been linked to either GYM or SPX, its “fast-acting” and ACh antagonistic capability as well as its occurrence in coastal areas across the globe should also be taken into account. It is therefore necessary to conduct further comprehensive studies on these toxins while using the baseline information provided by previous studies. Additional knowledge on the structural variability and MOA of the cyclic imines could provide insights on the potential pharmaceutical applications of the toxins.

## CHAPTER 2

### Aims and Outline of the Thesis

This study generally intends to investigate the structural variability and bioactivity of the cyclic imines gymnodimines and spiroolides. This study specifically aims to 1) isolate gymnodimine A (GYM A) and 13-desmethyl spiroolide C (SPX1) directly from *Alexandrium ostenfeldii*; 2) characterize novel spiroolides from *A. ostenfeldii* using mass spectrometry-based techniques; and, 3) evaluate the bioactivities of GYM A and SPX 1.

In **Chapter 3**, two *A. ostenfeldii* strains were mass cultivated to obtain structurally known GYM A and SPX 1 for bioassays. Mass cultivating *A. ostenfeldii* demonstrated that the content of toxin per cell and the capacity of the organism to reach high cell density influenced the overall toxin yield. Moreover, the amount of isolated toxins from *A. ostenfeldii* was limited by purification procedures used in the study.

Due to constraints posed by obtaining purified toxins, an alternative approach was sought to characterize the structure of unknown compounds. In **Chapter 4**, unknown spiroolides identified from the three clonal strains of *A. ostenfeldii* were characterized using combined mass spectral (MS) techniques. By using MS-based approach, new spiroolides were discovered and proposed as structural analogues of the existing C- and G-type spiroolides that has a 5:5:6 and 5:6:6 triketal ring system, respectively. Of the nine putative new spiroolides, one showed indications that it might belong to new spiroolide subclasses with a new trispiroketal ring configuration (i.e., 6:5:6 trispiroketal ring system).

The purified GYM A and SPX1 (Chapter 3) were subjected to cell line-based assays to determine the much-needed bioactivities of the toxins at the cellular level. In **Chapter 5**, the effect of GYM A and SPX 1 on rat pheochromocytoma (PC12) cells was investigated by monitoring intracellular calcium levels. This study demonstrated that under normal cellular functions (i.e., physiological conditions), both toxins target acetylcholine receptors and mimic acetylcholine. Furthermore, in **Chapter 6**, the effects of the toxins on the adaptive stress response pathways were examined through reporter gene assays. This chapter presents the capability of GYM A and SPX 1 to induce oxidative stress and inflammation response pathways.

Finally, **Chapter 7** provides an overall discussion of the implications of the structural characterization and bioassays done in this work. Perspectives for the future direction of research was also provided.

## CHAPTER 3

### Mass Cultivation of *Alexandrium ostenfeldii* and Isolation of Gymnodimine A and 13-desMethyl Spirolide C

#### Highlights:

- *A. ostenfeldii* strains OKNL 48 and X-LF-19-F10 were successfully grown in large scale (60 L and 210 L, respectively)
- Gymnodimine A (GYM A) and 13-desmethyl spirolide C (SPX 1) were extracted and purified to a final yield 345 µg and 559 µg, respectively for future studies.

#### Contribution of the Doctoral Researcher:

- Planning of experiments
- Data collection
- Data analysis and interpretation

---

The methodology of this chapter was used in:

Zurhelle, C.; Nieva, J.; Tillmann, U.; Harder, T.; Krock, B.; Tebben, J. Identification of Novel Gymnodimines and Spirolides from the Marine Dinoflagellate *Alexandrium ostenfeldii*. *Mar. Drugs* 2018, 16, 446. <https://doi.org/10.3390/md16110446>

### 3.1. Introduction

There has been an increasing interest in harmful algal bloom (HAB)-causing microalgae and their associated toxins because of their influence on the safety of shellfish industry and their potential medical applications (Munday *et al.*, 2004). Initial studies on the toxicological assessment and structural elucidation of HAB-related toxins used contaminated shellfish samples in isolating the toxins (Yasumoto and Murata, 1993). This approach was demonstrated by the early studies of okadaic acid (OA)-group toxins, brevetoxins (BTXs), saxitoxins (STXs), yessotoxins (YTXs), domoic acid, and pectenotoxins (PTXs) (Rundberget *et al.*, 2006). For cyclic imines (CIs), contaminated shellfish organisms *Tiostrea chilensis* (MacKenzie *et al.*, 1995) and *Mytilus edulis* (Hu *et al.*, 1995) were used as source for isolation and purification of compounds to identify the chemical structure and toxicity of gymnodimines (GYM) and spirolides (SPX), respectively. The use of shellfish samples relies on availability of contaminated shellfish samples. Thus, direct isolation of the toxins from toxigenic microalgae is an alternative approach. In this case, identification and isolation of the toxin-producing microalgae species is a prerequisite. The identification of *Karenia selliformis* (Seki *et al.*, 1995; Miles *et al.*, 2000; 2003) and *Alexandrium ostenfeldii* (Cembella *et al.*, 2000) as the toxin-producing species for GYM and SPX, respectively thus enabled studies to shift from the use of shellfish to the use of the specific microalgae.

Although the extraction of toxins from microalgal samples looks promising, it poses a challenge especially if culture of microalgae of interest proved to be difficult in the laboratory. Such as the case for *Dinophysis* spp., where the microalgal culture conditions limited the production of its associated toxin dinophysistoxin-2 (DTX-2) (Rundberget *et al.*, 2007). In some cases, this limitation can be overcome by optimizing the growth conditions of the microalgae and by subjecting them to serial bulk cultures (Miles *et al.*, 2003; Munday *et al.*, 2004; Rhodes *et al.*, 2004; Dragunow *et al.*, 2005). The use of large-scale cultures in obtaining toxins have also been applied in CI-producing species (Miles *et al.*, 2000; 2003; Ciminiello *et al.*, 2007; Roach *et al.*, 2009). While culturing in large volumes has been used in most toxin isolation studies, there are also difficulties that come with it, one of them includes particular growth requirements of many dinoflagellates and their lower growth rate compared to other microalgae (e.g., diatoms). Dinoflagellates have relatively low growth rates and also maximum yield of biomass and associated toxins yields are comparatively low. In addition, most dinoflagellates are also found to have low threshold for shear forces (Beuzenberg, *et al.*, 2012), which result from mixing, circulation, aeration and pumping (Wang and Lan, 2018). For these reasons,



challenges in obtaining dinoflagellate mass cultures with high biomass have limited the production and the potential applications of toxins.

Culture conditions of dinoflagellates, including those that produce GYM and SPX, must be thoroughly considered in order to come up with large-scale cultures. *Alexandrium ostenfeldii* have been subjected to mass cultivation in several studies (Ciminiello *et al.*, 2007; Roach *et al.*, 2009). The culture conditions of *A. ostenfeldii* was investigated through the use of photobioreactors (Beuzenberg, *et al.*, 2012; Medhioub, *et al.*, 2011). In these set-ups, culture conditions and growth rates were continuously monitored. Simultaneous to the monitoring, physico-chemical conditions, such as pH (controlled by CO<sub>2</sub> injections), turbidity, light regimes, mixing and temperature, were also controlled throughout the experiment. Doubtlessly, sophisticated and fully controlled photobioreactors are useful in obtaining high cell density, however, alternative and simple approaches are also feasible. Bulk cultures can also be made by using large-volume flasks or carboys using simple aeration for mixing and/or CO<sub>2</sub> addition. Use of this technique effectively provided *A. ostenfeldii* cells in large quantities for detailed studies on both known and previously unknown toxins (Ciminiello *et al.*, 2007; Roach *et al.*, 2009).

In this chapter, we investigated the feasibility of using simple large-scale batch cultures of the two clonal isolates of *A. ostenfeldii*, with the specific aim to isolate gymnodimine A (GYM A) and 13-desmethyl spirolide C (SPX 1) and use them for subsequent bioassay studies.

## 3.2. Materials and Methods

### 3.2.1 Culture Conditions

*Alexandrium ostenfeldii* strains analyzed in this chapter were collected in the Netherlands and Denmark. The clonal strains OKNL 48 from the Netherlands was collected in the Ouwkerkse Kreek, the Netherlands while X-LF-19-F10 was collected in Limfjord, Denmark. *A. ostenfeldii* strains were grown in 70 mL plastic culture flasks with filtered K medium (Keller, 1987) adjusted to pH 8 at salinity 30 (X-LF-19-F10) or 15 (OKNL 48) and were kept under a 16:8 light-dark cycle at 15 °C with 50  $\mu\text{mol m}^{-2} \text{s}^{-1}$  photon flux density.

Growth rate of *A. ostenfeldii* strains was calculated based on the cell density difference between  $t=0$  and  $t=7-11$  days (equation 3.1) (Guillard, 1973). The growth rate of a 200 mL culture was measured during the early exponential phase. Cell density (P) was determined by fixing 1 mL of

microalgal culture sub-samples in a counting chamber with Lugol's iodine solution and counting the cells under 100× magnification with an Axiovert 40C optical microscope (Zeiss, Göttingen, Germany).

$$\mu = \frac{\ln(Pt_1) - \ln(Pt_0)}{t_1 - t_0} \quad 3.1$$

where  $\mu$ : Growth rate,

$Pt_1$ : cell concentration at time  $t_1$ , and

$Pt_0$ : initial cell number.

### 3.2.2. Toxin Measurement

#### 3.2.2.1 Toxin Extraction

Small-scale (200 mL) toxin extraction was carried out once to determine the cell quota of the microalgal strains. Cultures that reached cell densities of  $>1500$  cells  $\text{mL}^{-1}$  were harvested by centrifugation of 50 mL culture at  $3,220 \times g$  for 10 min (Eppendorf 5810R, Hamburg, Germany). The cell pellets were transferred to 1 mL microtubes, centrifuged at  $16,000 \times g$  for 5 min (Eppendorf 5415R, Hamburg, Germany) and stored at  $-20$  °C until extraction.

Cell pellets were suspended in 500  $\mu\text{L}$  methanol and mixed twice in a vortex mixer for 30 seconds (Heidolph, Schwabach, Germany). The suspension was transferred into a spin-filter (pore-size 0.45 mm, Millipore Ultrafree, Eschborn, Germany) and centrifuged at  $16,000 \times g$  for 15 min (Eppendorf 5415R, Hamburg, Germany). The filtrate was transferred into LC vials for mass spectrometric measurement.

#### 3.2.2.2 Parameters of Liquid Chromatography-Tandem Mass Spectrometry (LC-MS/MS)

A triple-quadrupole mass spectrometer (API 4000 Q Trap, Sciex, Darmstadt, Germany) with a Turbo V ion source coupled to a 1100 LC liquid chromatograph (Agilent, Waldbronn, Germany) was used in the quantification of toxins from the two *A. ostenfeldii* strains.

The LC and mass spectrometric parameters used in this chapter were adapted from the procedure described by Martens *et al.* (2017). The LC component, composed of solvent reservoir, in-line degasser (G1379A), binary pump (G1311A), refrigerated autosampler (G1329A/G1330B) and a temperature-controlled column oven (G1316A) was employed for the toxin separation which was

conducted using an analytical C8 reverse phase column (50 mm × 2 mm) packed with 3 μm Hypersil BDS 120 Å (Phenomenex, Aschaffenburg, Germany) and thermostated at 20 °C. A gradient elution was then performed with water and methanol/water (95:5 v/v) as eluent A and B, respectively, and a buffer system made of ammonium formate and formic acid was added to both eluents with final eluent concentrations of 2.0 mM and 50 mM, respectively. A flow rate of 0.2 mL min<sup>-1</sup> was used to generate a gradient flow of 5% eluent B during the initial condition, a linear gradient to 100% B up to 10 min after injection, an isocratic elution for 20 min, 5% B for 1 min and finally 9 min for column equilibration. The total run time was 30 min.

The mass spectrometry component has the following parameters: Curtain gas: 20 psi, CAD (collision activated dissociation) gas: medium, ion-spray voltage: 5500 V, temperature: 650 °C, nebulizer gas: 40 psi, auxiliary gas: 70 psi, interface heater: on, declustering potential: 121 V, entrance potential: 10 V, exit potential: 22 V. The collision energy was 57 V for each transition. Measurements were performed in the positive ion-mode and 40 ms dwell times were used for each transition, which was  $m/z$  508 > 490 for gymnodimine A (GYM A) and  $m/z$  692 > 164 for 13-desmethyl spirolide C (SPX 1). Certified reference materials (NRC, Halifax, NS, Canada) of GYM A and SPX 1 were used to determine the toxin content in the microalgal samples.

### 3.2.3. Mass Extraction and Purification of Gymnodimine A (GYM A) and 13-desmethyl spirolide C (SPX 1)

While different types of gymnodimines and spirolides were identified in the two microalgal strains, this chapter focused only on describing the extraction and purification of GYM A and SPX 1.

#### 3.2.3.1 Mass Culture of *A. ostenfeldii*

*A. ostenfeldii* cultures were upscaled in a gradual manner. A 40-mL aliquot was collected from high cell density 70mL cultures (> 1500 cells mL<sup>-1</sup>) and were mixed with 160 mL K medium (20% final concentration of stock cultures). Using the same volume ratio, the cultures that exceeded 1500 cells mL<sup>-1</sup> were further upscaled to give a total volume of 1 L, 5 L and finally 10 L. A total of 64 L and 210 L of OKNL 48 and X-LF-19-F10 were produced for this experiment.

#### 3.2.3.2 Solid-phase Extraction (SPE) Methods

Prior to mass extraction, four batches of 1 L OKNL 48 cultures (from Section 3.2.2) were used to determine which SPE conditions provide high recovery and purity of GYM A and SPX 1. Sep-Pak C18 SPE cartridge (Merck Supelco, Darmstadt, Germany) and HP-20 resin (3 g, Diaion Supelco,

Steinheim, Germany) were conditioned by sequentially eluting two column volumes of methanol and water. After the cultures were loaded into two separate sets of cartridge and resin, either methanol (MeOH) or acetonitrile (ACN) were used to elute the toxins. Different concentrations of the solvents were sequentially used to elute different fractions. Percent recovery and purity was measured in all the set-ups using equation 3.2 and 3.3, respectively.

$$\% \text{ Recovery} = \frac{\text{Toxin content after purification}}{\text{Toxin content before purification}} \times 100 \quad (3.2)$$

$$\% \text{ Purity} = \frac{\text{Height (Area) of the toxin peak}}{\text{Total height (area) of peaks in the fraction}} \times 100 \quad (3.3)$$

### 3.2.3.3 Extraction and Purification

Six batches of 10 L OKNL 48 (with a mean cell density of  $4.1 \times 10^3$  cell mL<sup>-1</sup>) and a total volume of 210 L X-LF-19-F10 (with a mean cell density of  $5.4 \times 10^3$  cell mL<sup>-1</sup>) were treated with acetone (7% final concentration) to lyse the cells and thus to transfer all toxins into the dissolved phase. Toxins were extracted using conditioned HP-20 (~15 g per 10 L, 48 h, Diaion Supelco). The resin was collected by filtration and desalted, dried, and stored at -20 °C. The pooled resin (460 g) from a total of 270 L was eluted with acetonitrile (ACN) and the eluate was dried under vacuo before loading into the preparative reversed phase chromatography (C18, 25 × 310 mm, 5 mL min<sup>-1</sup>). The elution was done with a stepwise gradient from aqueous:acetonitrile (ACN) (water/ACN, 80:20 v/v) to 100% ACN (a total of 30 fractions). The presence of GYM A and SPX 1 was confirmed by LC-MS and the toxin-containing fractions dried, resuspended in water-ACN (1:1) (2 mL) and applied to (high-performance liquid chromatography) HPLC reversed-phase purification on a C8 column (10 × 150 mm, Machery & Nagel) with solvent A: water and solvent B: acetonitrile (ACN) both containing 0.1% formic acid. The samples were eluted isocratically at 15% B for 5 min, followed by a 20 min gradient to 100% B and held at 100% B for 5 min. The reequilibration phase at 15% B was 5 min. The final purification step was performed under isocratic elution with water-ACN 45:55 over for 30 min on a Phenyl-hexyl column (4.6 mm × 150 mm, 1.5 mL·min<sup>-1</sup>, Machery & Nagel) (Zurhelle *et al.*, 2018).

### 3.3. Results and Discussion

#### 3.3.1 Growth rate and cell quota differs Among *A.ostenfeldii* Strains

*A. ostenfeldii* strains OKNL 48 and X-LF-19-F10 that were grown in 200 mL cultures have a growth rate of 0.14 day<sup>-1</sup> (Table 3.1). This is within the range of growth rates of *A. ostenfeldii* strains reported in literature. Strains from the Netherlands had growth rates that ranged from 0.16–0.22 day<sup>-1</sup> (Van de Waal *et al.*, 2015) or a previously studied Danish strain that has a growth rate range of 0.08–0.16 day<sup>-1</sup> (Medhioub *et al.*, 2011).

**Table 3.1** Growth rates ( $n = 2$ ) and toxin cell quotas from 200 mL *A. ostenfeldii* strains. Standard error was measured for the growth rates.

Strain	Growth Rate ( $\mu$ ), day <sup>-1</sup>	Toxin Cell Quota (pg cell <sup>-1</sup> )	
		GYM A	SPX 1
OKNL 48	0.14 ± 0.01	3.1	0.3
X-LF-19-F10	0.14 ± 0.02	0.3	1.2

The toxin cell quota was different between both *A. ostenfeldii* strains (Table 3.1). OKNL 48 contained more GYM A than SPX 1 and strain X-LF-19-F10 contained more SPX 1 than GYM A. Among many *A. ostenfeldii* strains collected from the same area as OKNL 48, many strains had significantly higher SPX cell quota (up to 4.4 pg cell<sup>-1</sup>; Van de Waal *et al.*, 2015) but few other strains have a SPX cell quota of less than 1.8 pg cell<sup>-1</sup> (Martens *et al.*, 2017), that is more comparable to the low cell quota of strain OKNL 48 observed in the present culture set-up. With respect to GYM, the current cell quota of strain OKNL 48 was ten-fold lower as compared to a previous analysis of the same strain (Martens *et al.*, 2017), but it is unknown if this is due to a potential reduction in toxin production of the strain as it ages. As for X-LF-19-F10, it has a higher SPX cell quota as compared to an earlier study that reported a SPX cell quota of 1–5 pg cell<sup>-1</sup> (Medhioub *et al.*, 2011).

#### 3.3.2 Different Solid-phase extraction (SPE) methods for GYM A and SPX 1

The two SPE methods, each eluted with either MeOH or ACN (Figure 3.1), showed different recoveries and purities of GYM A and SPX 1 (Table 3.2). In C18 cartridge eluted with ACN (Figure 3.1A), low recovery (less than 10%) and low purity (less than 15%) was measured in the second fraction (F2). Toxin-rich fraction with high purity was observed in F3. The lowest recovery was found in F4 yet; GYM A has a purity of greater than 70% (Table 3.2). In a separate C18 cartridge set-up (Figure 3.1B), a high percent recovery was only measured when 80% MeOH was used (F3), with

SPX 1 having a recovery of 43%. Toxin purity was at 48% and 28% for GYM A and SPX 1, respectively. The use of 100% MeOH (for F4) provided a recovery of less than 3% but with a purity 71% (for GYM A). No toxin was detected in F2, where 50% MeOH was used to elute the toxin fraction. A different trend was observed in the second SPE method using HP-20 resin. The use of ACN in eluting GYM A and SPX (Figure 3.1C) consistently gave a percent recovery of ~10% or more at all three fractions (Table 3.2). Moreover, GYM A purity was within the range of ~60 in F2 to F4. The use of 80% ACN (F3) provided a recovery of almost 30% and a purity of ~22% for SPX 1 (Table 3.2). In a different HP-20 resin (Figure 3.1D), a high recovery (~10% and ~25% for GYM A and SPX 1, respectively) and purity (~60% and ~25% for GYM A and SPX 1, respectively) was described only in F4.

From the different SPE methods conducted in this study, HP-20 eluted with ACN (Figure 3.1C) was the chosen procedure for the initial purification of the large-scale microalgal culture. The method was prioritized because of the adequate proportion of recovery and purity of all its fractions (F2-F4). Other fractions that were eluted with ACN (i.e., F3 in C18 cartridge) could also be considered. However, since the recovery and purity have similar values to that F3 in HP-20 eluted with ACN, the former was disregarded as an option.

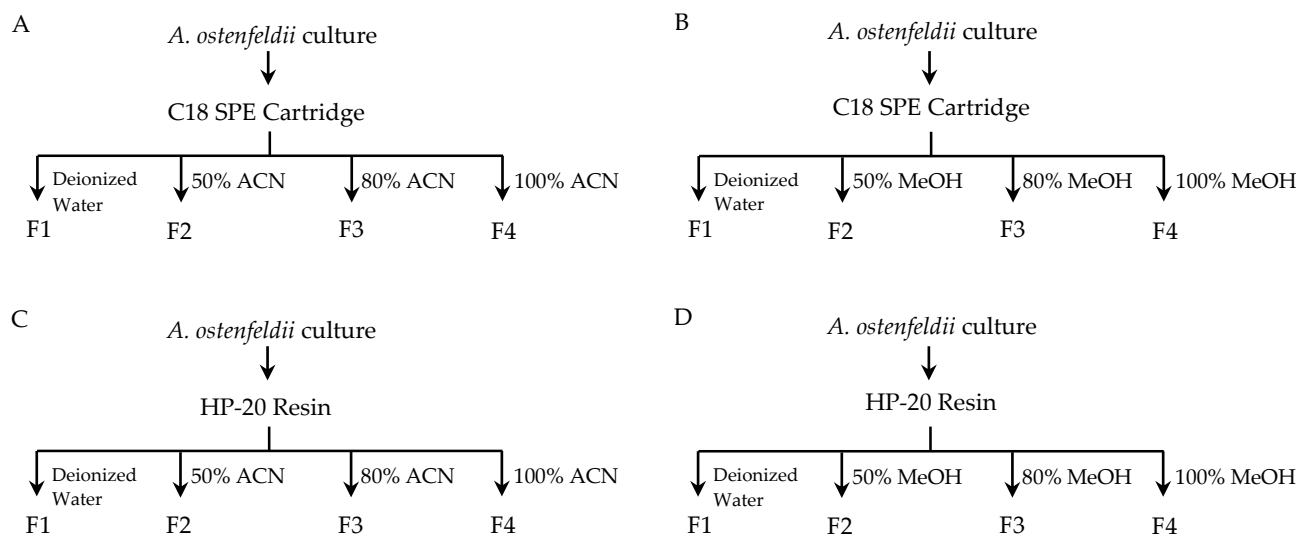


**Figure 3.1.** Schematic diagram of the SPE methods tested in this study. Fractions 1 – 4 (F1-F4) were obtained using C18 cartridge eluted with (A) ACN and (B) Methanol (MeOH). HP-20 adsorption resin F1-F4 were collected after the column was eluted with (C) ACN and (D) MeOH.

**Table 3.2.** Recovery and purity of toxins from the fractions using C18 SPE Cartridge and HP-20 adsorption resin. The percent recovery described the percentage of toxin recovered in each experiment.  $n=1$

SPE	Fraction	ACN				Fraction	MeOH			
		GYM A		SPX 1			GYM A		SPX 1	
		Recovery (%)	Purity (%)	Recovery (%)	Purity (%)		Recovery (%)	Purity (%)	Recovery (%)	Purity (%)
C18 Cartridge	F2	6	13	8	3	F2	0	n/a	0	n/a
	F3	9	59	29	30	F3	10	48	43	28
	F4	<1	72	<1	15	F4	2	71	2	11
HP-20 Resin	F2	7	61	10	16	F2	0	n/a	0	n/a
	F3	12	62	27	22	F3	1	56	1	15
	F4	10	67	17	20	F4	11	59	26	23

In a separate experiment, a different ACN gradient was tested with HP-20 resin (Figure 3.2) and it showed an increase in toxin recovery (Table 3.3). Aside from the ACN fractions (F2-F4), F5 that was obtained from HP-20 using MeOH had a recovery of less than 1%. The low recovery in F5 indicates that GYM A and SPX 1 were eluted at ACN-mediated fractions. Among the fractions, F3 was identified as the toxin-rich fraction.

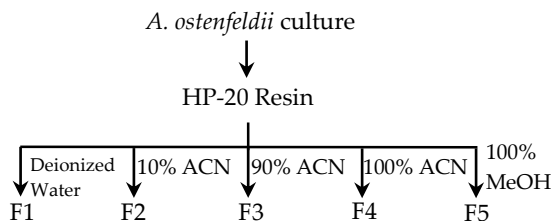


**Figure 3.2** Schematic diagram of fractions obtained from using HP-20 resin.

**Table 3.3.** Toxin recovery and purity using HP-20 eluted with 90% ACN (F2) and 100% ACN (F4).

Fraction	GYM A		SPX 1	
	Recovery (%)	Purity (%)	Recovery (%)	Purity (%)
F3	27	57	37	17
F4	6	29	6	12

The difference in recoveries between GYM A and SPX 1 could be ascribed to their degree of polarity and their extent of solubility to either MeOH or ACN. The difference in purity, on one hand, could be attributed to the presence of other structural types of gymnodimine or spirolides in the fraction. In particular, the low purity of SPX 1, is likely influenced by the presence of two other types of spirolides (Zurhelle *et al.*, 2018). Moreover, the different recoveries and purities from two SPE methods could indicate that toxins might have different affinities to the SPE columns. However, although C18 cartridge and HP-20 resin are of different material, both use reverse-phase chromatography technique in separating compounds. As such, both columns are suitable for the

purification of a wide array of compounds (e.g., polar and non-polar compounds) upon the use of polar organic desorbing solvents. The polar nature of GYM A and SPX 1 allows them to be readily soluble in MeOH, ACN or any other polar solvents (Otero *et al.*, 2009). For this reason, there are many SPE-mediated purification steps that could be applied to crude toxin extracts. Previous studies have described the use of Sephadex LH-20 and MeOH as the eluting solvent for the pre-purification method for spirolides (Hu *et al.*, 1995; 2001; Gill *et al.*, 2003, MacKinnon *et al.*, 2006) while another study demonstrated the use of Sephadex LH-20 eluted with acetone (Otero *et al.*, 2009). Pre-purification through C18 cartridge was also used in earlier studies (Aasen *et al.*, 2005; Roach *et al.*, 2009). In this experiment, HP-20 resin eluted with ACN gradient was employed as the SPE-mediated purification method (Figure 3.2), which is the same technique used from a previous study (Ciminiello *et al.*, 2007). While there are no distinct criteria on the type of SPE method to be used for the cleaning method, the aforementioned procedure (i.e., HP-20 in ACN) was chosen because of its suitability to the target compounds GYM A and SPX 1. In samples where there are many types of toxin present, it is important to consider the method that incorporates a high recovery and purity of most of the toxins of interest, if not all. This consideration to the methods was demonstrated in a study by Otero *et al.* (2009), where they identified 50% ACN and acetone as the solvents appropriate for the elution of two types of SPX from silica-based SPE.

SPE is an extraction method that is commonly performed to clean-up or remove impurities from the crude extracts before subjecting them to further downstream chromatographic purification (i.e., HPLC). For marine microalgal samples, SPE could also function as a desalting process. Such as the case for the first fraction (F1), wherein deionized water was used to elute the unwanted buffer salts in the column. As SPE in itself is versatile (Wells, 2013), it is thus significant to identify which conditions (type of SPE and solvent) will provide a high percent recovery for every samples.

### 3.3.3 Purified GYM A and SPX 1

The extraction and isolation of GYM A and SPX 1 was conducted by subjecting the toxin-rich fraction, obtained from the HP-20 resin eluted with ACN, to chromatographic purification (Figure 3.3). A total of 345  $\mu\text{g}$  GYM A and 559  $\mu\text{g}$  SPX 1 were purified (greater than 95% purity) from the microalgal strains. The collective recovery of pure toxin was ~10% (Table 3.4).



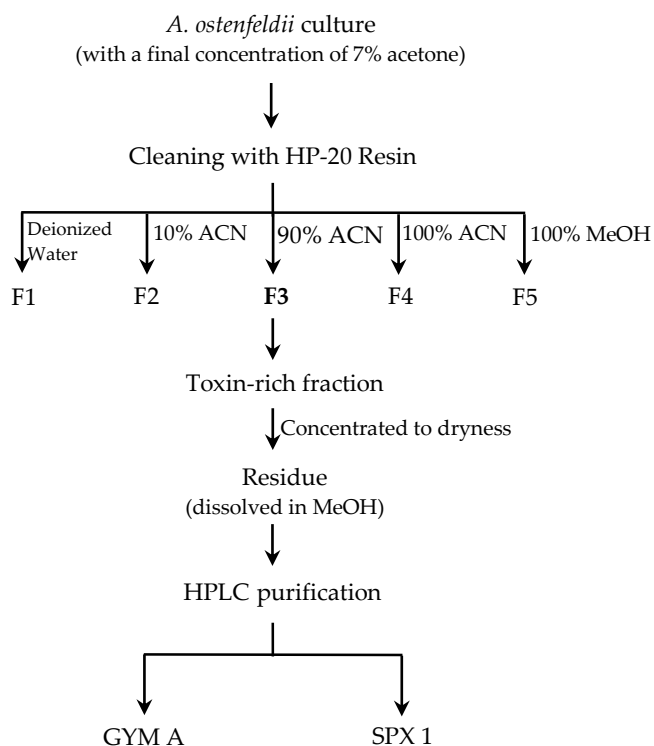


**Table 3.4.** Total amount of toxin recovered from the extraction and purification procedure conducted in this study.

Toxin	Weight ( $\mu\text{g}$ )	Recovery (%)	Purity (%)
GYM A	345	9	> 95
SPX 1	559	10	> 95

**Figure 3.3** Schematic diagram of the extraction and purification procedure performed in this study.

Purified GYM A and SPX 1 were identified by comparing retention time from *A. ostenfeldii* extracts with those from standard solutions (Fig. 3.4). The similarity in retention times illustrates that the target toxins from the microalgal strains are the same as those from the standard solutions. Furthermore, this is an indication that the extraction and purification method established in this study was potentially applicable in isolating GYM A and SPX 1 with high purity. Although the isolation processes used in the experiment purified the target compounds, the recovery is ~10%. Most of the losses could be attributed to the SPE-mediated purification procedure. A way to increase the recovery is to elute the toxins with the same desorbing solvent several times. This method was applied in earlier studies wherein SPE column, which was extracted twice with MeOH, was used for the purification of SPX from shellfish and microalgal samples (Aasen *et al.*, 2005; 2006; Ciminiello *et al.*, 2006).

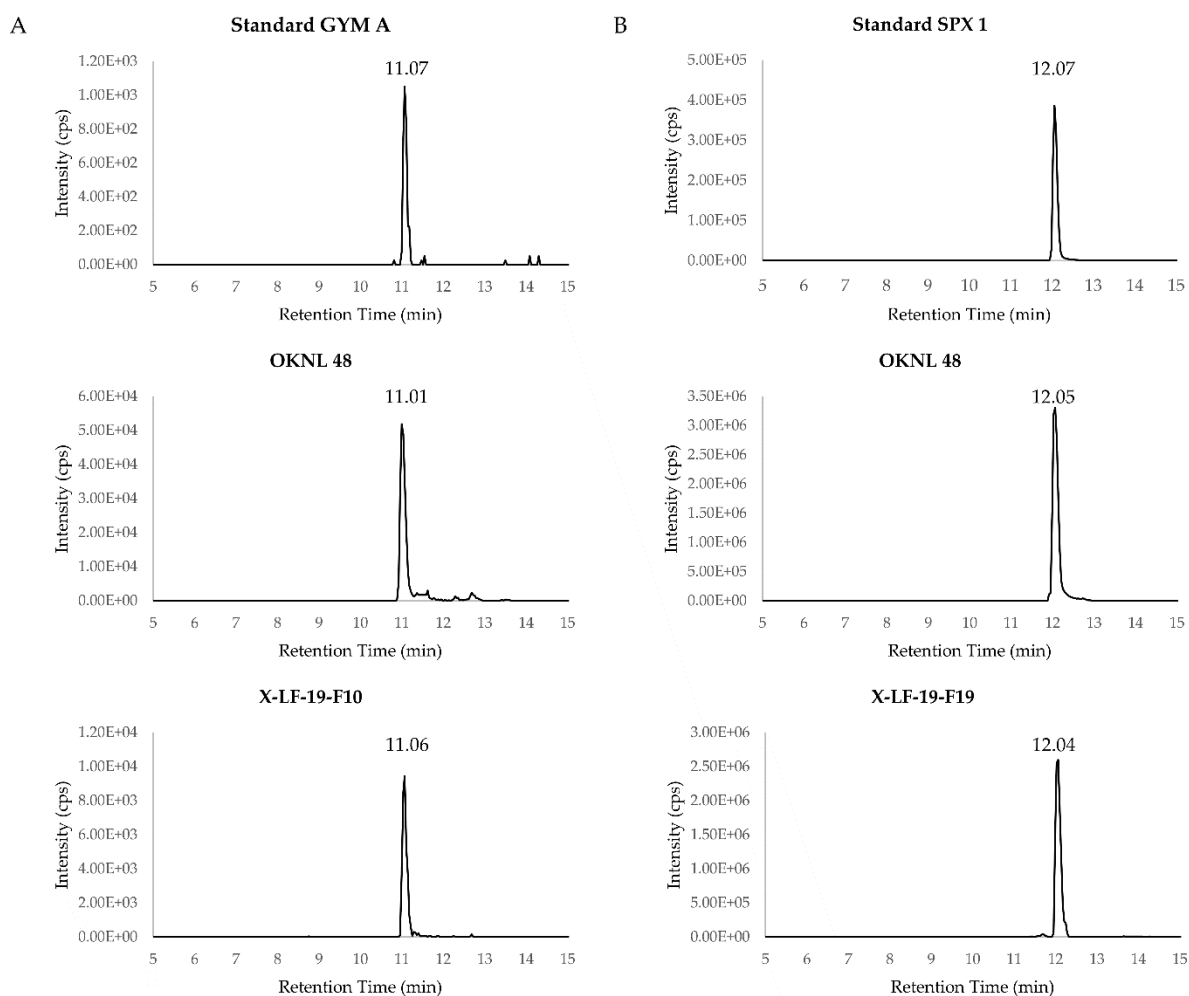


**Figure 3.4** Ion chromatograms of (A) GYM A ( $m/z$  508 > 490) from the standard reference material and from *A. ostenfeldii* strains OKNL 48 and X-LF-19-F10; and (B) SPX 1 ( $m/z$  692 > 164) from the standard reference material and from *A. ostenfeldii* strains OKNL 48 and X-LF-19-F10.

### 3.3.4 Implications on Toxin Isolation

Large-scale methods for extraction of the toxins is necessary to obtain pure compounds that will be used for further experiments. While this chapter focused only on describing structurally known compounds (i.e., GYM A and SPX 1), unknown cyclic imines could likewise be considered in the extraction and purification steps of mass cultures of *A. ostenfeldii*. In fact, the culture, extraction and purification methods described in this chapter was used to isolate two new spirolides identified from OKNL 48 (Zurhelle *et al.*, 2018). Compared to GYM A and SPX 1, the two SPX types were present in low amounts but were sufficient for structural characterization assays.

The amount of isolated microalgal toxins to a large extent depend on the capacity of the organism to reach high cell density. In addition, growth rate and more importantly, toxin content

per cell of the microalgal strain play a role on the production of toxins. While the growth rate and cell quota values of the *A. ostenfeldii* strains are within the range from the previous studies (Medhioub et al., 2011; Van de Waal et al., 2015), it is relatively low compared to other *A. ostenfeldii* strain (Suikkanen et al., 2013).

The extraction and purification procedures also contribute to the yield of pure compounds. As there are different variations of the extraction methods, initial experiments focused on determining the most suitable isolation process for the target compounds is useful in order to increase the recovery of the toxins. Aside from recovery, the use of pre-HPLC purification steps (i.e., SPE) that could effectively remove impurities should also be considered. Both recovery and purity play significant roles in the isolation of target compounds. In toxin isolation, particularly those that focused on SPX, variations in the SPE-mediated purification method are more commonly applied than the purification step through HPLC. Previous studies used Sephadex LH-20, Silica gel or HP-20 in the pre-purification procedures by SPE (Hu et al., 1995; 2001; Gill et al., 2003, Aasen et al., 2005; MacKinnon et al., 2006; Ciminiello et al., 2007; Roach et al., 2009; Otero et al., 2009). By employing different SPE techniques, the isolation of known and novel spirolides was carried out successfully.

With these above-mentioned conditions, mass cultivation of *A. ostenfeldii* and extraction, purification and isolation of cyclic imines entailed a big challenge especially in gathering enough toxins for experimental use. This study focused only on the structurally known toxins—GYM A and SPX 1. Thus, isolation of other toxins present in the microalgal samples could also be explored including novel toxins. In isolating novel toxins, which at times are present in trace amounts, optimized large-scale culture conditions as well as efficient extraction and purification procedures must be further studied in order to isolate sufficient amounts for both structural characterization and bioassays.

## CHAPTER 4

### Mass Spectrometry-Based Characterization of New Spirolides from *Alexandrium ostenfeldii* (Dinophyceae)

#### Highlights:

- In depth analysis of three strains of *Alexandrium ostenfeldii* revealed the presence of nine novel spirolides.
- Compound **1** was suggested to have a truncated side chain in lieu of the commonly observed butenolide ring in spirolides.
- Other compounds were proposed as C- and G-type SPX analogues.
- Compound **5** might belong to new spirolide subclasses with a trispiroketal ring configuration having a 6:5:6 trispiroketal ring system.
- Compound **7** was proposed as the first G-type SPX with a 10-hydroxylation as usually observed in C-type SPX.

#### Contribution of the Doctoral Researcher:

- Planning of experiments
- Data collection
- Data analysis and interpretation
- Manuscript writing

---

This chapter appeared in:

**Nieva, J.A.;** Tebben, J.; Tillmann, U.; Wohlrab, S.; Krock, B. Mass Spectrometry-Based Characterization of New Spirolides from *Alexandrium ostenfeldii* (Dinophyceae). *Mar. Drugs*. 2020, *18*, 505. <https://doi.org/10.3390/md18100505>

#### 4.1. Introduction

Since the discovery of spirolides (SPX) in 1995 (Hu *et al.*, 1995), more information has been reported on the types of cyclic imine toxin. To date, 16 SPX of microalgal origin have been structurally elucidated (Table 4.1). The first characterized SPX, which were gathered from Canadian microalgal and contaminated shellfish samples, included spirolides A-D and the 13-desmethyl analogues of SPX C (=SPX 1) (Hu *et al.*, 1995; 2001) and D (Sleno *et al.*, 2004a). These A–D spirolides are generally classified as C-type SPX because they all share a 5:5:6 trispiroketal ring system in their structural configuration. In addition, new spirolide subclasses, G-type (Aasen *et al.*, 2005) and SPX H/I (Roach *et al.*, 2009) were discovered. In contrast to C-type SPX, G-type spirolides have a 5:6:6 trispiroketal ring configuration and H/I-type SPX contain a 5:6 dispiroketal ring system (Table 4.1). Over the years, different spirolide analogues, mostly belonging C-type spirolides, were also elucidated from different microalgal samples (MacKinnon *et al.*, 2006; Ciminiello *et al.*, 2007; 2010; Zurhelle *et al.*, 2018).

The occurrence of SPX subtypes in *A. ostenfeldii* strains has also been observed across European waters (Hummert *et al.*, 2002; Aasen *et al.*, 2005; MacKinnon *et al.*, 2006; Villar González *et al.*, 2006; Touzet *et al.*, 2008; Katikou *et al.*, 2010; Tillmann *et al.*, 2014; Van de Waal *et al.*, 2015; Martens *et al.*, 2017), in the Gulf of Maine (Gribble *et al.*, 2005) and the South American Atlantic and Pacific coasts (Álvarez *et al.*, 2010; Almandoz *et al.*, 2014; Guinder *et al.*, 2018), demonstrating the global distribution of SPX-producing *A. ostenfeldii* strains. While some strains primarily produce SPX 1 (Hu *et al.*, 2001; Ciminiello *et al.*, 2010; Van der Waal *et al.*, 2015; Qui *et al.*, 2018) other strains have SPX A (Gribble *et al.*, 2005), SPX C (Touzet *et al.*, 2008), 20-methyl SPX G (Aasen *et al.*, 2005; Qui *et al.*, 2018) or 13,19-didesmethyl SPX C (MacKinnon *et al.*, 2006) as their major component. Next to their major SPX, other strains also contain minor constituents, which rarely have been characterized in detail.

The increasing knowledge on the distribution and structural diversity of SPX were based on different structural characterization techniques used to identify the novel SPX. Nuclear magnetic resonance (NMR), which is the only technique for unambiguous structural elucidation of novel compounds, have been widely used in SPX structural elucidation (Hu *et al.*, 1995; 2001; Sleno *et al.*, 2004a; Aasen *et al.*, 2005; MacKinnon *et al.*, 2006; Ciminiello *et al.*, 2007; 2010; Roach *et al.*, 2009; Zurhelle *et al.*, 2018). This method is a non-destructive technique and gives absolute structural configuration; yet high amounts of pure compound are required. As described in **Chapter 3**, growth conditions of the *A. ostenfeldii* strains and the purification procedures play a crucial role in producing

**Table 4.1** Structurally elucidated spirolides from *Alexandrium ostenfeldii* and their corresponding mass transition.

Spirolide	R <sub>1</sub>	R <sub>2</sub>	R <sub>3</sub>	R <sub>4</sub>	R <sub>5</sub>	R <sub>6</sub>	$\Delta^{C2,3}$	Mass transition	Structure	
A	H	CH <sub>3</sub>	CH <sub>3</sub>	H	H	OH	+	692 > 150		
B	H	CH <sub>3</sub>	CH <sub>3</sub>	H	H	OH	-	694 > 150		
C	CH <sub>3</sub>	CH <sub>3</sub>	CH <sub>3</sub>	H	H	OH	+	706 > 164		
13-desMethyl C	CH <sub>3</sub>	H	CH <sub>3</sub>	H	H	OH	+	692 > 164		
13,19-didesMethyl C	CH <sub>3</sub>	H	H	H	H	OH	+	678 > 164		
20-Hydroxy-13,19-didesMethyl C	CH <sub>3</sub>	H	H	OH	H	OH	+	694 > 164		
27-Hydroxy-13-desMethyl C	CH <sub>3</sub>	H	CH <sub>3</sub>	H	OH	OH	+	708 > 180		
27-Hydroxy-13,19-didesMethyl C	CH <sub>3</sub>	H	H	H	OH	OH	+	694 > 180		
27-Oxo-13,19-didesMethyl C	CH <sub>3</sub>	H	H	H	O	OH	+	692 > 178		
D	CH <sub>3</sub>	CH <sub>3</sub>	CH <sub>3</sub>	H	H	OH	-	708 > 164		
13-desMethyl D	CH <sub>3</sub>	H	CH <sub>3</sub>	H	H	OH	-	694 > 164		
20-Hydroxy-13,19-didesMethyl D	CH <sub>3</sub>	H	H	OH	H	OH	-	696 > 164		
G	CH <sub>3</sub>	H	H	H	H	H	+	692 > 164		
20-Methyl G	CH	H	CH <sub>3</sub>	H	H	H	+	706 > 164		
H	CH <sub>3</sub>	H	CH <sub>3</sub>	H	H	OH	+	650 > 164		
I	CH <sub>3</sub>	H	CH <sub>3</sub>	H	H	OH	-	652 > 164		

pure toxins. Considering that marine toxins, including spirolides, are usually produced at  $\text{pg cell}^{-1}$  levels, extensive biomass production and toxin isolation efforts are needed to obtain samples suitable for NMR (Dell'Aversano and Tartaglione, 2017). As the requirement of relatively high amounts of pure toxins poses a severe limitation in many cases, alternative methods such as tandem mass spectrometry coupled to liquid chromatography (LC-MS/MS) have also been applied for structural characterization. LC-MS/MS, as a complementary technique, can provide partial structural information and requires only several orders of magnitude lower amounts of samples relative to NMR. LC-tandem high-resolution mass spectrometry (LC-HRMS/MS) has successfully complemented low resolution MS in the screening for unknown phycotoxins as well as in the characterization of structural information when the toxin concentration is too low for NMR analysis (Zendong *et al.*, 2015).

Structural analyses based on mass spectral techniques require at least one compound, for which has the absolute structural configuration (from NMR) and a defined fragmentation pattern (from LC-MS/MS) is available. The structural characterization of unknown compounds is conducted by comparing the fragmentation pattern of the unknown compound with that of a related compound with known structures (Figure 4.1).

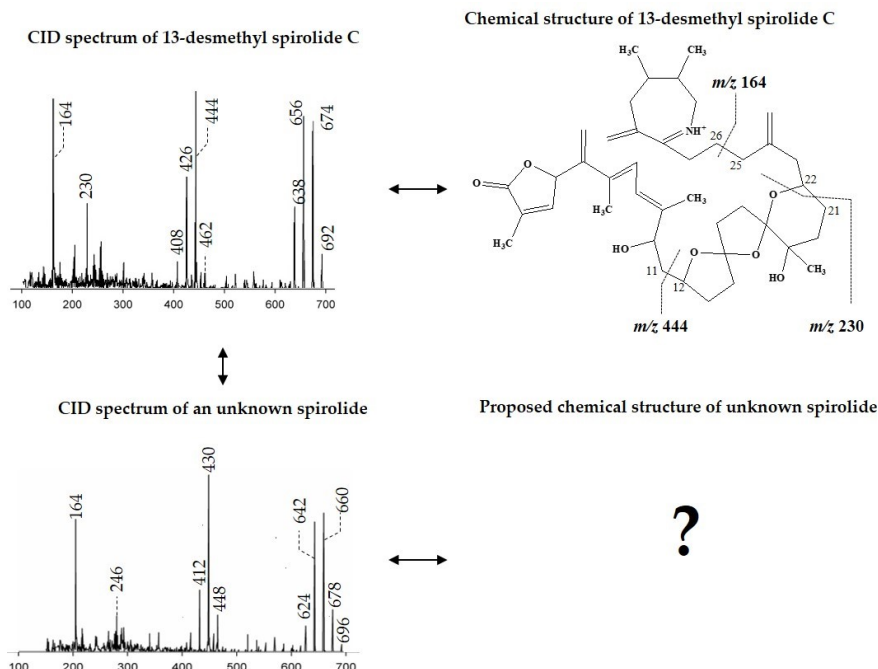


**Figure 4.1.** Mass spectrometry-based structural characterization of unknown compounds. Structural insights of unknown compounds are obtained by comparing its fragmentation pattern to known compounds. Similarity in fragments infer that the structural configuration corresponding to the fragment is likely conserved in both known and unknown compounds. Difference in fragments implies a structural modification (e.g., change or loss of a functional group) in the unknown compound. The proposed structural configuration pertains to the difference and similarity of fragmentation patterns between the known and unknown compounds.

The structural information depends on the fragmentation of the compounds, thus, only partial structural insights including several options can be deduced within a certain fragment. Although the absolute structural configuration cannot be deduced from LC–MS/MS in most cases, the probability of the structural proposals is increased with the application of LC–HRMS/MS. This technique distinguishes compounds with same nominal mass based from the chemical formula predicted from the exact mass. For example,  $-\text{CH}_4$  and an oxygen atom (O), both have a nominal mass of 16 Daltons (Da). The exact masses for  $-\text{CH}_4$  and O from LC–HRMS/MS measurements are 16.0312 and 15.9949, respectively. As such, combined mass spectral techniques provide an excellent alternative for the structural characterization of novel phycotoxins.

Much of our knowledge on the structural variability of phycotoxins is based on mass spectral data (Aasen *et al.*, 2005; Zendong *et al.*, 2015; Martens *et al.*, 2017; Krock *et al.*, 2017). Examples in the case of SPX were the description of SPX variability among *A. ostenfeldii* strains as well as structural characterization were acquired through mass spectrometry being conducted from strains isolated from Canada (Sleno *et al.*, 2004a), the Netherlands (Van de Waal *et al.*, 2015) and Argentina (Guinder *et al.*, 2018). With the increased application of mass spectral based detection and identification methods in phycotoxins, this study aimed to use mass spectrometry methods in describing the SPX variability of *A. ostenfeldii* strains isolated from recent surveys in the Netherlands, Greenland and Norway.

## 4.2. Materials and Methods

### 4.2.1 Culture Conditions and Cell Harvest

The *Alexandrium ostenfeldii* strains analyzed in this study were collected in the Netherlands, Greenland and Norway. The clonal strains AON 24 from the Netherlands was collected in the Rhine–Meuse–Scheldt Delta, the Netherlands (51.73°N, 4.72°E), while MX-S-B11 and NX-56-10 were collected in Disko Bay, Greenland (69.03°N, 52.04°W) and Trondheim Fjord, Norway (63.52°N, 10.28°E), respectively (Figure 4.2). Strains MX-S-B11 and NX-56-10 were morphologically identified by plate pattern analysis using epifluorescence microscopy, and species identification was confirmed by rDNA large–subunit (LSU) sequence comparison (Tillmann, unpublished), and strain AON 24 was identified by microsatellite genotyping (Trautmann *et al.*, 2017) of loci published in Nagai *et al.* (2015). *A. ostenfeldii* strains were grown in 70 mL plastic culture flasks with filtered K medium (Keller, 1987) adjusted to pH 8 at salinity 30 (MX-S-B11 and NX-56-10) or 10 (AON 24) and were kept under a 16:8 light–dark cycle at 15 °C with 50  $\mu\text{mol m}^{-2} \text{s}^{-1}$  photon flux density. Cell density and



cell pellet preparation was conducted similar to the methods described in Section 3.2.1 and 3.2.2a, respectively.

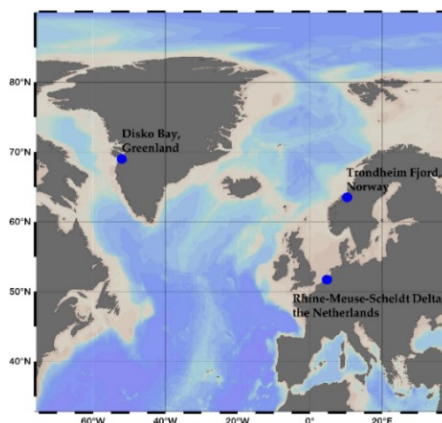


**Figure 4.2.** Sampling locations of the *Alexandrium ostenfeldii* strains used in this study

#### 4.2.2. Spirolide Extraction

Spirolide extraction was carried according to the method described in **Chapter 3**, Section 3.2.2.1.

#### 4.2.3. Parameters of Liquid Chromatography-Tandem Mass Spectrometry (LC-MS/MS)

A triple-quadrupole mass spectrometer (API 4000 Q Trap, Sciex, Darmstadt, Germany) with a Turbo V ion source coupled to a 1100 LC liquid chromatograph (Agilent, Waldbronn, Germany) was used in the detection of novel spirolides.

##### 4.2.3.1 Liquid Chromatography (LC)

The LC component parameters were the same as **Chapter 3**, Section 3.2.2.2.

##### 4.2.3.2. Scan Modes in Tandem Mass Spectrometry (MS/MS)

Different tandem mass spectrometry (MS/MS) scan modes were used in this study: Selected reaction monitoring (SRM), precursor ion scan and enhanced product ion (EPI) scan. SRM is a highly selective quantitative target analyte scan but requires prior information of the precursor and product ions of the compound of interest (Figure 4.3). In SRM, the precursor ion was selected in the first quadrupole (Q1), fragmented in the collision cell by collision-induced dissociation (CID) and the product ion was selected in the third quadrupole (Q3) for detection. The following mass spectrometric parameters were applied in SRM: Curtain gas: 20 psi, CAD (collision activated dissociation) gas: Medium, ion-spray voltage: 5500 V, temperature: 650 °C, nebulizer gas: 40 psi,

auxiliary gas: 70 psi, interface heater: On, declustering potential: 121 V, entrance potential: 10 V, exit potential: 22 V.

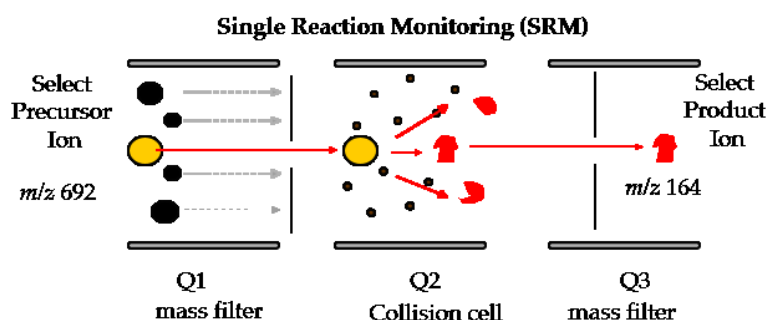


Figure 4.3. Triple quadrupole set-ups under single reaction monitoring mode.

In order to identify novel compounds, samples were subjected to precursor ion scan of  $m/z$  164, which is characteristic to spiroptides (Figure 4.4). Precursor ions were scanned in Q1 with a mass range set at 500-800 Da, fragmented in the collision cell and the product ion,  $m/z$  164, was selected in Q3. The following mass spectrometric parameters were applied in the precursor ion scan: Curtain gas: 20 psi, CAD (collision activated dissociation) gas: High, ion-spray voltage: 5500 V, temperature: 650 °C, nebulizer gas: 40 psi, auxiliary gas: 70 psi, interface heater: On, declustering potential: 121 V.

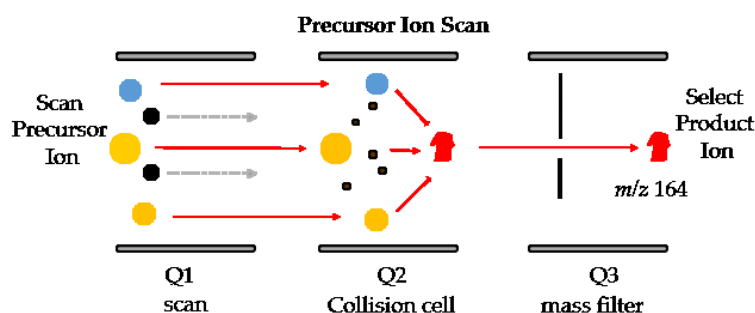


Figure 4.4. Triple quadrupole set-ups under precursor ion scan mode.

Finally, the compounds that were identified as potential spiroptides in the precursor ion scan were subjected to enhanced product ion (EPI) scan to obtain CID spectra (Figure 4.5). In the EPI scan, the precursor ion or the pseudo-molecular ion ( $[M + H]^+$ ) was scanned in Q1 and fragmented in Q2. As the fragmented ions exit from Q2, they enter in Q3 that accumulates the fragment ions by subjecting them to a highly sensitive ion trap mass scan. The following mass spectrometric parameters were applied in EPI: Curtain gas: 20 psi, CAD (collision activated dissociation) gas: High, ion-spray voltage: 5500 V, temperature: 650 °C, nebulizer gas: 40 psi, auxiliary gas: 70 psi, interface heater: On, declustering potential: 121 V, entrance potential: 10 V, exit potential: 22 V.

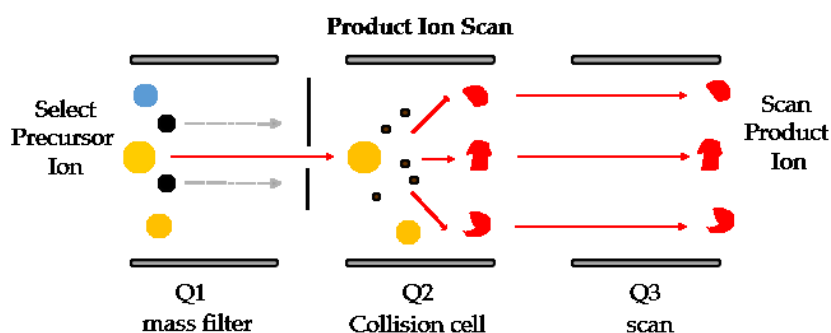


Figure 4.5. Triple quadrupole set-ups under product ion mode.

#### 4.2.4. Analyses of Spirolides by High Resolution Tandem Mass Spectrometry (HR-MS/MS)

High-resolution mass measurement and fragmentation spectra of novel spirolides were gathered using UHPLC system coupled to a hybrid quadrupole mass spectrometer (Vanquish UHPLC, Q Exactive Plus HR-MS, both Thermo Fisher Scientific, Schwerte, Germany) with a heated electrospray ionization source. Separation was performed on a C18 column (C18 BEH, 100 × 2 mm, 1.7 μm particle size, ACQUITY (Waters, Eschborn, Germany) equipped with guard column) with a column oven set to 32 °C. Samples were eluted using solvent A (H<sub>2</sub>O + 10 mM ammonium formate and 0.1% formic acid) and solvent B (ACN + 10 mM ammonium formate and 0.1% formic acid), which followed a stepwise gradient of A:B (90:10) to 100% B at a flow rate of 0.55 mL min<sup>-1</sup>. In addition, the elution of the first 0.6 min of each run were discarded to waste to minimize the presence of salt deposits. All measurements were performed with the capillary temperature set to 266 °C, the auxiliary gas heater to 400 °C, the spray voltage of 3.5 kV, the sheath gas flow of 51 and the auxiliary gas rate of 18. Positive Ion Calibration Solution (Pierce, Thermo Fisher) was used for the calibration of the instrument.

Assignment of elemental formulas were done from HRMS/MS spectra acquired in data independent acquisition (DIA) mode. DIA spectra were acquired with a resolution (RES) of 280000 FWHM ( $m/z$  200), automatic gain control (AGC) of  $5 \times 10^5$ , isolation range of 1.0–3.0  $m/z$  and normalized collision energy of 30 utilizing an inclusion list ( $m/z$  666.44, 670.44, 678.44, 694.47, 696.48, 708.48, 720.48, 722.50 and 738.46). The exact mass of the pseudo-molecular ion of compound 9 ( $m/z$  708) was taken from a full scan (RES = 280000 ( $m/z$  200), AGC =  $2 \times 10^5$ , MaxIT = 50, SR =  $m/z$  6500 to 750). Analytes with >3 point per peak were successfully detected in all experiments. The assignment for the molecular formulas of the  $[M + H]^+$  ions were set within the acceptable mass tolerance range of the instrument's error (<1ppm). After the application of the nitrogen rule as well as some general considerations (e.g., molecular formula or carbon number of the daughter ions in comparison to the

formula of the pseudo-molecular ion), generally only one theoretical elemental formula (C, H, O, N atoms only) corresponded to the measured  $m/z$  within 1 ppm.

### 4.3 Results and Discussion

#### 4.3.1. Interpretation of Collision-Induced Dissociation (CID) Spectra

In CID spectra, the pseudo-molecular ion ( $[M + H]^+$ ) of the compound in the CID spectrum is typically described as the peak with the highest mass-to-charge ( $m/z$ ) ratio. In the case of 13-desmethyl spiroside C (SPX 1), this is the pseudo-molecular ion  $m/z$ , 692 (Figure 4.6A), which represented the unfragmented form of the compound (Figure 4.7).

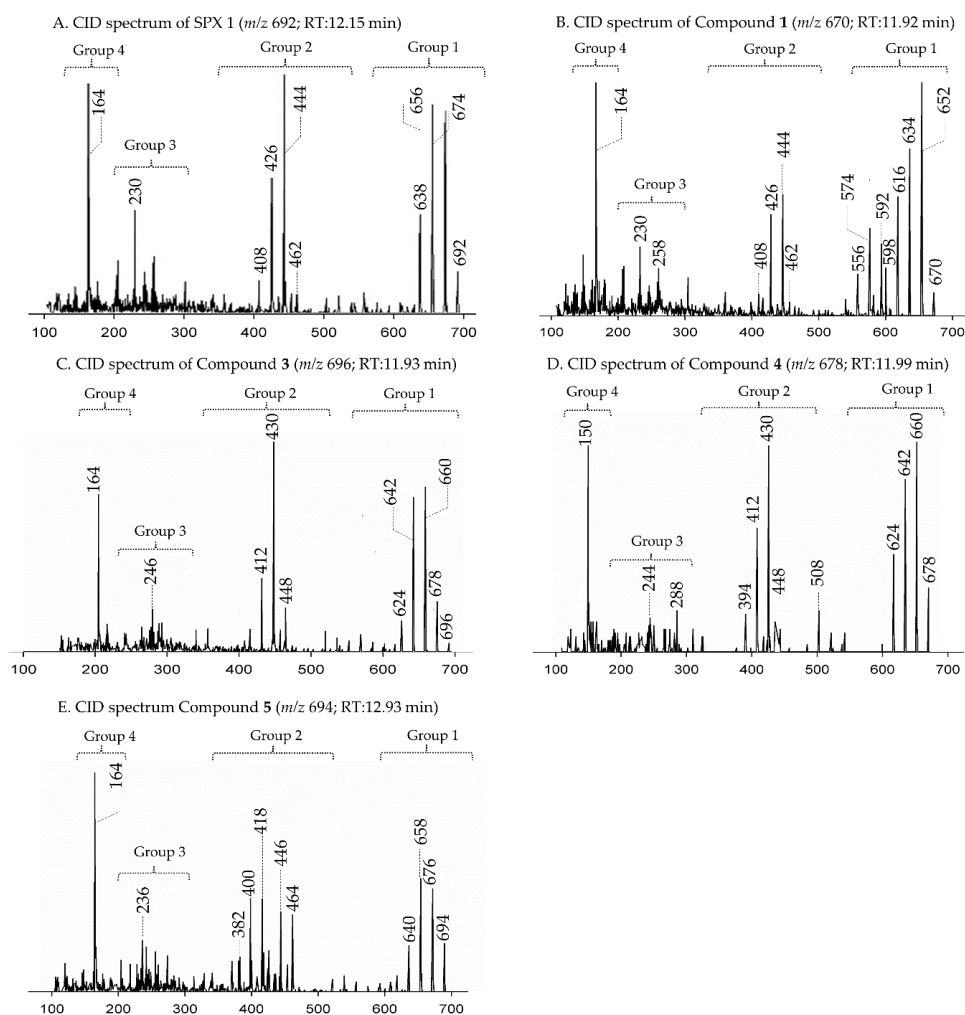


**Figure 4.6.** Collision-induced (CID) spectra of novel spiroside (SPX) detected in *A. ostensfeldii* strains related to C-type spiroside: (A) SPX 1; (B) Compound 1; (C) Compound 3; (D) Compound 4; and (E) Compound 5.

As the pseudo-molecular ion is fragmented in the collision cell, stable products including charged and neutral species are formed after the cleavage of the weakest bonds (McLafferty, 1993). For compounds that possess a cyclohexenyl moiety, the fragmentation is preceded by the opening of the macrocyclic system through retro-Diels-Alder (RDA) reaction, which converts the macrocyclic molecule into its linear form (Sleno *et al.*, 2004b). As shown in SPX 1, the fragment cluster produced by a RDA reaction and subsequent water losses, which are typically observed in polyether compounds such as SPX, is named group 1 cluster (Sleno *et al.*, 2004b). The fragment cluster caused by the fragmentation at C11-C12 (and subsequent water losses) is named group 2 cluster (e.g.,  $m/z$  444 in SPX 1, Figure 4.7).

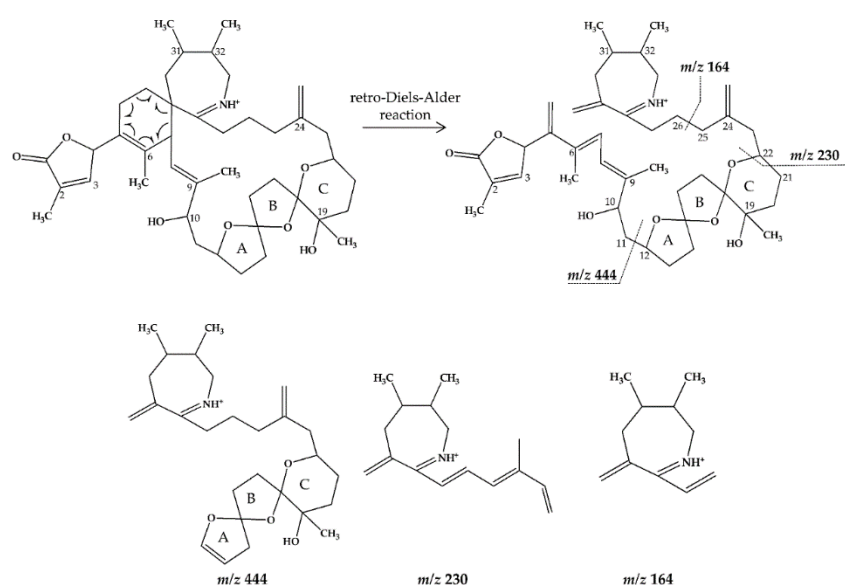


**Figure 4.7.** Chemical structure and fragmentation pattern of SPX 1 (modified from Sleno *et al.*, 2004b). Dashed lines indicate the cleavage sites resulting in the corresponding fragments.

Corresponding to the formation of the charged fragment  $m/z$  444, a neutral loss (NL) of many C-type SPX that have a 5:5:6 (ring A, B, C, respectively) trispiroketal ring system occurs. A rather rare fragmentation can often be observed for SPX involving the C11-C12 cleavage. In SPX 1, a fragment is formed with  $m/z$  462 at a lower intensity than  $m/z$  444 (difference of  $H_2O$ ). This fragment is most likely formed by the protonation of the ether oxygen stabilized by the neighboring hydroxyl group and subsequent charge mediated fragmentation of the C11/12 bond (OH transfer from C10 to C12 and C11/12 cleavage) (Hu *et al.*, 1995). Equivalent fragments were also observed for other SPX with a C10 hydroxyl group ( $m/z$  464, Zurhelle *et al.*, 2018). SPX G, which is isobaric with SPX 1 (same molecular mass), in contrast displays a different fragmentation pattern. The most abundant fragments of this compound ( $m/z$  378, 334 and 332) result from the C16–C17 cleavage of its second ketal (6-membered) ring B (Aasen *et al.*, 2005). Interestingly, no C11/12 cleavage is observed in either

SPX G or 20 Me SPX G, which are the only known SPX with no hydroxyl group at C10. This suggests that the C10 hydroxyl group is required for the C11/12 cleavage as well as the  $m/z$  462 formation. The smallest high abundant fragment of SPX usually is  $m/z$  164 (group 4), consisting of the cycloimine ring (Figure 4.7), but can be shifted to  $m/z$  150 (Hu *et al.*, 2001) or 180 (Sleno *et al.*, 2004a; Ciminiello *et al.*, 2010, Figures 4.6 and 4.8) depending on the degree of methylation or hydroxylation or both.

In this study, SPX with known structures, SPX 1 and a methyl analogue of SPX G, 20-methyl spiroside G (20-Me SPX G), with their CID spectra (Figures 4.6A and 4.8A, respectively) and fragmentation pattern (Figures 4.7 and 4.9, respectively), were used to deduce structural characteristics of the novel spiroside.

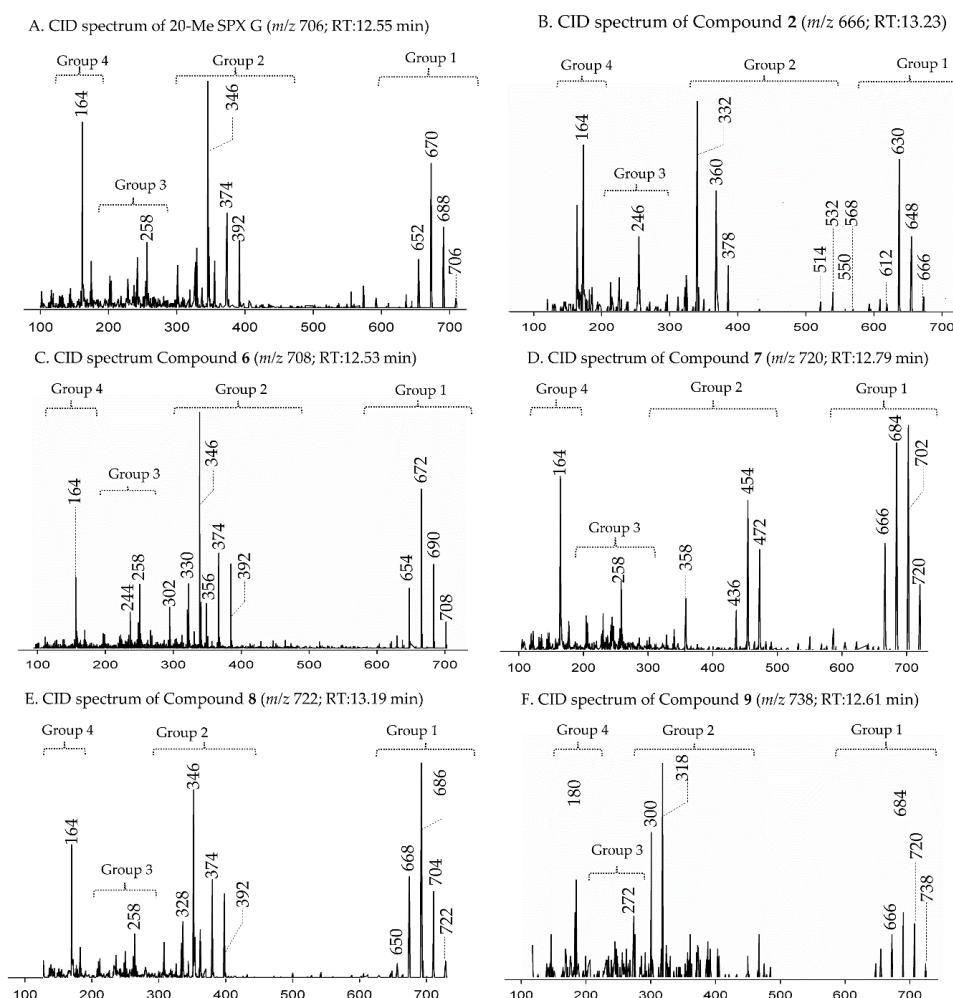


**Figure 4.8.** Collision-induced (CID) spectra of novel SPX detected in *A. ostensfeldii* strains related to G-type spiroside: (A) 20-Me SPX G; (B) Compound 2; (C) Compound 6; (D) Compound 7; (E) Compound 8; and (F) Compound 9.

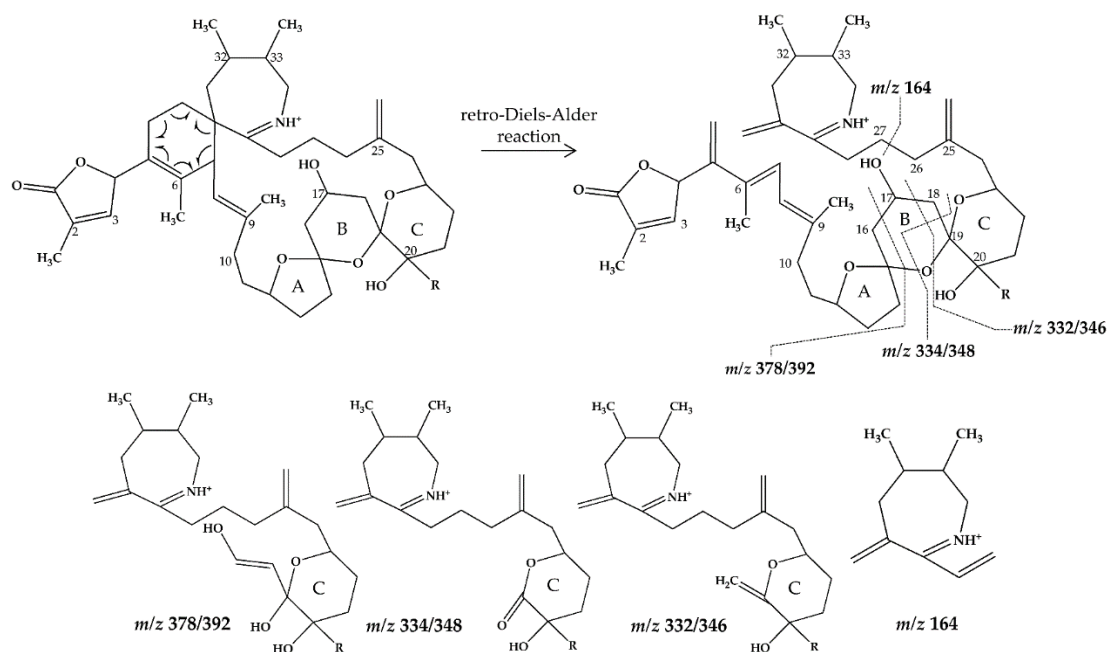


**Figure 4.9.** Chemical structure and fragmentation pattern of spirolide G (R=H) and 20-methyl spirolide G (R=CH<sub>3</sub>) (modified from Aasen *et al.*, 2005). Dashed lines indicate the cleavage sites resulting in the corresponding fragments.

#### 4.3.2. Characterization of Novel Spirolides

From the selected reaction monitoring (SRM) scans, the *A. ostensfeldii* strains isolated from the Netherlands, Greenland and Norway collectively revealed nine novel spirolides, which possessed the same masses as previously known spirolides but eluted at different retention times. The pseudo-molecular ions of these unknown spirolides were  $m/z$  666 (2),  $m/z$  696 (3),  $m/z$  678 (4),  $m/z$  694 (5),  $m/z$  708 (6),  $m/z$  720 (7),  $m/z$  722 (8) and  $m/z$  738 (9). In addition, another spirolide with pseudo-molecular ion  $m/z$  670 (1) was identified by precursor ion scans of the characteristic spirolide fragment at  $m/z$  164. The accurate masses of the pseudo-molecular ions and the elemental formula of compounds 1–9 were obtained by HR-MS measurements (Tables 4.2–4.4).

##### 4.3.2.1. Compound 1

Strain AON 24, originally isolated from North Sea water of the coast of the Netherlands, predominantly produced SPX 1 (Table 4.5). We also detected an unknown compound with a CID spectrum inferring an SPX (Figure 4.6B). Compound 1 had an accurate mass of 670.4678 (C<sub>40</sub>H<sub>64</sub>NO<sub>7</sub><sup>+</sup>, Tables 4.2 and S2), a difference of 22 Da (–C<sub>2</sub> and +H<sub>2</sub>) in comparison to 13 methyl SPX C (C<sub>42</sub>H<sub>62</sub>NO<sub>7</sub><sup>+</sup>).

**Table 4.2.** Measured and calculated accurate masses of the key product ions of compounds **1** from AON 24 and NX-56-10 obtained by HR-MS.

Strain	Compound	Elemental Formula	Measured	Calculated	$\Delta/\text{ppm}$
AON 24 (the Netherlands)	<b>1</b> (670 > 164)	C <sub>40</sub> H <sub>64</sub> NO <sub>7</sub> <sup>+</sup>	670.4678	670.4677	0.07
		C <sub>38</sub> H <sub>58</sub> NO <sub>4</sub> <sup>+</sup>	592.4363	592.4360	0.51
		C <sub>27</sub> H <sub>44</sub> NO <sub>5</sub> <sup>+</sup>	462.3219	462.3214	1.01
		C <sub>27</sub> H <sub>42</sub> NO <sub>4</sub> <sup>+</sup>	444.3111	444.3108	0.66
		C <sub>18</sub> H <sub>28</sub> N <sup>+</sup>	258.2217	258.2216	0.21
		C <sub>16</sub> H <sub>24</sub> N <sup>+</sup>	230.1904	230.1903	0.32
		C <sub>11</sub> H <sub>18</sub> N <sup>+</sup>	164.1435	164.1434	0.81
NX-56-10 (Norway)	<b>2</b> (666 > 164)	C <sub>40</sub> H <sub>60</sub> NO <sub>7</sub> <sup>+</sup>	666.4365	666.4364	0.14
		C <sub>35</sub> H <sub>50</sub> NO <sub>3</sub> <sup>+</sup>	532.3787	532.3785	0.38
		C <sub>22</sub> H <sub>36</sub> NO <sub>4</sub> <sup>+</sup>	378.2640	378.2639	0.32
		C <sub>22</sub> H <sub>34</sub> NO <sub>3</sub> <sup>+</sup>	360.2533	360.2533	-0.07
		C <sub>21</sub> H <sub>34</sub> NO <sub>2</sub> <sup>+</sup>	332.2584	332.2584	-0.13
		C <sub>17</sub> H <sub>28</sub> N <sup>+</sup>	246.2216	246.2216	0.09
		C <sub>11</sub> H <sub>18</sub> N <sup>+</sup>	164.1435	164.1434	0.62
	<b>3</b> (696 > 164)	C <sub>41</sub> H <sub>62</sub> NO <sub>8</sub> <sup>+</sup>	696.4471	696.4470	0.13
		C <sub>38</sub> H <sub>54</sub> NO <sub>3</sub> <sup>+</sup>	572.4100	572.4098	0.37
		C <sub>26</sub> H <sub>42</sub> NO <sub>5</sub> <sup>+</sup>	448.3060	448.3057	0.56
		C <sub>26</sub> H <sub>40</sub> NO <sub>4</sub> <sup>+</sup>	430.2954	430.2952	0.52
		C <sub>17</sub> H <sub>28</sub> N <sup>+</sup>	246.2217	246.2216	0.34
		C <sub>11</sub> H <sub>18</sub> N <sup>+</sup>	164.1435	164.1434	0.90

The ring opening via RDA and the subsequent fragmentation of the pseudo-molecular ion produced fragments  $m/z$  462 (C<sub>27</sub>H<sub>42</sub>NO<sub>5</sub><sup>+</sup>), 444 (C<sub>27</sub>H<sub>42</sub>NO<sub>4</sub><sup>+</sup>),  $m/z$  230 (C<sub>16</sub>H<sub>24</sub>N<sup>+</sup>) and  $m/z$  164 (C<sub>11</sub>H<sub>18</sub>N<sup>+</sup>), which are also observed for SPX 1, indicating that **1** features an identical triketal ring system and a hydroxyl group at C10 (SPX 1 numeration). In contrast to SPX 1, a fragment was observed at  $m/z$  592 (C<sub>38</sub>H<sub>58</sub>NO<sub>4</sub><sup>+</sup>, Tables 4.2 and S2), produced by a neutral loss (NL) of 78 (C<sub>2</sub>H<sub>6</sub>O<sub>3</sub>) for **1**. Assuming a structure identical to SPX 1 starting from C10, this NL can only be explained by a simultaneous loss of water and fragmentation of the butenolide ring 'part' of the molecule (one possible fragmentation pathway is shown in Figure 4.10A). The proposed structure of **1** with a vicinal dihydroxypropyl substituent instead of the butenolide is consistent with the  $m/z$  592 fragment formation (Figures 4.10A and S10), as this fragment can be formed by a nucleophilic attack of one of the hydroxyl groups, which is not possible in the case of the butenolide side chain. Accordingly, the  $m/z$  592 fragment usually is not observed in SPX CID spectra. In summary, a structural proposal with a butenolide ring part altered in comparison to SPX 1, featuring a side chain with two hydroxyl groups is the most likely conclusion. However, this structural proposal is based on the assumption that there are no structural changes between C10 and C33 (C-numbering of SPX 1) in comparison to SPX 1 and needs unambiguous confirmation by NMR.



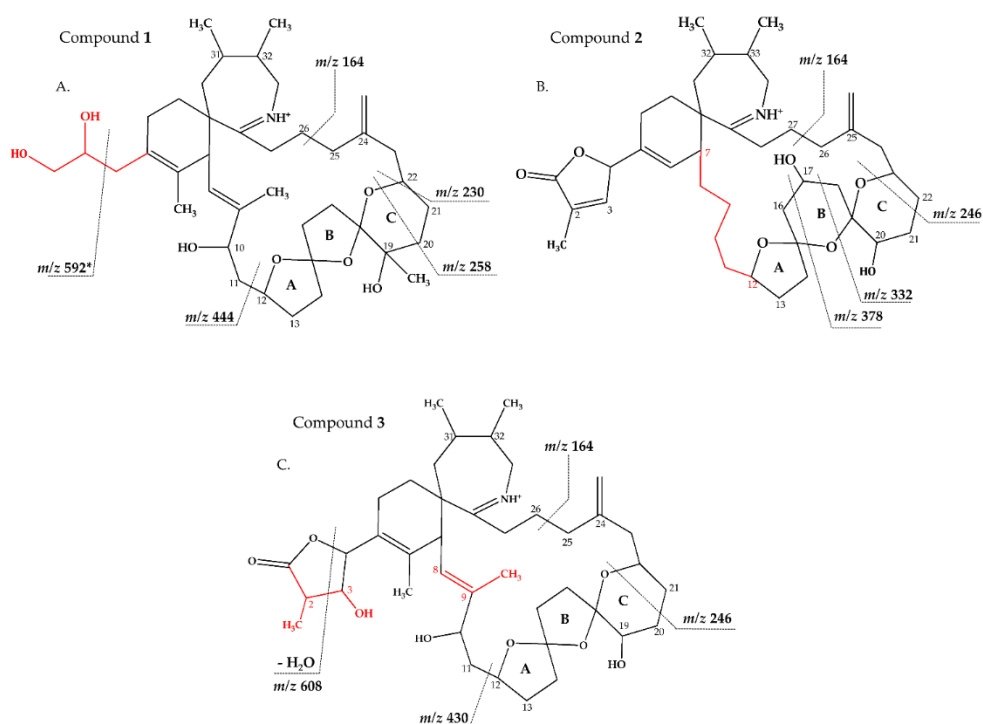


**Figure 4.10.** Proposed structures of compounds **1** (A) from AON 24 and compounds **2** (B) and **3** (C) from NX-56-10. Structural parts in red cannot unambiguously be assigned by mass spectrometry. Dashed lines indicate the cleavage sites resulting in the corresponding fragments. \*For more information about fragment  $m/z$  592, refer to Figure S10.

#### 4.3.2.2. Compound 2–3

Strain NX-56-10, originally isolated from Trondheim Fjord, Norway, produced SPX 1, 20-Methyl SPXG and trace amounts of SPX A, H and I (Table 4.5). Two unknown SPX were also detected in the CID spectra (**2** (Figure 4.8B) and **3** (Figure 4.6C)).

Compound **2** had an accurate mass of  $m/z$  666.4364 ( $C_{40}H_{60}NO_7^+$ , Tables 4.2 and S3). The CID spectrum indicated a G-type SPX for compound **2** (Figure 4.8B), characterized by group 2 ( $m/z$  378, 360, 342, 332) and group 3 ( $m/z$  246) that were similar to spirolide G (SPCX G). Group 4 ( $m/z$  164) cluster was identical to SPX G (Table S1) (Aasen *et al.*, 2005). The only difference between the SPX G and **2** were found in the group 1 cluster that is characterized by water losses of the parental molecule ( $m/z$  666 for **2**,  $m/z$  692 for SPX G). The structural difference between both compounds (26 Da,  $C_2H_2$ ) must be located between C1 and C16 (SPX G numeration). However, the low abundant fragment cluster  $m/z$  568, 550, 532, 514 (NL 98 Da, Figure 4.8B and Tables 4.2 and S3) that can be explained by the cleavage of the butenolide ring followed by several water losses indicates the presence of the butenolide side chain in **2** that is typical for SPX. The presence of the butenolide ring, however, further narrows down the location of structural differences between SPX G and **2** to C5–C11. As the

elemental difference of C<sub>2</sub>H<sub>2</sub> is impossible to explain by a single modification, several modifications must be present. The most likely assumption is the elimination of the methyl groups at C6 and C9 together with a hydration of a double bond. The only double bond that can be saturated without affecting the RDA macrocycle opening is between C5 and C6. In summary, a structural proposal of 8,9-dihydro-6,9-didesmethyl-SPX G is consistent with the recorded CID spectrum of **2** (Figure 4.10B). However, this structural proposal is preliminary and needs unambiguous confirmation by NMR.

Compound **3** is characterized by its accurate mass of  $m/z$  696.4471 (C<sub>41</sub>H<sub>62</sub>NO<sub>8</sub><sup>+</sup>, Tables 4.2 and S3). The pseudo-molecular ion of **3** (Figure 4.6C), showed a 4 Da (-C and +O) upshift in comparison to SPX 1 (C<sub>42</sub>H<sub>62</sub>NO<sub>7</sub><sup>+</sup>, Figure 4.6A) or an addition of H<sub>2</sub>O in comparison to 13,19-desmethyl SPX C ( $m/z$  678). The group 2 fragments of **3** ( $m/z$  448, 430, 412; Figure 4.6C and Tables 3.2 and S3) resemble the group 2 fragments of 13,19-didesmethyl SPX C (Table S1, Christian *et al.*, 2008)) indicating that **3** and 13,19-didesmethyl SPX C share the structural element comprising C12 to C34. This is in agreement with the elemental composition of  $m/z$  430 (C<sub>26</sub>H<sub>40</sub>NO<sub>4</sub><sup>+</sup>) as also observed in the CID spectrum of 13,19-didesmethyl SPX C (MacKinnon *et al.*, 2006). Fragment  $m/z$  246 (C<sub>17</sub>H<sub>28</sub>N<sub>7</sub><sup>+</sup>, Table 4.2) was also observed, indicating no oxygenation in the part of the molecule from C21 to C34 (SPX 1 numeration). The low abundant, but characteristic fragment cluster  $m/z$  608, 590, 572 (Tables 4.2 and S3) can be explained by a C2-C3 cleavage of the butenolide side chain followed by water losses. This cleavage usually is not observed in SPX, but we propose a 3-hydroxylation, which may cause a destabilization of the butenolide ring and thus explain the characteristic fragmentation by a formation of the  $m/z$  608, 590, 572 cluster (Table S3). In summary, the addition of H<sub>2</sub>O is only possible by the saturation of either double bond C2-C3 or C8-C9 or a hydroxylation of the methyl groups at C8 or C9. A structural proposal of 2-hydro-3-hydroxy-13,19-didesmethyl SPX C is consistent with the CID spectrum of **3** (Figure 4.10C), but the above-mentioned isoforms cannot be ruled out by mass spectrometry.

#### 4.3.2.3. Compounds 4–9

Strain MX-S-B11, originally isolated from Disko Bay, West Greenland, produced 20-Methyl SPXG, SPX H and I as well as trace amounts of SPX 1 and SPX C (Table 4.5). Six unknown SPX were also detected in the CID spectra (**4–9** (Figures 4.6D, 4.6E and 4.8C–F)).

Compound **4** had an accurate mass of  $m/z$  678.4363 ( $C_{41}H_{60}NO_7^+$ , Tables 4.3 and S4). This sum formula is identical to 13,19-desmethyl SPX C [37]. The group 2 cluster of **4** ( $m/z$  448, 430, 412, 394, Figure 3.6D and Tables 4.3 and S4) was also identical with **3** (Table S3) and 13,19-desmethyl SPX C (Table S1). However, we observed  $m/z$  150 ( $C_{10}H_{16}N^+$ ) as the most abundant group 4 ion, which indicated a 14 Da downshift ( $-CH_2$ ) in comparison to **3** and 13,19-desmethyl SPX C ( $m/z$  164,  $C_{11}H_{18}N^+$ ). The  $m/z$  150 fragment can also be observed for SPX A (=31-desmethyl SPX C) (Table S1, Hu *et al.*, 2001) which shows no C31 methylation. A structural configuration with a methyl group at C19 (often observed in A-, B-, C- and D-type SPX) and no methyl group of C31 would be in agreement with the observed cluster **4** as well as **2**. In summary, the CID spectrum of **4** is consistent with 13-desmethyl SPX A (Figure 4.11A). Theoretically, another demethylation of C19 instead of C13 is also possible. However, 13-desmethyl variants are more common among SPX.

**Table 4.3.** Measured and calculated accurate masses of the key product ions of compounds **4–6** from MX-S-B11 obtained by HR-MS.

Strain	Compound	Elemental Formula	Measured	Calculated	$\Delta/ppm$
MX-S-B11 (Greenland)	<b>4</b> (678 > 150)	$C_{41}H_{60}NO_7^+$	678.4363	678.4364	-0.22
		$C_{26}H_{42}NO_5^+$	448.3059	448.3057	0.42
		$C_{26}H_{40}NO_4^+$	430.2953	430.2952	0.38
		$C_{17}H_{26}N^+$	244.2061	244.2060	0.32
		$C_{10}H_{16}N$	150.1278	150.1277	0.64
	<b>5</b> (694 > 164)	$C_{42}H_{64}NO_7^+$	694.4679	694.4677	0.24
		$C_{29}H_{48}NO_4^+$	474.3581	474.3578	0.65
		$C_{27}H_{46}NO_5^+$	464.3374	464.3370	0.76
		$C_{26}H_{44}NO_3^+$	418.3318	418.3316	0.59
		$C_{15}H_{26}NO^+$	236.2010	236.2009	0.35
		$C_{11}H_{18}N^+$	164.1435	164.1434	0.90
	<b>6</b> (708 > 164)	$C_{43}H_{66}NO_7^+$	708.4836 *	708.4834	1.06
		$C_{23}H_{38}NO_4^+$	392.2798	392.2795	0.56
		$C_{22}H_{36}NO_2^+$	346.2744	346.2741	0.85
		$C_{11}H_{18}N^+$	164.1439	164.1434	-0.08

\*  $m/z$  taken from full scan (see comment Figure S6).

Compound **5** is characterized by its accurate mass of  $m/z$  694.4679 with an inferred elemental formula of  $C_{42}H_{64}NO_7^+$  from HR-MS (Tables 4.3 and S4). The CID spectrum and HR-MS of **5** (Figure 4.6E) showed a fragmentation pattern more similar to C-type SPX than G-type SPX. The group 4 fragment ( $m/z$  164,  $C_{11}H_{18}N^+$ ) was observed in **5** and SPX 1 (Figure 4.6E and 4.6A, respectively), indicating an identical cyclic imine moiety and  $C_{26}$ - $C_{33}$  for **5** and SPX 1. Furthermore, the elemental composition of **5** ( $C_{42}H_{64}NO_7^+$ ) and SPX 1 ( $C_{42}H_{62}NO_7^+$ ) differed by only two hydrogen atoms. The same was the case for the group 2 fragments  $C_{42}H_{64}NO_7^+$  464 and 462, respectively, indicating a

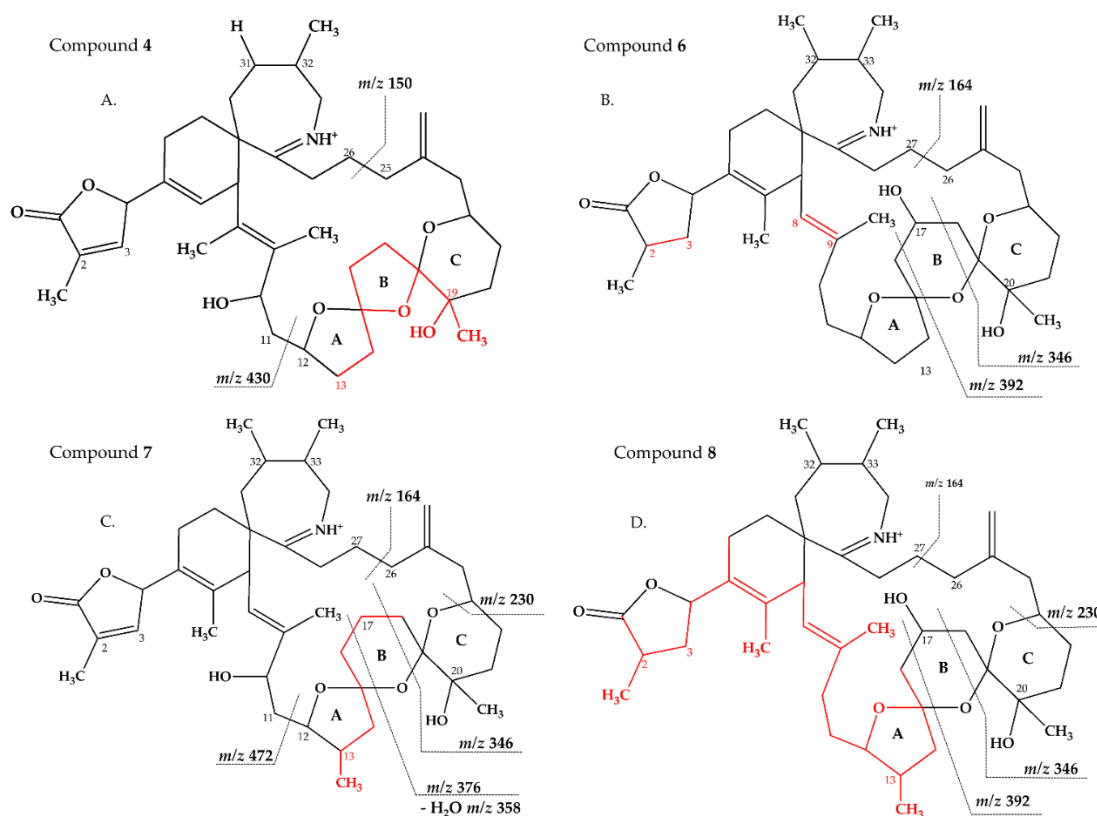


**Figure 4.11.** Proposed structures of compounds 4 (A), 6 (B), 7 (C) and 8 (D) from MX-S-B11. Structural parts marked in red cannot unambiguously be assigned by mass spectrometry. Dashed lines indicate the cleavage sites resulting in the corresponding fragments.

common neutral loss of 230 Da ( $C_{15}H_{18}O_3$ ) and a conserved structural element of C1–C11 between 5 and SPX 1. Interestingly, unusual ion clusters were observed in group 2 and 3 fragments of 5. The group 2 cluster showed an additional fragment  $m/z$  418 ( $C_{26}H_{44}NO_3^+$ ) with two corresponding water losses ( $m/z$  400 and 382). Fragment  $m/z$  418 (Tables 4.3 and S4) has not been observed in SPX yet, but could result from the ring opening of ring A (C12–C15) of a putative 5:5:6 ketal ring configuration (Figure 4.12A). However, an opening of ring A of SPX has not been observed, which suggests a structural difference of the ring A region among all known SPX and 5. A possible explanation of fragment  $m/z$  418 would be a structure that has a 6:5:6 ketal ring configuration (Figure 4.12C). This hypothesis is supported by the fact that the structurally related pinnatoxins, also with a 6:5:6 triketal ring configuration, in fact show an opening of ring A (Figure 4.12C).

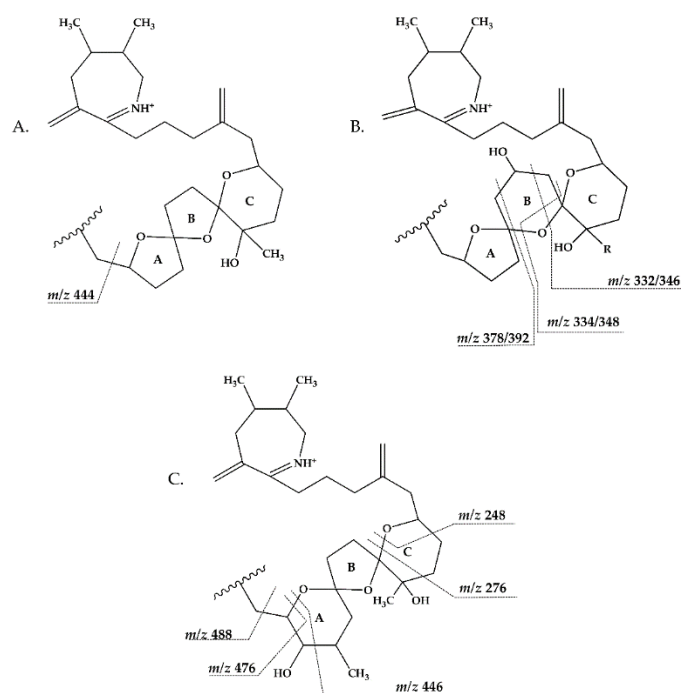


**Figure 4.12.** Triketal ring system of **A**: C-type spiroolides (modified from Sleno *et al.*, 2004b) **B**: G-type spiroolides (modified from Aasen *et al.*, 2005); and **C**: Pinnatoxin E/F (modified from Selwood *et al.*, 2010). Dashed lines indicate the cleavage sites resulting in the corresponding fragments.

The opening of the six-membered ketal ring A produces fragments  $m/z$  446 and 476 for both pinnatoxin E and F (Selwood *et al.*, 2010). Another characteristic feature in the group 2 fragments is the presence of a high intensity peak at  $m/z$  464 (Tables 4.3 and S4), which corresponds to the above-mentioned NL of 230 ( $C_{15}H_{18}O_2$ ). It is assumed to be the  $m/z$  462 equivalent of SPX 1. In contrast to **5**,  $m/z$  462 in SPX 1 [32] like in any other C-type spiroolides (Zurhelle *et al.*, 2018) shows a very low relative abundance, which might be explained by differing configuration of the adjacent ring. This is additional confirmation of the hypothesis that **5** might be composed by a 6:5:6 ring configuration. Another unusual fragment was also observed in group 3, at  $m/z$  236 ( $C_{15}H_{26}NO^+$ , Tables 4.3 and S4). This fragment could result from a structure with an addition of a hydroxyl group between C24–C26 and a missing methylene group likely at C25 (Figure 4.13) in comparison to SPX 1 (Figure 4.7), resulting in the difference of 6 Da ( $-C$  and  $+H_2O$ ) in comparison to the  $m/z$  230 ( $C_{16}H_{24}N^+$ ) fragment of SPX 1 (Figure 4.7). The position of the hydroxyl group at C28 can be ruled out for **5**; otherwise,  $m/z$  180 should be observed instead of  $m/z$  164 in group 4 [8,10]. The additional hydroxyl group at either C24–C26 also requires a missing hydroxyl group likely at C20 (Figure 4.13) in comparison to SPX 1 (Figure 4.7).

In summary, we suggest that **5** is a novel spiroide with a 6:5:6 triketal ring system, no methylene and hydroxyl group at C24 and C19 (C-numbering of SPX 1), respectively, and a hydroxyl group between C23–C25 (Figure 4.13). With the different combinations based from the unique fragments in **5**, it is not possible to propose a full structure with HR-MS data. An alternative structural proposal would include a G-type 5:6:6 ring configuration without a 17-hydroxylation. The absence of a hydroxylation might stabilize and this suppress a fragmentation of ring B (see Compound **7**) and thus explain the absence of the typical G-type fragments. An absence of a hydroxyl group at C10 requires a hydroxylation at a different site, namely of ring A to account for the observed fragments and elemental composition.

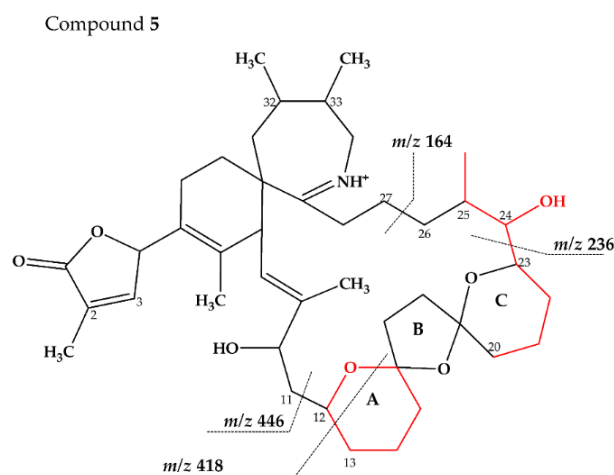


**Figure 4.13.** Proposed structure of compound **5** from MX-S-B11. Structural parts marked in red cannot unambiguously be assigned by mass spectrometry. Dashed lines indicate the cleavage sites resulting in the corresponding fragments.

Compound **6** had an accurate mass of  $m/z$  708.4836 ( $C_{43}H_{66}NO_7^+$ , Tables 4.3 and S4). The pseudo-molecular ion of **6** (Figure 4.8C), showed a 2 Da upshift ( $+H_2$ ) in comparison to 20-Me SPX G (Figure 4.8A), while group 2 cluster resulting from the cleavage of ring B ( $m/z$  392/346) was identical. The most likely conclusion is that the C2–C3 double bond in the butenolide ring is saturated in **6** (Figure 4.11B) in comparison to 20-Me SPX G, which also is the case in SPX of the B- and D-type. Alternatively, a saturation could also be located at C8–C9, which is less frequently observed in SPX.

Compound **7** had an accurate mass of  $m/z$  720.4836 ( $C_{44}H_{66}NO_7^+$ , Tables 4.4 and S4). Interestingly, **7** (Figure 4.8D) showed B-ring fragments ( $m/z$  376, 358, 346) but also fragments  $m/z$  490 and 472. Despite of an overall low intensity in the spectrum, the ratio between  $m/z$  490 and 272 was akin to the  $m/z$  462 to 444 of SPX 1. Fragment  $m/z$  462 in SPX 1 is most likely formed by the charge mediated fragmentation of the C11/12 bond (OH transfer from C10 to C12 and C11/12

cleavage) (Figure 4.7, Nielsen *et al.*, 2013). Both  $m/z$  444 as well as the less abundant  $m/z$  462 were only reported for 10-hydroxylated SPX and not for any known G-type SPX (Aasen *et al.*, 2005). The  $m/z$  490/472 (Tables 4.4 and S4) cluster of **7** could therefore be equivalent to the  $m/z$  462/444 cluster in SPX **1** (Table S1) and point towards a hydroxylation at C10. The fragments of the B-ring cluster showed one hydroxyl group less in comparison to 20-Me SPX **G** ( $m/z$  392, 346, Table S1) indicating no hydroxylation at C18 in **7**. A methyl group between C10 and C18 is also required to satisfy the sum formula, most likely at C13. Contrary to  $m/z$  462/444 in the SPX **1** spectrum,  $m/z$  490/470 were not most abundant daughter ions (next to  $m/z$  164 ion). Instead, the most abundant fragments were observed for the  $m/z$  376 cluster. We speculate that the fragmentation of the six-membered B-ring is favored over the hydroxyl attach and subsequent cleavage of the C11–C12 bond. However, this hypothesis needs further investigation as no previous G-type SPX with hydroxyl at C10 is known. In summary, a structure proposal similar to 20-Me SPX **G** but with a hydroxyl group at C10, no hydroxyl at C18 and methyl group at C13 (Figure 4.11C) would satisfy all observed fragmentation characteristics.

**Table 4.4.** Measured and calculated accurate masses of the key product ions of compounds **7–9** from MX-S-B11 obtained by HR-MS.

Strain	Compound	Elemental Formula	Measured	Calculated	$\Delta$ /ppm
MX-S-B11 (Greenland)	<b>7</b> (720 > 164)	C <sub>44</sub> H <sub>66</sub> NO <sub>7</sub> <sup>+</sup>	720.4836	720.4834	0.37
		C <sub>29</sub> H <sub>46</sub> NO <sub>5</sub> <sup>+</sup>	490.3530	490.3527	0.60
		C <sub>29</sub> H <sub>44</sub> NO <sub>4</sub> <sup>+</sup>	472.3425	472.3421	0.70
		C <sub>23</sub> H <sub>38</sub> NO <sub>3</sub> <sup>+</sup>	376.2849	376.2846	0.77
		C <sub>23</sub> H <sub>36</sub> NO <sub>2</sub> <sup>+</sup>	358.2741	358.2741	0.05
		C <sub>22</sub> H <sub>38</sub> NO <sub>2</sub> <sup>+</sup>	346.2743	346.2741	0.21
		C <sub>16</sub> H <sub>24</sub> N <sup>+</sup>	230.1905	230.1903	0.58
		C <sub>11</sub> H <sub>18</sub> N <sup>+</sup>	164.1435	164.1434	0.72
	<b>8</b> (722 > 164)	C <sub>44</sub> H <sub>68</sub> NO <sub>7</sub> <sup>+</sup>	722.4994	722.4990	0.50
		C <sub>23</sub> H <sub>38</sub> NO <sub>4</sub> <sup>+</sup>	392.2796	392.2795	0.17
		C <sub>23</sub> H <sub>36</sub> NO <sub>3</sub> <sup>+</sup>	374.2691	374.2690	0.28
		C <sub>22</sub> H <sub>38</sub> NO <sub>3</sub> <sup>+</sup>	364.2691	364.2846	-0.12
		C <sub>22</sub> H <sub>36</sub> NO <sub>2</sub> <sup>+</sup>	346.2741	346.2741	0.24
		C <sub>18</sub> H <sub>28</sub> N <sup>+</sup>	258.2217	258.2216	0.32
		C <sub>16</sub> H <sub>24</sub> N <sup>+</sup>	230.1904	230.1903	0.45
		C <sub>11</sub> H <sub>18</sub> N <sup>+</sup>	164.1435	164.1434	0.72
	<b>9</b> (738-180)	C <sub>43</sub> H <sub>64</sub> NO <sub>9</sub> <sup>+</sup>	738.4579	738.4576	0.44
		C <sub>23</sub> H <sub>38</sub> NO <sub>6</sub> <sup>+</sup>	424.2697	424.2694	0.68
		C <sub>22</sub> H <sub>36</sub> NO <sub>3</sub> <sup>+</sup>	362.2693	362.2690	0.79
		C <sub>20</sub> H <sub>32</sub> NO <sub>3</sub> <sup>+</sup>	336.2537	336.2533	1.10
		C <sub>20</sub> H <sub>32</sub> NO <sub>2</sub> <sup>+</sup>	318.2429	318.2428	0.42
C <sub>15</sub> H <sub>26</sub> NO <sup>+</sup>		236.2010	236.2009	0.67	
C <sub>11</sub> H <sub>18</sub> NO <sup>+</sup>		180.1384	180.1383	0.59	

Compound **8** had an accurate mass of  $m/z$  722.4994 ( $C_{44}H_{68}NO_7^+$ , Tables 4.4 and S4). The CID spectrum of **8** (Figure 4.8E) displayed an identical fragment pattern as 20-Me SPX G (Table S1) with the exception of an upshift of 16 Da ( $+CH_4$ ) in the group 1 fragments in **8**. The upshifted NL resulting from the cleavage between C16 and C17 ( $m/z$  314 in 20-Me SPX G,  $m/z$  330 in **8**) indicates a methyl group between C3 and C16 and a saturation at either C8-C9 or C2-C3 of **8**. In summary, the proposed structure of **8** is made up of a methyl analogue of 20-Me SPX G (Figure 4.11D).

Compound **9** had an accurate mass of  $m/z$  738.4579 ( $C_{43}H_{64}NO_9^+$ , Tables 4.4 and S4). The CID spectrum of **9** (Figure 4.8F) showed fragment  $m/z$  180 that is found in 27-hydroxy SPX analogues (Sleno *et al.*, 2004a; Ciminiello *et al.*, 2010) (corresponding to 28-hydroxy G-type SPX). At first sight, the intensities did neither resemble a G-type nor a C-type SPX fragmentation. However, low intensity fragments indicated a G-type spirolide with an upshift of 16 ( $O_2$ ) in the B-ring fragment ( $m/z$  424, Tables 4.4 and S4) indicating two more hydroxyl groups in comparison to 20-Me SPX G ( $m/z$  392, 346, Table S4). A fragment at  $m/z$  362 was also observed which could correspond to the B-ring cleavage after a loss of water elsewhere. In contrast to 20-Me SPX G, the most intense fragments of this cluster were observed for the additional loss of  $H_2O$  ( $m/z$  406, 362, Tables 4.4 and S4). A similar observation was made for the most abundant fragment ion ( $m/z$  318, Tables 4.4 and S4) of the spectrum, which indicated one loss of water from  $m/z$  336 ( $C_{20}H_{34}NO_3^+$ ). This study suggests that the unusually high abundance of this C-ring fragment is due to an additional hydroxyl group at C21, which destabilize the ring and favors the  $m/z$  336/318/300 over the B-ring cluster formation. In summary, the mass spectrum suggests a structure with two more hydroxyl groups between C21 and C28 in comparison to 20-Me SPX G, with one hydroxyl most likely at C28 and the other at C21 (Figure 4.14).

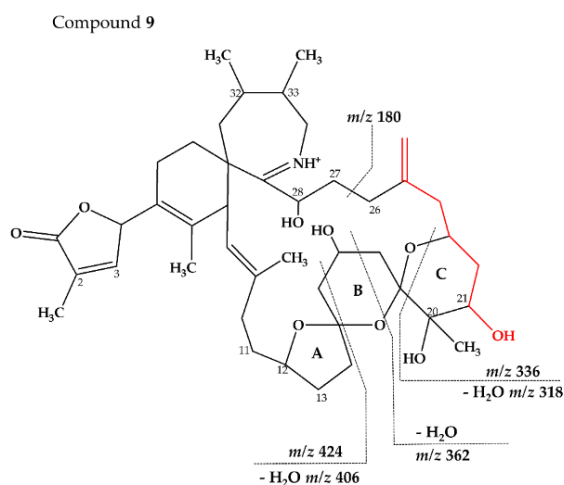


**Figure 4.14.** Proposed structures of compounds **9** from MX-S-B11. Structural parts marked in red cannot unambiguously be assigned by mass spectrometry. Dashed lines indicate the cleavage sites resulting in the corresponding fragments.



### 4.3. Structural Variability of Spirolides

This mass spectrometry-based study confirms previous studies which also indicate a high structural diversity of spirolide congeners produced by *Alexandrium ostenfeldii* (Hu *et al.*, 2001; Sleno *et al.*, 2004a; Ciminiello *et al.*, 2010; Aasen *et al.*, 2005; Roach *et al.*, 2009; Tillmann *et al.*, 2014; Van de Waal *et al.*, 2015; Guinder *et al.*, 2018). Moreover, this study provides first evidence for a new SPX subclass with a novel triketal ring system configuration. All other previously described SPX only differ in ring B configuration (five or six carbon atoms for C-type or G-type SPX, respectively) and have a similar configuration of their ring A and C (Van Wagoner *et al.*, 2014). The only reported exceptions are dispiroketal H/I-type SPX that do not have a ring C, but a 5:6 configuration, instead. Most SPX of this study belong to either C-type or G-type SPX with 5:5:6 and 5:6:6 triketal ring system configuration. However, mass spectral data of **5** suggest a six-membered ketal ring A (6:5:6 configuration). The postulated 6:5:6 triketal ring system of **5** was previously only observed in pinnatoxins, which otherwise feature a seven-membered ether ring instead of a butanolide side chain. Pinnatoxins and spirolides resemble each other in the last 2/3rds of the chain covering the ketal ring system (Figure 4.12) indicating that they may share common nascent polyketide chain in the biosynthesis of this part of the molecule (Van Wagoner *et al.*, 2014). While both toxins contain the same cyclic imine moiety (represented by *m/z* 164), they produce different fragmentation patterns and no compound with pinnatoxin-type fragmentation was detected in the present study nor is any reported in previous studies of *A. ostenfeldii*. Similarly, spirolides compounds are not detected in *Vulcanodinium rugosum* that produces pinnatoxins (Rhodes *et al.*, 2011). On the other hand, the remaining part of SPX including the butanolide side chain is identical to that of gymnodimines (Van Wagoner *et al.*, 2014), again suggesting that identical biosynthetic steps are involved in the synthesis of both compounds. Contrary to pinnatoxins, gymnodimines, initially identified in *Karenia selliformis* (Seki *et al.*, 1995), have not been reported to co-occur with spirolides in *A. ostenfeldii* (Van Wagoner *et al.*, 2014; Van de Waal *et al.*, 2015; Marten *et al.*, 2017).

Aside from the fundamental change in the triketal ring system, other proposed structural differences of compound **1–9** include the degree of saturation and number of attached methyl or hydroxyl groups. These structural differences can result from small differences in ketoreduction (KR), dehydration (DH) and enoyl reduction (ER). The presence of double bonds, for example, results from omitting the ER process, while the presence of hydroxyl group results from omission of the DH process.

SPX variability in *Alexandrium ostenfeldii* is obvious between different strains often having different SPX profiles (Hu *et al.*, 2001; Sleno *et al.*, 2004a; Ciminiello *et al.*, 2010; Aasen *et al.*, 2005; Roach *et al.*, 2009; Tillmann *et al.*, 2014; Van de Waal *et al.*, 2015; Guinder *et al.*, 2018). The toxin profile of a given strain is thought to be genetically fixed and, consistent with that, the relative spirolide composition of the strains studied here remained constant at least over a period of ten months in culture (data not shown). It is thus valid to discuss toxin profile differences among strains (Table 4.5).

**Table 4.5.** Cell quota and relative SPX content of *A. ostenfeldii* strains from the Netherlands (AON 24), Norway (NX-56-10) and Greenland (MX-S-B11). Nd refers to *not detected* and LOD refers to the *limit of detection*.

Spirolide	MX-S-B11 (Greenland)		NX-56-10 (Norway)		AON 24 (the Netherlands)		Ketal Ring System (A:B:C)
	Cell quota (fg cell <sup>-1</sup> )	Relative Content (%)	Cell quota (fg cell <sup>-1</sup> )	Relative Content (%)	Cell quota (fg cell <sup>-1</sup> )	Relative Content (%)	
<i>Known</i>							
13-desMethyl spirolide C	34.5	0.73	146.1	6.37	740.3	99.90	5:5:6
20-Methyl spirolide G	2086.4	44.41	5.1	0.22	0.4	0.05	5:6:6
Spirolide A	384.3	8.18	0.3	0.01	<LOD (0.06)	Nd	5:5:6
Spirolide C	33.9	0.72	0.1	0.01	0.1	0.02	5:5:6
13,19-didesMethyl spirolide C	<LOD (0.16)	Nd	2037.9	88.85	<LOD (0.06)	Nd	5:5:6
Spirolide H	257.3	5.48	0.4	0.02	<LOD (0.06)	Nd	5:6
Spirolide I	158.4	3.37	0.3	0.01	<LOD (0.06)	Nd	5:6
<i>Unknown</i>							
Compound 1	<LOD (0.16)	Nd	<LOD (0.07)	Nd	0.2	0.03	5:5:6
Compound 2	<LOD (0.16)	Nd	81.0	3.53	<LOD (0.06)	Nd	5:6:6
Compound 3	<LOD (0.16)	Nd	22.3	0.97	<LOD (0.06)	Nd	5:5:6
Compound 4	19.6	0.42	<LOD (0.07)	Nd	<LOD (0.06)	Nd	5:5:6
Compound 5	233.7	4.98	<LOD (0.07)	Nd	<LOD (0.06)	Nd	6:5:6
Compound 6	883.2	18.80	<LOD (0.07)	Nd	<LOD (0.06)	Nd	5:6:6
Compound 7	423.5	9.02	<LOD (0.07)	Nd	<LOD (0.06)	Nd	5:6:6
Compound 8	182.0	3.87	<LOD (0.07)	Nd	<LOD (0.06)	Nd	5:6:6
Compound 9	0.8	0.02	<LOD (0.07)	Nd	<LOD (0.06)	Nd	5:6:6

While all three strains share the presence of SPX 1 and 20-methyl SPX G, the relative contribution of each single known compound may vary significantly. For example, SPX 1 is the major compound in strain AON 24 (99.90%) but only a minor compound in strain NX-56-10 (6.37%) and MX-S-B11 (0.73%). Notably, 13,19-didesmethyl spirolide C was the major component of NX-56-10 (88.85%). All new compounds are minor components in terms of relative percentage, with the exception of **6** that contributes 18.51% in strain MX-S-B11. Moreover, certain SPX types only were produced in a single strain (Table 4.5). The high structural variability of secondary compounds of microalgae such as phycotoxins is not uncommon and also has been observed in other species than *A. ostenfeldii*, for example in *Protoceratium reticulatum* with more than 90 yessotoxin variants (Miles *et al.*, 2005) or in

*Prymnesium parvum* with more than 50 prymnesin variants (Binzer *et al.*, 2019). A possible explanation for a high structural variability of SPX could be that some variants might be biosynthetic precursors of others. However, the fact that different variants are found as major compounds in several strains argues against this hypothesis. Another, more likely explanation may be that chemical variability may be an evolutionary trait in order to improve chemical plasticity and thereby better allow species to adapt to environmental changes. However, since the biological function of most phycotoxins including SPX still remain unknown, this hypothesis still needs confirmation and certainly more research is needed to address the biological functions of microalgal secondary metabolites.

#### 4.4. Conclusions

The mass spectrometry-based structural characterization used in this study resulted in the proposal of eight novel SPX that have either a 5:5:6 or 5:6:6 triketal ring configuration and one SPX that may have a 6:5:6 ring configuration otherwise known from closely related pinnatoxins. However, future studies by NMR will be needed to confirm the structural features derived from mass spectrometric analyses of this work. Even though each strain seems to have a dominance of one or the other triketal ring system, these ring systems are not exclusive of one strain, but different ring systems are usually present indicating a high variability of biosynthetic pathways in this species. As the genes encoding for SPX biosynthesis have not been described yet, unravelling of the involved PKS genes in SPX biosynthesis will add valuable information for the understanding of the expression of this class of secondary metabolites and their putative physiological and/or ecological functions. In addition, toxicity of the novel SPX needs to be assessed to get more insights into structure-toxicity relationships. Structurally related pinnatoxins have an increased oral toxicity compared to SPX (**5**), which might be due to their 6:5:6 ketal ring configuration, which also may be the case for SPX with a 6:5:6 ketal ring configuration. Less is known of other structural elements of SPX such as 10-hydroxylation, which is a commonly observed feature of C-type SPX, but also in **7**, which is the first report on a 10-hydroxy G-type SPX, and of the butenolide side chain, which is shared by almost all SPX and also gymnodimines. In this sense, toxicity testing of the novel compounds, especially of **1** (truncated butenolide side chain), **5** (6:5:6 ketal ring configuration) and **7** (10-hydroxy G-type SPX), would be of special interest. However, for both NMR analysis and toxicity testing, relatively high amounts of purified compounds in the  $\mu\text{g}$  range are necessary, which currently hampers progress in this area.

## CHAPTER 5

### Gymnodimine A and 13-desMethyl Spirolide C Alter Intracellular Calcium Levels via Acetylcholine Receptors

#### Highlights:

- Using rat pheochromocytoma (PC12), the presence of 0.5  $\mu\text{M}$  of Gymnodimine A (GYM A) or 13-desmethyl spirolide C (SPX 1) induced an increase in intracellular calcium ( $[\text{Ca}]_i$ ) mediated by acetylcholine receptors (AChRs) and inhibited further activation of AChRs by acetylcholine (ACh).
- GYM A and SPX 1 activated nicotinic AChRs (nAChRs) and inhibited the further activation of nAChRs by ACh, indicating that both toxins mimicked the activity of ACh.
- A differential response was observed between the two toxins in muscarinic AChRs (mAChRs). Only GYM A activated mAChRs resulting in elevated  $[\text{Ca}]_i$  but both toxins prevented a subsequent activation by ACh.
- GYM A and SPX 1 induced no changes in  $[\text{Ca}]_i$  when nAChRs and mAChRs were inhibited simultaneously, indicating that both toxins target AChRs.

#### Contribution of the Doctoral Researcher:

- Planning of experiments
- Data collection
- Data analysis and interpretation
- Manuscript writing

---

This chapter appeared in:

Nieva, J.A.; Krock, B; Tillmann, U.; Zurhelle, C.; Tebben, J.; Bickmeyer, U.; Gymnodimine A and 13-desmethyl spirolide C alter Intracellular Calcium Levels via Acetylcholine Receptors. *Toxins* 2020, 12, 751. <https://doi.org/10.3390/toxins12120751>

## 5.1. Introduction

Gymnodimine A (GYM A) and 13-desmethyl spirolide C (SPX 1) are known to co-occur in a number of *A. ostenfeldii* strains (Van Wagoner *et al.*, 2011; Van de Waal *et al.*, 2015; Harju *et al.*, 2016; Martens *et al.*, 2017; Zurhelle *et al.*, 2018). The presence of structurally related gymnodimines and spirolides in a single microalgal species suggests that both toxins may share a common biosynthetic pathway. In addition to the cyclic imine moiety, the butenolide side chain is also identical for gymnodimines and spirolides, which may indicate a common function of both toxin types (Van Wagoner *et al.*, 2014).

Functional bioassays on GYM A and SPX 1 revealed a similar bioactivity. Both GYM A and SPX 1 induce the same rapid neurotoxic symptoms in mice, suggesting that both are “fast-acting toxins” (Munday *et al.*, 2012; Otero *et al.*, 2012). However, mouse toxicity assays showed that both compounds are less toxic in oral administration as compared to intraperitoneal injection treatments. *In vivo* inhibition binding assays were also performed to determine the binding selectivity of GYM A and SPX 1 to certain cell receptors. Results showed that the time for symptoms to manifest shortened and the onset of death accelerated when anticholinergic or acetylcholinesterase inhibitors were simultaneously administered. These observations prompted studies to determine the mechanism by which the toxins affect acetylcholine receptors (AChRs) (Gill *et al.*, 2003; Munday *et al.*, 2004).

To gain a better understanding of the effect of GYM A and SPX 1 on AChRs, electrophysiological measurements were conducted. This method uses clonal cells that have a specific type of overexpressed receptor (Friis *et al.*, 2009). Clonal cells with both homomeric and heteromeric subtypes such as  $\alpha 7$ ,  $\alpha 1\beta 1\gamma\delta$ ,  $\alpha 7$ -5HT<sub>3</sub>,  $\alpha 3\beta 2$  and  $\alpha 4\beta 2$  were used to evaluate the binding activity of the toxins to nicotinic AChRs (nAChRs). On the other hand, cells with subtypes M<sub>1</sub>–M<sub>5</sub> were used to determine the activity of GYM A and SPX 1 on muscarinic AChRs (mAChRs). Electrophysiological measurements demonstrated that while GYM A as well as SPX 1 broadly targets nAChRs (Kharrat *et al.*, 2008; Aráoz *et al.*, 2015; Bourne *et al.*, 2010; Hauser *et al.*, 2012), only GYM A showed a reversible effect (Kharrat *et al.*, 2008). The particular observation means that even when the toxins were washed off with buffer, SPX-treated cells retained its antagonistic effect to the nAChRs. On the other hand, the effect of SPX 1 on mAChRs showed the antagonistic effect of the toxin that resulted in a reduced function and decreased specificity of mAChRs (Wandscheer *et al.*, 2010). However, recent studies contradicted this model and showed that neither SPX 1 (Aráoz *et*

*al.*, 2015; Hauser *et al.*, 2012) nor GYM A (Hauser *et al.*, 2012) strongly interact with mAChR subtypes M<sub>1</sub>–M<sub>5</sub>.

Considering that GYM A and SPX 1 have shown anticholinergic effects on AChRs in recombinant cells (Gill *et al.*, 2003; Munday *et al.*, 2004; Kharrat *et al.*, 2008; Aráoz *et al.*, 2015; Bourne *et al.*, 2010; Hauser *et al.*, 2012; Wandscheer *et al.*, 2010), it is important to determine the effects on cellular signaling. Through cellular signaling, cell membrane structures such as voltage-gated channels and receptor-mediated channels (i.e., AChRs) transmit signals, which are in the form of cations (i.e., Na<sup>+</sup>, K<sup>+</sup>, Ca<sup>2+</sup>, etc), into the cells. In neuroendocrine cells such as rat pheochromocytoma (PC 12) cells, many different types of receptors and ion channels are simultaneously present (Seta *et al.*, 2002; Catterall *et al.*, 1995). Voltage-gated calcium (Ca) channels and AChRs are known to permeate calcium ions (Ca<sup>2+</sup>) into the cell when the channels are opened as a result of depolarization or binding of acetylcholine (ACh), respectively. Voltage-gated Ca channels are selective gates that regulate the majority of the Ca<sup>2+</sup> influx into the cell (Catterall *et al.*, 1995) while nAChRs are non-selective cation channels that are permeable not only to Ca<sup>2+</sup> but also to other cations (Gotti *et al.*, 2006). AChRs can be classified into nicotinic and muscarinic AChRs. While nAChRs function as ionotropic receptors inducing as a fast response in the cell (Hurst *et al.*, 2013), mAChRs are coupled to G-proteins which use the transmitted signal to activate a cascade of reactions and produce a secondary messenger. Compared to nAChRs, mAChRs provide an indirect response to a series of reactions (Brann *et al.*, 1993).

This chapter, thus, investigated the effects of GYM A and SPX 1 (from **Chapter 3**) on the intracellular Ca<sup>2+</sup> ([Ca]<sub>i</sub>) alterations mediated by ion channels and receptors. PC12 cells were chosen in order to be able to investigate the effects of toxins on more than one type of receptor and many different ion channels (Shafer *et al.*, 1991). This study specifically aimed to determine the influence of GYM A and SPX 1 on voltage-gated plasma-membrane Ca channels and nicotinic and muscarinic AChRs of PC 12 cells under physiological conditions. Since PC12 cells contain the nAChR subtypes  $\alpha$ 3,  $\alpha$ 5,  $\beta$ 2- $\beta$ 4 (Takahashi *et al.*, 1999) as well as atypical mAChR subtypes (Michel *et al.*, 1989), the approach of this study is more general than previously published works (Kharrat *et al.*, 2008; Aráoz *et al.*, 2015; Bourne *et al.*, 2010; Hauser *et al.*, 2012; Wandscheer *et al.*, 2010).

## 5.2. Materials and Methods

### 5.2.1. Extraction and purification of gymnodimine A and 13-desmethyl spiroside C

The extraction and purification of the toxins was conducted using the procedure described in **Chapter 3**, Section 3.2.3.3.

### 5.2.2. PC 12 culture methods

Prior to cell cultivation, cover slips were placed into the Petri dishes, coated with 0.5 mg mL<sup>-1</sup> collagen A (Biochrom, Berlin, Germany) and dried for 24 hours. The Petri dishes were filled with 100 mL of culture medium composed of Roswell Park Memorial Institute (RPMI) medium 1640, 10% fetal calf serum, 5% horse serum, and 100 units penicillin/streptomycin per milliliter. Rat pheochromocytoma (PC12) cells (ATCC, Wesel, Germany) were then seeded into thus prepared Petri dishes. The cells were kept in an incubator at 37 °C, 90% humidity, and 5% CO<sub>2</sub> and medium changes were conducted after three to five days of cultivation.

### 5.2.3. Fluorimetric measurements of intracellular Calcium levels

For fluorometric measurements of [Ca]<sub>i</sub>, cover slips adhered with PC12 cells were incubated in Na<sup>+</sup> buffer (in mM: 125 NaCl, 2.5 KCl, 1 MgCl<sub>2</sub>, 2 CaCl<sub>2</sub>, 1.3 NaH<sub>2</sub>PO<sub>4</sub>, 30 Glucose, 26 Na HEPES (4-(2-hydroxyethyl)-1-piperazineethanesulfonic acid)) with a final concentration of 10 μM Ca<sup>2+</sup> fluorescent dye, Flou-3 acetoxymethylester (Flou-3 AM), for 1 hour at 37°C. Then the physiological Na<sup>+</sup> buffer was removed and replaced with fresh Na<sup>+</sup> buffer. The cell fluorescence was monitored using an inverted confocal laser scanning microscope (Leica SP5, Wetzlar, Germany) equipped with an argon ion laser for fluorescence excitation (exc 488nm, em 520-550 nm). Images were taken every second. The beam of the laser scanned the object plane through a Zeiss (Jena, Germany) 20× water immersion objective. A plastic inlay was constructed to reduce the exchangeable volume to 250 μL, increase the speed of solution exchange and minimize the amount of toxins used in the experiment. To increase speed, the compounds were manually pipetted, instead of pumping or gravity filtration. The experiment took place in an Utermöhl chamber.

10 PC12 cells (n = 10) were selected in the cover slips and were analyzed independently using region of interest (ROI)s in the Leica Application Suite Advanced Fluorescence (LAS AF, Wetzlar, Germany) software. The dye intensity represents the calcium concentration inside the cell. Ten individual cells were measured simultaneously in all treatments. The cellular fluorescence emission of the selected PC12 cells was normalized by dividing the fluorescence measured by the initial

values ( $t_0$ ) and then multiplying them by 100. All experiments were replicated using a different cell culture batch obtaining comparable results.

#### 5.2.4. $[Ca]_i$ measurements using $K^+$ depolarization

Cover slips with adhered cells were mounted on the microscope using a chamber with a volume capacity of 250  $\mu$ L. The fluorescence of the PC12 cells was measured and cells were subsequently depolarized by submerging  $K^+$  buffer (in mM: 55 NaCl, 80 KCl, 1 MgCl<sub>2</sub>, 2 CaCl<sub>2</sub>, 1.3 NaH<sub>2</sub>PO<sub>4</sub>, 30 Glucose, 26 Na HEPES) through manual pipetting. The effects of the toxin were determined by spiking the  $K^+$  buffer with GYM A or SPX 1 reaching a final concentration of 0.5  $\mu$ M.

#### 5.2.5. $[Ca]_i$ measurements with application of acetylcholine

Cells were stimulated by application of 100  $\mu$ M Acetylcholine-Cl (ACh) (Sigma, Darmstadt, Germany) in  $Na^+$  buffer (described in Section 4.2.3). The effects of the toxin were determined by spiking the buffer with either GYM A or SPX 1 resulting in final concentrations of 0.005, 0.05 and 0.5  $\mu$ M. In addition, AChR subtype blockers, atropine and tubocurarine, were utilized in order to investigate the mechanism of action against nAChR and mAChR, respectively. Both substances were used at a final concentration of 100  $\mu$ M.

### 5.3. Results

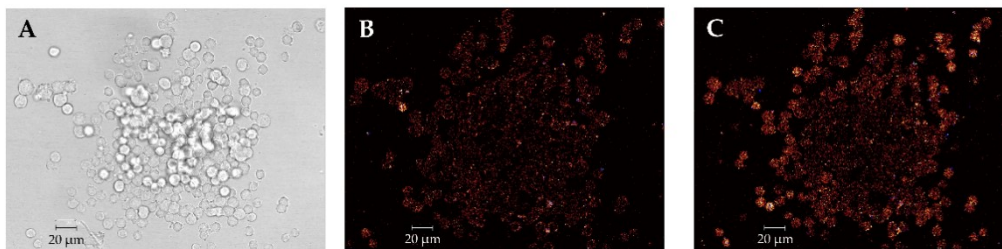


**Figure 5.1.** (A) Transmission image of PC12 cells and (B) fluorescence images of flou-3 acetoxymethylester (Flou-3 AM)-stained PC 12 cells before and (C) during depolarization.

#### 5.3.1. Depolarization of $Ca$ channels using $K^+$

To account for the possibility of the toxins inhibiting voltage-dependent calcium channels, this study investigated the toxin's influence on depolarization-induced  $[Ca]_i$  changes (Figure 5.1). This was done to avoid misinterpretation on toxin induced calcium channel inhibition with effects on AChRs. In the controls, an elevation of  $[Ca]_i$ , induced by high concentrations of  $K^+$  was associated with a change in fluorescence emission intensity of the Flou-3 AM dye. Baseline recovery of  $[Ca]_i$  to the baseline was observed after depolarization (Figure 5.2A).



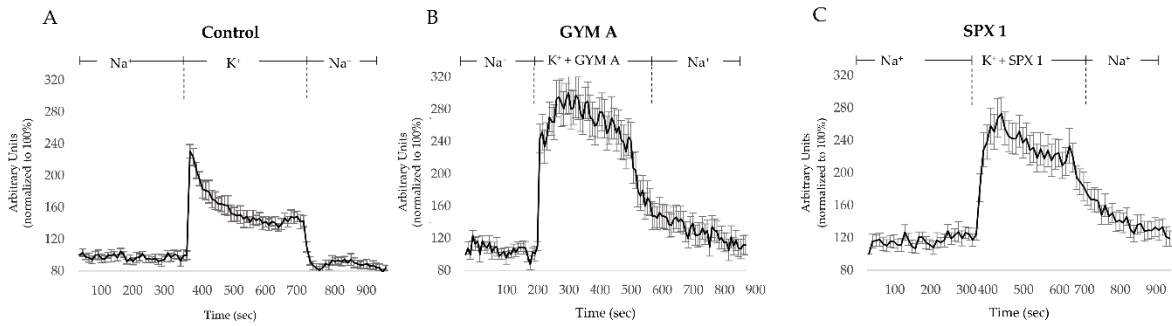


**Figure 5.2.** Alteration of fluorescence intensity (FI) induced by 80 mM  $K^+$ . (A) Intracellular calcium ( $[Ca]_i$ ) level changes (shown as arbitrary FI units) induced by activation of voltage-gated calcium channels ( $K^+$ ) under control conditions and (B) in cells treated with 0.5  $\mu M$  GYM A or (C) SPX 1.

Cells incubated with GYM A or SPX 1 (0.5  $\mu M$ ) showed an increase of  $[Ca]_i$  during depolarization and no calcium channel inhibition (Figure 5.2B and 5.2C, respectively). In both treatments, the baseline recovery was delayed (Figure 5.2B and 5.2C) compared to the control (Figure 5.2A).

### 5.3.2. $[Ca]_i$ changes induced by ACh

A  $[Ca]_i$  elevation, as described by an increase of  $[Ca]_i$  from the baseline, was also mediated by ACh (Figure 5.3A). To reveal the effects of the toxins on  $[Ca]_i$ , GYM A or SPX 1 were applied before ACh (Figure 5.3B and 5.3C).

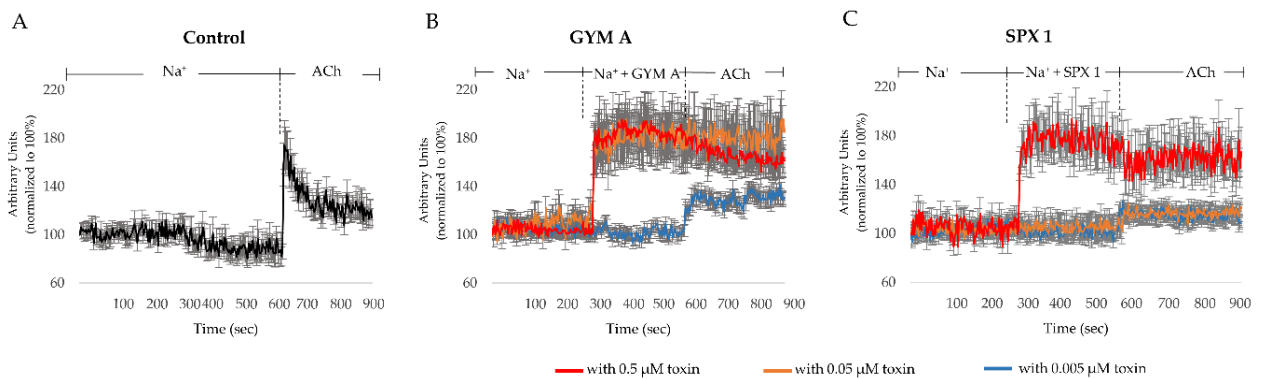


**Figure 5.3.**  $[Ca]_i$  changes induced by ACh, GYM A and SPX 1. (A)  $[Ca]_i$  level changes induced by activation of AChRs under control conditions and (B) in cells treated with GYM A in the concentrations 0.005  $\mu M$  (blue), 0.05  $\mu M$  (orange) and 0.5  $\mu M$  (red) and (C) SPX 1 in the concentrations 0.005  $\mu M$  (blue), 0.05  $\mu M$  (orange) and 0.5  $\mu M$  (red).

In cells treated with either 0.5  $\mu\text{M}$  (Figure 5.3B, in red) or 0.05  $\mu\text{M}$  (Figure 5.3B, in orange) GYM A, an increase of  $[\text{Ca}]_i$  was observed after the toxins were applied. The successive application of ACh induced no further  $[\text{Ca}]_i$  elevation (Figure 5.3B, in red and orange). A different pattern was observed for 0.005  $\mu\text{M}$  GYM A (Figure 5.3B, in blue). In this case, no increase in  $[\text{Ca}]_i$  was observed after the addition of GYM A but instead after the ACh was applied.

The application of 0.5  $\mu\text{M}$  of SPX 1 did also result in an increase in  $[\text{Ca}]_i$  (Figure 5.3C, in red). Following the application of ACh, no further  $[\text{Ca}]_i$  response was detected. As for the lower concentrations, no increase in  $[\text{Ca}]_i$  was observed after the addition of 0.05 and 0.005  $\mu\text{M}$  SPX 1. When ACh was subsequently applied, a  $[\text{Ca}]_i$  elevation was observed (Figure 5.3C, in orange and blue).

To differentiate the effects of both toxins on AChRs present in the cells, we pharmacologically isolated the effect of the toxins on nAChRs by using the mAChR-blocker atropine (Figure 5.4A, 5.4B and 5.4C). Under control conditions, a response in  $[\text{Ca}]_i$  was observed upon the addition of ACh to nAChRs (Figure 5.4A). In cells treated with atropine and 0.5  $\mu\text{M}$  GYM A (Figure 5.4B, in red) and 0.05  $\mu\text{M}$  GYM A (Figure 5.4B, in orange), a  $[\text{Ca}]_i$  response was observed. The subsequent application of ACh induced no further increase in  $[\text{Ca}]_i$ . For 0.005  $\mu\text{M}$  GYM A (Figure 5.4B, in blue), only a slight increase of fluorescence intensity (FI) (~10%) was observed when the toxin was added along with atropine. Upon application of ACh (Figure 5.4B, in blue),  $[\text{Ca}]_i$  increased further (~30% FI increase). When SPX 1 (0.5, 0.05 and 0.005  $\mu\text{M}$ ; Figure 5.4C, in red, orange and blue, respectively) was applied together with atropine, an increase in  $[\text{Ca}]_i$  was observed at all three concentrations. Upon application of ACh, no additional  $[\text{Ca}]_i$  response was observed in 0.5 and 0.05  $\mu\text{M}$  SPX 1-treated cells. However, in cells treated with 0.005  $\mu\text{M}$  SPX 1 (Figure 5.4C, in blue), an increase in  $[\text{Ca}]_i$  by ACh was evident.

The effect of the toxins on mAChRs was investigated by adding nAChR-blocker tubocurarine. Under control conditions, a response in  $[\text{Ca}]_i$  was observed upon the addition of ACh to mAChRs (Figure 5.4D). In cells treated with 0.5, 0.05 and 0.005  $\mu\text{M}$  GYM A, a dose-dependent increase of  $[\text{Ca}]_i$  was observed (Figure 5.4E, in red, orange and blue, respectively). At the highest concentration used in this study (0.5  $\mu\text{M}$ ) no further  $[\text{Ca}]_i$  response was observed after additional ACh was applied (Figure 5.4E, in red). For the two lower concentrations, 0.05 and 0.005  $\mu\text{M}$ , an increase of  $[\text{Ca}]_i$  (~20% FI increase) was observed (Figure 5.4E, in orange and blue, respectively). A different response was

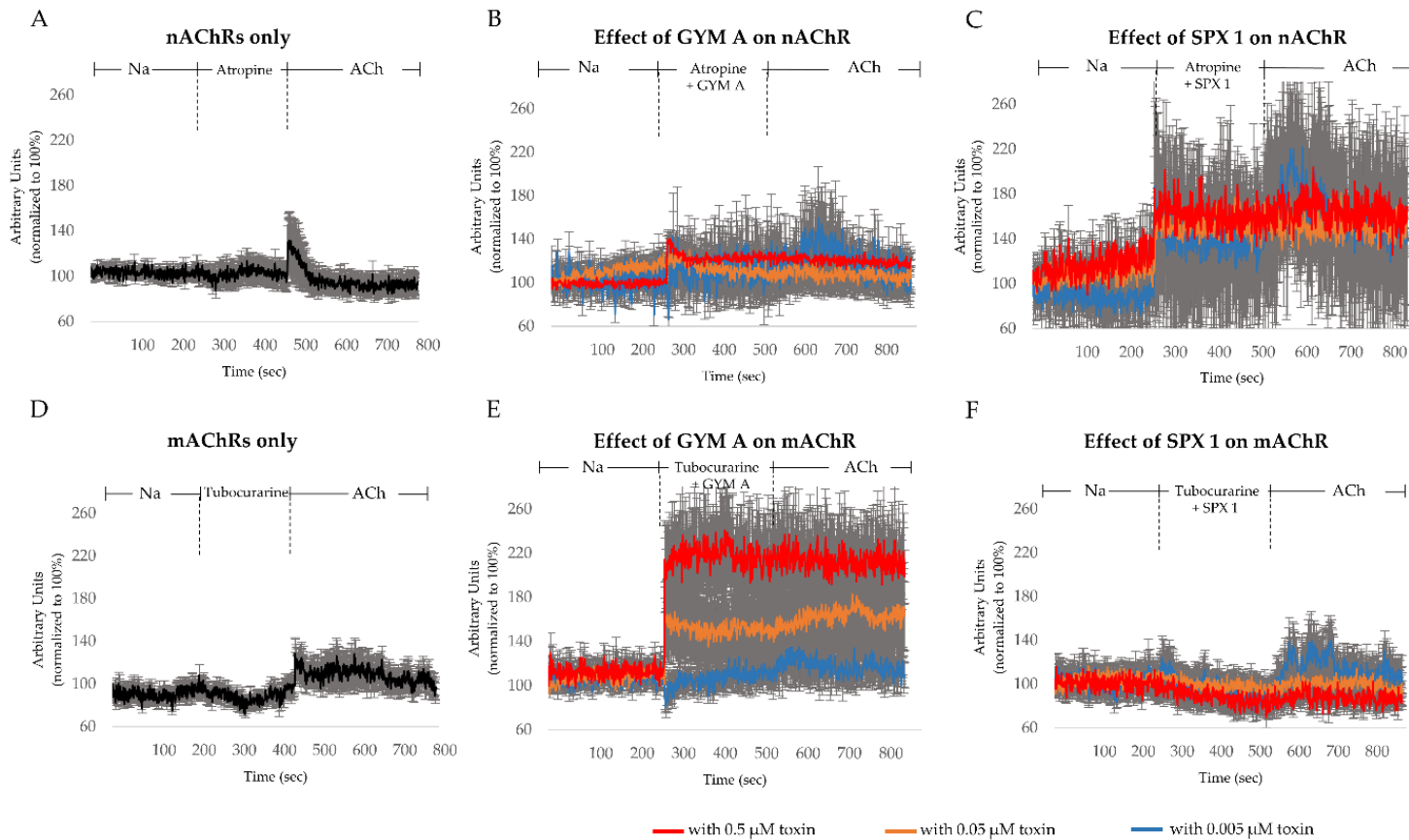


**Figure 5.4.**  $[Ca]_i$  changes induced by ACh, GYM A and SPX 1 through pharmacologically isolated nAChRs or mAChRs. (A)  $[Ca]_i$  level changes in cells pretreated with only mAChR-blocker atropine and (B) atropine with GYM A in the concentrations 0.005  $\mu$ M (blue), 0.05  $\mu$ M (orange) and 0.5  $\mu$ M (red) followed by the application of ACh. (C)  $[Ca]_i$  level changes in cells pretreated with mAChR-blocker atropine and SPX 1 in the concentrations 0.005  $\mu$ M (blue), 0.05  $\mu$ M (orange) and 0.5  $\mu$ M (red) followed by the application of ACh. (D)  $[Ca]_i$  level changes in cells pretreated with only nAChR-blocker tubocurarine and (E) tubocurarine with GYM A in the concentrations 0.005  $\mu$ M (blue), 0.05  $\mu$ M (orange) and 0.5  $\mu$ M (red) followed by the application of ACh. (F)  $[Ca]_i$  level changes in cells pretreated with nAChR-blocker tubocurarine and SPX 1 A in the concentrations 0.005  $\mu$ M (blue), 0.05  $\mu$ M (orange) and 0.5  $\mu$ M (red) followed by the application of ACh.

observed when SPX 1 was applied on mAChRs. A decrease of  $[Ca]_i$  (~5-10% FI) was measured in cells treated with SPX 1 (Figure 5.4F, in red, orange and blue, respectively). In cells treated with 0.5 and 0.05  $\mu\text{M}$  SPX 1 (Figure 5.4F, in red and orange, respectively), the addition of ACh resulted in no further change in  $[Ca]_i$ . In cells treated with 0.005  $\mu\text{M}$  SPX 1 (Figure 5.4F, in blue), however, the addition of ACh induced a  $[Ca]_i$  elevation (~ +40% FI).

In order to rule out effects of the toxins on cellular targets involved in  $[Ca]_i$  signaling other than AChRs, either GYM A or SPX 1 (0.5  $\mu\text{M}$ ) was applied to cells while simultaneously inhibiting nAChRs and mAChRs. In both treatments, no obvious change in  $[Ca]_i$  was observed. In addition, no  $[Ca]_i$  response was observed after ACh addition (Figure 5.5A and 5.5B).

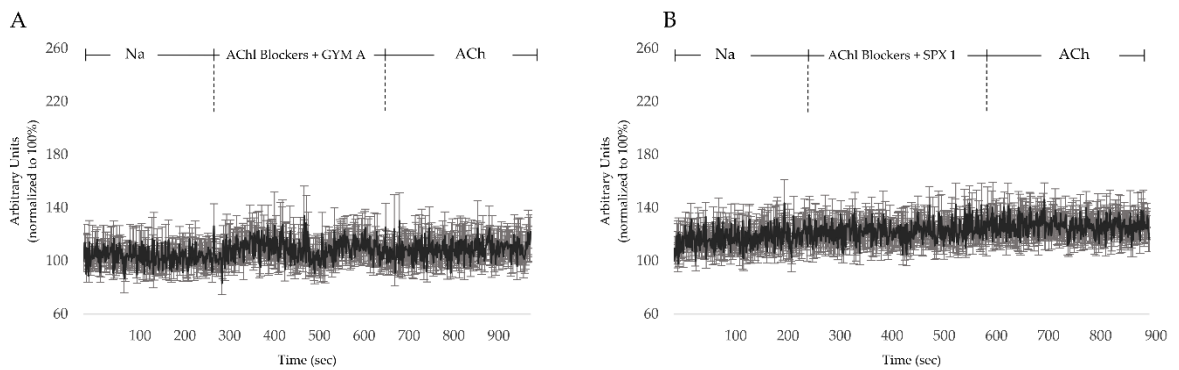


**Figure 5.5.** (A)  $[Ca]_i$  level changes in cells pretreated with mAChR-blocker atropine and nAChR-blocker tubocurarine with 0.5  $\mu\text{M}$  GYM A and (B) SPX 1.

## 5.4. Discussion

### 5.4.1. GYM A and SPX 1 do not inhibit the influx of $[Ca]_i$ through voltage-gated Ca channels

First, the influence of voltage-gated Ca channels on toxin-induced  $[Ca]_i$  changes was excluded. During depolarization, voltage-gated Ca channels mediate the influx of  $Ca^{2+}$  into the cell. Free  $Ca^{2+}$  is removed from the cytosol by uptake into the endoplasmic reticulum and mitochondria and by extrusion mechanisms such as calcium pumps and ion exchangers (Berridge *et al.*, 2000; Bickmeyer *et al.*, 2010).  $[Ca]_i$  measurements during depolarization in controls as well as in GYM A- and SPX 1-exposed cells indicate that the toxins do not reduce the influx of  $[Ca]_i$  through voltage-gated Ca channels. The gradual decrease in  $[Ca]_i$  following depolarization in GYM A- and SPX 1-treated cells (Figure 5.2B and 5.2C, respectively) indicates either an inhibition of transport proteins (e.g.,  $Ca^{2+}$  ATPases) that remove  $Ca^{2+}$  from the cell or that the influx of  $Ca^{2+}$  into the cell is mediated by other means (Berridge *et al.*, 2000). Since AChRs depolarize the cellular membrane and permeate  $Ca^{2+}$  into

the cells (Gotti *et al.*, 2006), and GYM A and SPX 1 bind to those receptors, AChRs were chosen as targets for further experiments.

#### 5.4.2. GYM A and SPX 1 alter $[Ca]_i$

The binding of a stimulating compound such as ACh to AChRs initiate the influx of  $Ca^{2+}$  into the cell. GYM A or SPX 1 tested here had the same effect: the application of 0.05, 0.5  $\mu$ M GYM A and 0.5  $\mu$ M SPX 1 induced  $[Ca]_i$  elevations (Figure 5.3B, in red and orange and 5.3C, in red). The activation of AChRs by either GYM A or SPX 1, particularly at the concentration of 0.5  $\mu$ M, may be the reason why a slow and gradual decrease in  $[Ca]_i$  was observed in the  $K^+$ -depolarized cells (Figure 5.2B and 5.2C). The response observed in  $[Ca]_i$  infers that toxins mimic ACh and thereby initiate the influx of  $Ca^{2+}$  into the cell. The resulting AChR-toxin complex further inhibits a subsequent activation of AChRs by ACh (Figure 5.3B, in red and orange and Figure 5.3C, in red). Both toxins activated AChRs at varying concentrations, with GYM A acting as a more potent activator than SPX 1. Compared to GYM A (at 0.05  $\mu$ M, Figure 5.3B, in orange), SPX 1 of a higher concentration (at 0.5  $\mu$ M, Figure 5.3C in red) was needed to induce comparable  $Ca^{2+}$  influx into the cell. At the lowest concentrations (0.005  $\mu$ M) of both toxins, no activation of AChRs was measurable.

#### 5.4.3. GYM A and SPX 1 show a similar effect on nAChRs and a differential response to mAChRs

The difference in response in  $[Ca]_i$  between the atropine-treated cells (Figure 5.4A) and atropine-toxin-treated cells indicate an interaction of GYM A (Figure 5.4B) and SPX 1 (Figure 5.4C) with nAChRs. Both toxins activate nAChRs, induce entry of  $Ca^{2+}$  into the cells and block the binding of ACh to nAChRs. At low concentrations (0.005  $\mu$ M), activation of nAChRs appears in SPX 1- (Figure 5.5C, in blue) but not in GYM A-treated cells (Figure 5.4B, in blue), demonstrating dose dependent differences. For both toxin, low concentrations did not inhibit the activation of nAChRs by ACh, resulting in an increase in  $[Ca]_i$ . The results support previous studies that showed SPX to have a higher efficacy for nAChRs than GYM A (2–15 fold difference) (Bourne *et al.*, 2010; Hauser *et al.*, 2012).

The contrasting response between cells treated only with tubocurarine and cells which were additionally treated with GYM A or SPX 1 suggests that toxins may have also interacted with mAChRs. GYM A activates mAChRs dose-dependently. ACh only activate mAChRs at low concentrations of GYM A (0.005  $\mu$ M) (Figure 5.4E, in blue) where an inhibition of a constitutive activity of receptors may have happened. For SPX 1, a decrease in  $[Ca]_i$  was observed which could have been caused by an inhibition of a constitutive activity of mAChRs (Spalding *et al.*, 2006).

Following the observed decrease in  $[Ca]_i$  upon addition of SPX 1, high and moderate concentrations of the toxin inhibit the subsequent activation of mAChRs by ACh (Figure 5.4F, in red and orange). A low concentration of SPX 1, on the other hand, had no effect (Figure 5.4F, in blue). GYM A (Hauser *et al.*, 2012) and SPX 1 (Hauser *et al.*, 2012; Aráoz *et al.*, 2015) have previously been described to have a low ability to interact with mAChRs, with the latter having a lower affinity (Hauser *et al.*, 2012). This study describes a differential effect of GYM A and SPX 1 on mAChRs.

#### 5.4.4 GYM A and SPX alter $[Ca]_i$ through nAChRs and mAChRs

At a concentration of 0.5  $\mu$ M, GYM A and SPX 1 activate nAChR (GYM A also activates mAChRs) and inhibit the response to ACh.  $[Ca]_i$  was not affected by GYM A and SPX 1 (0.5  $\mu$ M) when both AChR subtypes were blocked simultaneously by atropine and tubocurarine (Figure 5.5A and 5.5B). The lack of  $[Ca]_i$  response shows that nAChRs and mAChRs must be the primary targets of GYM A and SPX 1 related to  $[Ca]_i$  signaling.

Previous studies have demonstrated that both GYM A and SPX 1 acted as antagonists to nAChRs (Kharrat *et al.*, 2008, Bourne *et al.*, 2010, Wandscheer *et al.*, 2010, Hauser *et al.*, 2012, Aráoz *et al.*, 2015), while neither interacted strongly with mAChRs (Hauser *et al.*, 2012; Aráoz *et al.*, 2015). This study shows that GYM A and SPX 1 activate nAChR at 0.5  $\mu$ M and dose-dependently interact with a successive ACh stimulation. GYM A was observed to additionally activate mAChRs at 0.5  $\mu$ M, demonstrating that mAChRs are also a target of GYM A. The disparity on the response elicited in this study may be due to different receptor subtypes present in PC12 cells (nAChR subtypes  $\alpha$ 3,  $\alpha$ 5,  $\beta$ 2- $\beta$ 4 (Takahashi *et al.*, 1999) and atypical mAChR subtypes (Michel *et al.*, 1989) as compared to subtypes used in studies published previously (nAChR subtypes  $\alpha$ 7,  $\alpha$ 1 $\beta$ 1 $\gamma$  $\delta$ ,  $\alpha$ 7-5HT $_3$ ,  $\alpha$ 3 $\beta$ 2 and  $\alpha$ 4 $\beta$ 2 and M $_1$ -M $_5$  mAChR subtypes) (Kharrat *et al.*, 2008; Bourne *et al.*, 2010; Hauser *et al.*, 2012; Wandscheer *et al.*, 2010; Aráoz *et al.*, 2015). To investigate structure-activity relations and to investigate functional measurements due to desensitization mechanism, future electrophysiological studies are required. The potentiation of nAChRs by atropine is described for specific subunits of the receptor ( $\alpha$ 4 $\beta$ 4) (Zwart *et al.*, 1997), which are not present in PC12 cells. A potential interaction site of atropine with nAChRs (inhibition) is the  $\alpha$ 3 $\beta$ 4 subunit, which is present in PC12 cells (Parker *et al.*, 2003). It is therefore possible that in this experiment atropine potentiated the effect of SPX 1 on certain nAChR subunits and has a small effect during application of a low dose of GYM A.

The response of cells following direct application of higher concentrations of toxins has not been described previously. This study demonstrates GYM A and SPX 1 to dose-dependently interact

with AChRs of neuroendocrine PC12 cells. Furthermore, SPX 1 has the capability to inhibit the constitutive activity of mAChRs.

The activation of receptors at high toxin concentrations and inhibition of subsequent activation by ACh at lower concentrations hint to a cooperativity of molecules. In this case, e.g., one molecule binds to one receptor's binding site preventing further activation by ACh, and when more toxin molecules together bind to more receptor sites, this leads to activation of receptors. The cooperativity can be calculated by the steepness of dose response relationships. This is unfortunately not feasible in this study due to limited amounts of compounds being available and therefore limited dose response related data points.

In summary, this study demonstrates that under physiological conditions, both toxins act as agonists for nAChRs and that GYM A induces an increase in  $[Ca]_i$  through mAChRs. This study further provides clear evidence that GYM A and SPX 1 mimic the action of ACh preventing further activation of receptors. The macrocyclic nature of GYM A and SPX 1 allows the toxins to conform to the same binding sites of nAChRs with the cyclic imine as the pivot point of the molecule (Bourne *et al.*, 2010). Absence of a triketal ring system may provide a basis for selective activation of mAChRs by GYM A as compared to SPX 1. The difference in activity regarding nAChRs and mAChRs observed between the toxins may be due to the subtype-selectivity of these receptors. Subtypes of nAChRs, which can be homomeric or heteromeric in form, have different permeabilities to  $Ca^{2+}$  and affinities to ACh (Albuquerque *et al.*, 2008). mAChR subtypes couple to different G-protein types initiating different secondary induction pathways (Eglen *et al.*, 2005). Structural conformation of the toxins (presence or absence of a triketal ring system) as well as of the AChR subunits play crucial roles in the selectivity and specificity of toxin-receptor interactions.

## CHAPTER 6

### Activation of Oxidative Stress and Inflammation Response Pathways by Gymnodimine A and 13-desMethyl Spirolide C

#### Highlights:

- This study provides the preliminary information on the effects of gymnodimine A (GYM A) and (13-desmethyl spirolide C) SPX 1 in AREc32 (Luciferase reporter gene assay) and NfκB- BLA (Beta-lactamase reporter gene assay) assays.
- GYM A and SPX 1 differed in their induction effects towards oxidative stress and inflammatory response pathways.
- Induction of oxidative stress response pathways was observed only through SPX 1.
- GYM A and SPX 1 induces inflammatory response pathway in the nanomolar concentration range.

#### Contribution of the Doctoral Researcher:

- Planning of experiments
- Data collection
- Data analysis and interpretation

---

This chapter is a collaborative study between Alfred-Wegener-Institut, Helmholtz-Zentrum für Polar- und Meeresforschung (AWI) and Helmholtz-Zentrum Umweltforschung GmbH (UFZ) under the supervision of Dr. Bernd Krock and Prof. Dr. Beate I. Escher, respectively.



## 6.1. Introduction

Harmful algal blooms (HABs)-associated toxins exhibit significantly diverse bioactivities mainly due to their structural variability, resulting to their respective modes of action (MOA) (Beuzenberg *et al.*, 2012). As such, these compounds present a large pool of potential medical applications; hence, mechanistic understanding of intoxications in the medical context is imperative (García Camacho *et al.*, 2007). For example, a known antifungal polyether phycotoxin goniodomin-A produced by a few species of *Alexandrium* (Murakami *et al.*, 1988) inhibited the migration of endothelial cells, indicating that this toxin is capable of inhibiting growth of new blood vessels (commonly described as anti-angiogenesis property). Their properties further imply that the toxin could potentially act as anti-tumor and anti-cancer agent because of its ability to inhibit angiogenesis, a precursor for tumor and cancer cells (Abe *et al.*, 2002). Studies on toxin MOA have provided understanding of their capability as anti-tumor, anti-inflammatory, antileukemic and neurotoxic activities, among others (García Camacho *et al.*, 2007).

Insights on the potential MOA of the toxins are determined by their response to a cellular signal transduction pathway (Cardenas *et al.*, 1998). Among the signal transduction pathways, adaptive stress responses are used to infer the possible MOA of a particular toxin. Adaptive stress responses are cellular adaptations that result from a change in physico-chemical conditions or the presence of stimuli or stressors. To restore homeostasis, various adaptive stress response pathways are activated (Figure 6.1; Simmons *et al.*, 2009).

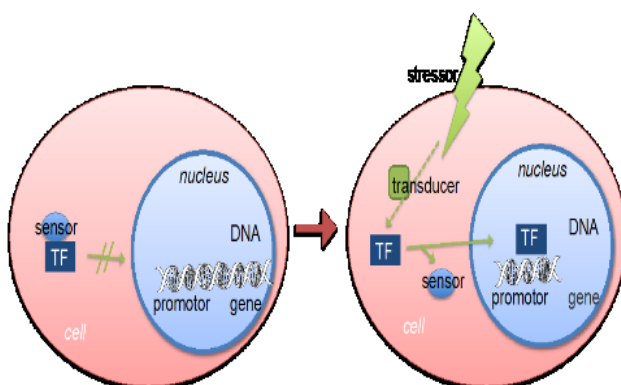


**Figure 6.1.** Activation of an adaptive stress response pathway (adapted from Escher and Leusch, 2012). The activation for these pathways is mediated by transcription factors (TFs). Under normal cell conditions, TFs are bound to a sensor molecule in the cell. As stimulants are introduced to the cell, transducers activate the release of TFs from the sensor molecule. The unbound TF enters the nucleus and initiates the expression of its target genes that further expresses proteins, which proceeds to cellular damage repair (Simmons *et al.*, 2009). Refer to Table 6.1 for examples of TF-sensor complex.

**Table 6.1.** Examples of transcription factor-sensor complex involved in the induction of selected adaptive stress response pathways.

Pathway	Sensor	Transcription Factor (TF)	Inducing Chemicals
Oxidative Stress	Keap 1	Nrf2	Reactive oxygen species producing chemicals
Inflammation	I $\kappa$ B	Nf $\kappa$ B	Inflammation-causing stimuli

When these response pathways are activated, cells synthesize protective molecules (i.e., cryoprotective proteins) or induce damage repair in order to modulate, if not prevent apoptosis or cell death (Milisav *et al.*, 2012). For instance, Schmidt *et al.* (1995) suggested that okadaic acid (OA) indirectly activates oxidative stress response through production of reactive oxidative intermediates (ROI). When OA was added in both tumor and primary cell lines, high concentrations of ROI species (i.e., H<sub>2</sub>O<sub>2</sub> and O<sub>2</sub>) were observed. The correlation between presence of OA and production of ROI suggests that the functionality of OA could be attributed to its tumor promoting and prooxidant activity (Schmidt *et al.*, 1995). Based on the effect of a toxin to a targeted adaptive response pathway, preliminary information regarding its possible MOA might be presumed.

For a number of phycotoxins, such as cyclic imines (CIs), MOA experiments have rarely been conducted. Usually, bioassays performed with these compounds include mouse bioassays (Munday *et al.*, 2012; Otero *et al.*, 2012) and electrophysiological and inhibition assays (Aráoz *et al.*, 2015; Cuesnon *et al.*, 2016). Regarding on gymnodimine A (GYM A) and 13-desmethyl spirolide C (SPX 1), electrophysiological and inhibition assays confirmed that these toxins bind to AChRs (Kharrat *et al.*, 2008; Bourne *et al.*, 2010; Wandescheer *et al.*, 2010; Hauser *et al.*, 2012; Aráoz *et al.*, 2015, Cuesnon *et al.*, 2016). Moreover, as described in the previous chapter (**Chapter 5**), GYM A and SPX 1 can alter intracellular calcium level by acting via acetylcholine receptors. With their capability to modify intracellular calcium concentrations, questions on other MOA as well as possible effects of GYM A and SPX 1 on other cellular pathway needs further investigation.

Further understanding on the MOA of GYM A and SPX 1 could be inferred from determining the effect of the toxins to specific adaptive stress response pathways (Cardenas *et al.*, 1998). To date, adaptive stress response pathway studies are visualized through reporter gene assay techniques (Figure 6.2). In this approach, genetic reporters (i.e., translated protein or enzyme) provide information whether signaling pathways or cellular events have been activated or repressed. The translated proteins, which are proportionate to the level of gene expression, are monitored through color change reactions such as fluorescence, luminescence or chromogenesis (Liu *et al.*, 2009). In

essence, reporter gene assays provide a sensitive approach in terms of determining the target pathway for the toxin (Escher and Leusch, 2012). Thus, this chapter specifically aimed to determine the response of purified GYM A and SPX 1 to oxidative stress and inflammation response pathways using AREc32 and NfκB-*bla* THP-1 cell lines, respectively.

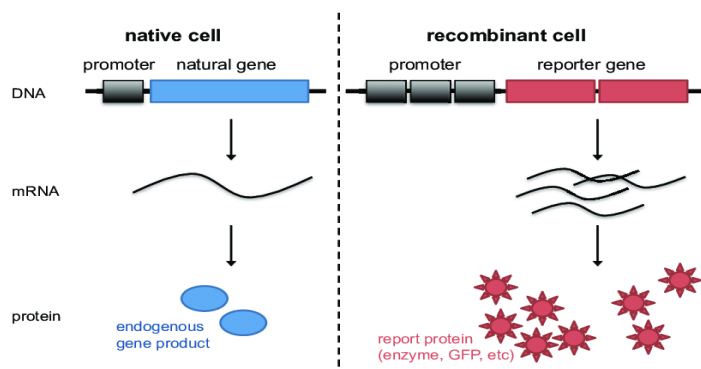


**Figure 6.2.** Difference between native and recombinant cell that uses reporter gene. In the recombinant cell, a reporter gene is linked to a promoter and cloned into an expression vector that is then transfected into the cells. After mRNA translation, the reporter gene encodes a reporter protein, which has an easily measurable activity (Escher and Leusch, 2012).

## 6.2. Materials and Methods

### 6.2.1 Sample Preparation

Gymnodimine A (GYM A) and 13-desmethyl spiroside C (SPX 1) were extracted and purified as previously described (**Chapter 3**, Section 3.2.3.3). Sample aliquots, initially dissolved with 300  $\mu$ L methanol (MeOH), were reduced to dryness through rotary evaporation. Approximately 1  $\mu$ g of toxins were used to prepare for the highest concentration needed for the dose-response curves (Table 6.2).

**Table 6.2.** Amount to toxins used in the adaptive stress response assays. Ten-fold serial dilution concentrations were prepared from the highest concentration of GYM A and SPX 1.

Toxin	Molecular Weight (g mol <sup>-1</sup> )	Oxidative Stress Response Assay (using AREc32 cells)		Inflammation Response Assay (using NfκB- <i>bla</i> THP-1)	
		Amount used ( $\mu$ g)	Highest Concentration ( $\mu$ M)	Amount used ( $\mu$ g)	Highest Concentration ( $\mu$ M)
GYM A	507	0.45	1.85	0.6	2.5
SPX 1	691	0.45	1.36	0.6	1.8

A process blank (i.e., MeOH blank) was also included in the analysis to determine the effect of the residue of the dissolving solvent. The MeOH blank was prepared by blowing down 300  $\mu$ L

MeOH into the dosing vial. Arbitrary concentration units (that have similar range as the toxins) were assigned to the MeOH blank so that the results can be plotted in the dose-response curve.

## 6.2.2 AREc32 for oxidative stress response

### 6.2.2.1 Cell and culture conditions

AREc32 reporter cell line was derived from the MCF7 human breast cancer cell lines that were transfected with an antioxidant response element (ARE) reporter plasmid. It contained copies of the rat glutathione S-transferase (GST) ARE element linked to a luciferase gene. The concentration of translated luciferase (from the reporter gene *Luc*) was determined by the response measured from the bioluminescent reaction (Wang *et al.*, 2006).

Cell lines were maintained in T75 flasks filled with a growth medium composed of 11 mL Dulbecco's Modified Eagle's medium (DMEM), 10% Fetal Bovine Serum (FBS), 1% penicillin–streptomycin, 1% Glutamax, 1.6% Geneticin (G418)) and were kept in an incubator at 37 °C, and 5% CO<sub>2</sub> and sub-cultured ever 2–5 days when cells were 80% confluent.

**Table 6.3.** Experimental parameters for the induction of oxidative stress and inflammation response.

Pathway	Cell Line	Reference Compound	Endpoint	Data Evaluation	Detection Method
Oxidative Stress	AREc32	<i>t</i> BHQ (tert-butylhydroquinone)	Oxidative stress response pathway	Induction (luminescence) for AREc32	Luciferase reporter gene assay
Inflammation	Nf-κB- <i>bla</i> THP-1	TNFα (tumor necrosis factor alpha)	Inflammatory response pathway	Induction (FRET) for GeneBLAzer assays	βlac reporter gene assay

### 6.2.2.2 Exposure experiments

After the growth medium was removed, AREc32 cells (30 μL of 1.2×10<sup>5</sup> cells per mL) were seeded in each well of a white polystyrene tissue culture (TC) treated 96-well microplate (Corning BV Life Sciences, Amsterdam, The Netherlands). The cell suspension or the assay medium consisted of the growth medium (described in Section 6.2.2.1) but without Geneticin (Escher *et al.*, 2012).

Experiment was set up in duplicates in 384-well microplates (Corning BV Life Sciences, Amsterdam, The Netherlands). Stimulated control wells were dosed with ten-fold serially diluted concentrations of the reference compound *tert*-butylhydroquinone (*t*BHQ). Test compound wells had either serially diluted (10-fold) GYM A or SPX 1 (Table 6.2). Unstimulated control wells were also prepared such as the medium blank, which contained AREc32 cells in the assay medium, and

the MeOH blank. The same arbitrary units assigned for MeOH was also used for the medium blank. Aside from the stimulated and unstimulated exposure conditions, cell-free control wells, which contained the assay medium only, were also included in the assay for background correction. The microplate was then covered with PCR-SP plate sealer (Axygen, Corning GmbH, Kaiserslautern, Germany) and incubated for 24 h before cytotoxicity or induction was assessed. The luminescence was measured at t=0 and t=24 hrs.

#### 6.2.2.3 Cell viability

Viability of adherent cell lines, such as AREc32, was measured through confluence or the percentage of the area covered by adherent cells in the microplate (Efremov *et al.*, 2013). In this study, the confluency of AREc32 cells dosed in 384-well plates was measured using an IncuCyte S3 live cell imaging system (Essen BioScience, Ann Arbor, Michigan, USA) at 37 °C and 5% CO<sub>2</sub> and quantitatively analyzed using the IncuCyte S3 software. Confluence was obtained by subtracting the luminescence measurements right after dosing (t=0) from measurements after 24 hours of incubation (t=24) (Neale *et al.*, 2018; Nivala *et al.*, 2018).

#### 6.2.3 CellSensor® NfκB-bla THP-1 assay for inflammation

##### 6.2.3.1 Cell and culture conditions

THP-1 human leukemia cell lines were transfected with lentivirus to express the β-lactamase (βlac) reporter gene that is under the control of the Nuclear Factor-kappa B (NF-κB) response element. The activity of βlac was determined by fluorescence resonance energy transfer (FRET) technique (Figure 6.3). FRET technique used two fluorescent substrates– coumarin and fluorescein. In the absence of βlac, the substrate complex remains intact. The excitation of coumarin at 409 nm resulted in FRET to fluorescein, which emits a green fluorescence signal (520 nm). In the presence of βlac, the lactam ring of the substrate complex was cleaved. As a result of the substrate being enzymatically separated from one another, FRET was disrupted. At this state, the excitation of coumarin at 409 nm emits a blue fluorescence signal at 447 nm. The ratio of the fluorescence emission signal, blue:green, was determined by the translation of βlac in cells (Miller *et al.*, 2010).

The commercially available CellSensor® NF-κB-bla THP-1 Cell Line (Invitrogen, Thermo Fisher Scientific, Scoresby, Australia) was used in this study. The cell lines were maintained in T75 flasks with 10 mL Roswell Park Memorial Institute (RPMI) medium, 1% sodium pyruvate, 10% Fetal Bovine Serum (FBS), 1% non-essential amino acid (NEAA), 1% penicillin–streptomycin, 1% Glutamax, 5 µg mL<sup>-1</sup> Blastcidin.

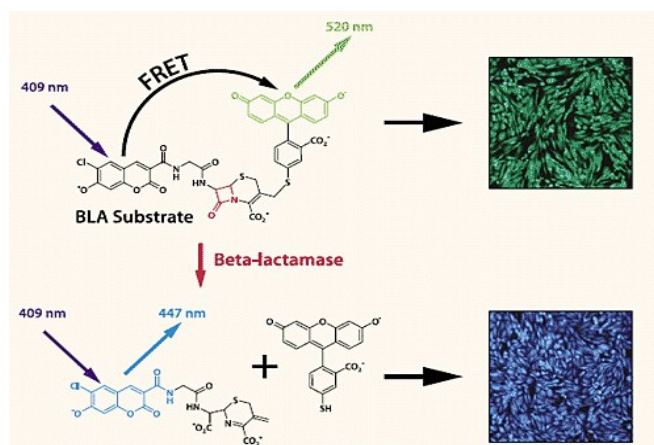


**Figure 6.3.** Measurement of  $\beta$ lac induction in Nf- $\kappa$ B-bla THP-1 using FRET (fluorescence resonance energy transfer) (Miller *et al.*, 2010).

### 6.2.3.2 Exposure experiments

Exposure experiments were adapted from König *et al.* (2017). NF- $\kappa$ B-bla THP-1 cells (30  $\mu$ L of  $6.25 \times 10^5$  cells per mL) were seeded and grown for > 6 hours in a black-coated clear bottom 384-well Falcon Becton-Dickinson (BD) plates (Corning BV Life Sciences, Amsterdam, The Netherlands). The assay medium consisted of the growth medium (described in Section 6.2.3.1) but without Blasticidin. Similar to exposure experiments in AREc32, three exposure conditions (i.e., stimulated, unstimulated and cell-free conditions), in duplicates, were performed for NF- $\kappa$ B-bla THP-1 cells.

The toxin extracts were serially diluted using 1:2 dilution series. An aliquot of 8  $\mu$ L sample solution with 0.5% dimethylsulfoxide (DMSO) were added into the cell plate containing cell mixtures in 32  $\mu$ L assay medium leading to a final DMSO concentration of 0.1%. Aside from GYM A or SPX 1, Tumor Necrosis Factor alpha (TNF $\alpha$ , Life Technologies, Mulgrave, Australia) served as the positive reference compounds. Similar to AREc32 (described in 6.2.2.2), MeOH and medium blanks were also prepared to obtain readings under unstimulated conditions. After dosing, plates were sealed with Breathe-Easy sealing membrane (Sigma-Aldrich, Steinheim, Germany) and incubated at 37°C and 5% CO<sub>2</sub>. FRET reagent with resazurin was added to the cell plates. Fluorescence was measured at 460 nm (blue) and 520 (green) directly after the addition of resazurin (t=0) and after incubation for 2 hours (t=2).

### 6.2.3.3 Cell Viability

The cell viability of NF- $\kappa$ B-bla THP-1 cells was determined by measuring the fluorescence at 665 nm of all three exposure conditions—stimulated, unstimulated and cell-free. (König *et al.*, 2017; Nivala *et al.*, 2018).

### 6.2.4. Data evaluation method

Toxicity data are normally visualized in log-sigmoidal concentration response curves (CRCs), where response is measured as a function of the concentration. For adaptive stress response pathways, where the maximum (100%) response or endpoint could not be reached, the use of log-sigmoidal CRCs is not suitable. Instead, the low-level linear concentration scale that is up to 30% of the maximum CRCs (Escher *et al.*, 2013; 2018) was used in this experiment.

#### 6.2.4.1 Cell viability and Cytotoxicity

Cell viability was first measured to determine the maximum concentration at which cells remained viable. Cell viability were measured from the confluence (described in 6.2.2.3) and fluorescence readings (described in 6.2.3.3) and calculated using equations 6.1 and 6.2, respectively (Escher *et al.*, 2012; König *et al.*, 2017; Nivala *et al.*, 2018).

$$\text{Cell viability}_{\text{AREc32}} = \frac{\% \text{ confluency}_{(\text{exposed cells})}}{\% \text{ confluency}_{(\text{unexposed cells})}} \quad (6.1)$$

$$\text{Cell viability}_{\text{NF-}\kappa\text{B}} = \frac{F_{665\text{nm}}(\text{sample}) - F_{665\text{nm}}(\text{cell free})}{F_{665\text{nm}}(\text{unexposed cell}) - F_{665\text{nm}}(\text{cell free})} \quad (6.2)$$

Cell toxicity was calculated as:

$$\text{Cell toxicity} = 1 - \text{Cell viability} \quad (6.3)$$

By applying the low-level linear CRC, the inhibitory concentration IC<sub>10</sub> for 10% reduction of cell viability was derived from the slope regression of % reduction of confluency against the dosed concentration (equation 6.4).

$$\text{IC}_{10} = \frac{10\%}{\text{slope}} \quad (6.4)$$

#### 6.2.4.2 IR: Induction of adaptive response pathway

##### *Data evaluation Induction (luminescence) for AREc32*

To avoid any cytotoxic interferences, only concentrations below the IC<sub>10</sub> (described in 6.2.4.1) were considered for the evaluation of the activation of oxidative stress response visualized by the Antioxidant Response Element (ARE).

The induction of ARE is proportional to the luciferase measured by a Luciferase Assay System (Promega E1500, Promega GmbH, Walldorf, Germany). The bioluminescent assay was used according to the Promega protocol and luminescence quantified with a FLUOstar Optima plate reader (BMG Labtech, Ortenberg, Germany). From the assay system, luciferase concentration was measured using relative light units (RLU). The induction ratio (IR) is defined as the ratio of the RLU of the sample divided by the average RLU of the controls (equation 6.5).

$$IR = \frac{RLU_{(sample)}}{\frac{\sum_{i=1}^n RLU_{(control)}}{n}} \quad (6.5)$$

##### *Data evaluation Induction (FRET) for GeneBlazer assay*

The induction of NF- $\kappa$ B is proportional to the beta-lactamase ( $\beta$ lac) production. The presence of  $\beta$ lac was measured by the FRET signal as a result of excitation at 409 nm and emission at 447 nm (blue; for activated response element) and at 520 nm (green; for inactive response element). It was recommended by Invitrogen (2006) that the fluorescence from the cell-free control wells should be subtracted from the fluorescence readings of the stimulated (TNF $\alpha$ ) and test compound wells.

$$\text{Signal}_{447\text{nm}} = [F_{447\text{nm}}(2 \text{ hrs}) - (F_{447\text{nm}}(0 \text{ hr, sample}) - F_{447\text{nm}}(0 \text{ hr, unexposed cells})) - F_{447\text{nm}}(2 \text{ hrs, cell free})] \quad (6.6)$$

$$\text{Signal}_{520\text{nm}} = [F_{520\text{nm}}(2 \text{ hrs}) - (F_{520\text{nm}}(0 \text{ hr, sample}) - F_{520\text{nm}}(0 \text{ hr, unexposed cells})) - F_{520\text{nm}}(2 \text{ hrs, cell free})] \quad (6.7)$$

The resulting blue:green ratio provides the quantitative measure of NF- $\kappa$ B activation as described by the production of  $\beta$ lac.

$$\frac{B}{G} = \frac{\text{Signal}_{447\text{nm}}}{\text{Signal}_{520\text{nm}}} \quad (6.8)$$

The induction ratio IR is the ratio between B/G of a given sample well and the associated control (cell or cell with solvent control (blown down methanol)). IR was calculated using equation 6.5.



#### 6.2.4.3 EC<sub>IR1.5</sub>: Effective concentration needed for the induction of adaptive response pathway

IR values were then plotted against the concentration and the effect levels up to an IR of less than 4 were used to derive a linear concentration-effect curve. As this experiment focused on the low level linear concentration scale, it follows equation 6.9 (Escher *et al.*, 2018).

$$\text{IR} = \text{slope} \times \text{concentration} + 1 \quad (6.9)$$

EC<sub>IR1.5</sub> is the effective concentration that causes an IR of 1.5 or an induction 50% over the control. The EC<sub>IR1.5</sub> was derived using the linear regression function forcing the line through the point x=0, y=1 (control).

$$\text{EC}_{(\text{IR}1.5)} = \frac{0.5}{\text{slope}} \quad (6.10)$$

#### 6.2.4.4 SR: Specificity Ratio

Specificity ratio (SR) is defined as the ratio between cytotoxicity (IC<sub>10</sub>) and the effective concentration (EC<sub>IR1.5</sub>) (Escher *et al.*, 2020)

$$\text{SR} = \frac{\text{IC}_{10}}{\text{EC}_{(\text{IR}1.5)}} \quad (6.11)$$

### 6.3. Results and Discussion

#### 6.3.1 AREc32 for oxidative response

##### 6.3.1.1 Reference compound *tert*-butylhydroquinone (*t*BHQ)

*t*BHQ is a known food antioxidant and is commonly used reference material for determining the induction of the oxidative stress pathway. AREc32 cells remained viable and there was no cytotoxicity observed in set-ups with *t*BHQ (Table 6.4 and Figure 6.A, in orange). The concentration that induced an induction ratio (IR) of 1.5 (EC<sub>IR1.5</sub>) was 3.0 ± 0.09 μM for *t*BHQ. This EC<sub>IR1.5</sub> is comparable to a previous study, where EC<sub>IR1.5</sub> of 1.32 ± 0.38 μM was determined (Escher *et al.*, 2012).

##### 6.3.1.2 Blank

The methanol and medium blank showed no cytotoxicity and no activation of AREc32 cells (Figure 6.4A, in green and blue (in circle), Table 6.4). The methanol in the solvent blank had been blown down (as is done for the samples) prior to the addition of the assay medium. The lack of cytotoxicity and activation indicates that the solvent residue and the assay medium did not induce cell cytotoxicity and did not induce an oxidative response.

**Table 6.4.** Inhibition concentrations ( $IC_{10}$ ) and effective concentrations ( $EC_{IR1.5}$ ) for the AREc32 assay. Experiments were performed in duplicates ( $n=2$ ) and the standard error for each concentration was measured.

	<b><i>t</i>BHQ (<math>\mu</math>M)</b>	<b>GYM A</b>	<b>SPX 1 (nM)</b>	<b>Methanol Blank</b>	<b>Medium</b>
$IC_{10}$	No cytotoxicity (up to 69.1 $\mu$ M)*	No cytotoxicity (up to 1.85 $\mu$ M)*	871 $\pm$ 162 (up to 1.36 $\mu$ M)*	No cytotoxicity	No cytotoxicity
$EC_{IR1.5}$	3.00 $\pm$ 0.09	No activation	393 $\pm$ 36	No activation	No activation
Specificity Ratio	-	-	2.2	-	-

\*highest tested concentration

### 6.3.1.3 GYM A and SPX 1

AREc32 cells administered with either GYM A or SPX 1 provided a different response on the oxidative stress pathway. No cytotoxicity and no activation of the response pathway was observed in cells treated with GYM A up to the highest tested concentration at 1.85  $\mu$ M (Figure 6.4, in violet, Table 6.4). The lack of cytotoxicity and activation indicates that GYM A (at 1.85  $\mu$ M) might not have the capacity to induce potential oxidative stress response. In contrast, cells treated with SPX 1 showed cytotoxicity at  $IC_{10} = 871.0 \pm 161.6$  nM and induction of the oxidative stress response pathway at  $EC_{IR1.5} = 393 \pm 36$  nM (Figure 6.4, in blue, Table 6.4). The difference in activity indicates that SPX 1, as compared to GYM A, is more likely to induce the oxidative stress response by activating the antioxidant response element (ARE) in the cells. Transcriptional activation of ARE offers an important role in modulating the oxidative stress (Reddy, 2008) as well as providing cryoprotective proteins against possible excess prooxidant stimuli such as reactive oxygen species (ROS) (Nguyen *et al.*, 2009; Giudice *et al.*, 2010; Zhang *et al.*, 2010). Moreover, the two-fold ratio between the  $EC_{IR1.5}$  and  $IC_{10}$  values of SPX 1 is indicative that cytotoxicity ( $IC_{10} = 871 \pm 162$  nM) did not interfere with the induction of oxidative stress response pathway ( $EC_{IR1.5} = 393 \pm 36$  nM). It is crucial that induction of oxidative stress response pathway is initiated at a concentration where cells are still viable in order to maintain suitable ARE and ROS concentration needed for cell homeostasis (Patel *et al.*, 2017). The specificity ratio (SR = 2.2, Table 6.4) of SPX 1 shows that the oxidative response in AREc32 cells is activated but not with a high specificity. A SR of  $1 \leq SR \leq 10$  describes that a compound is moderately specific to the induction of the adaptive response (Escher *et al.*, 2020).

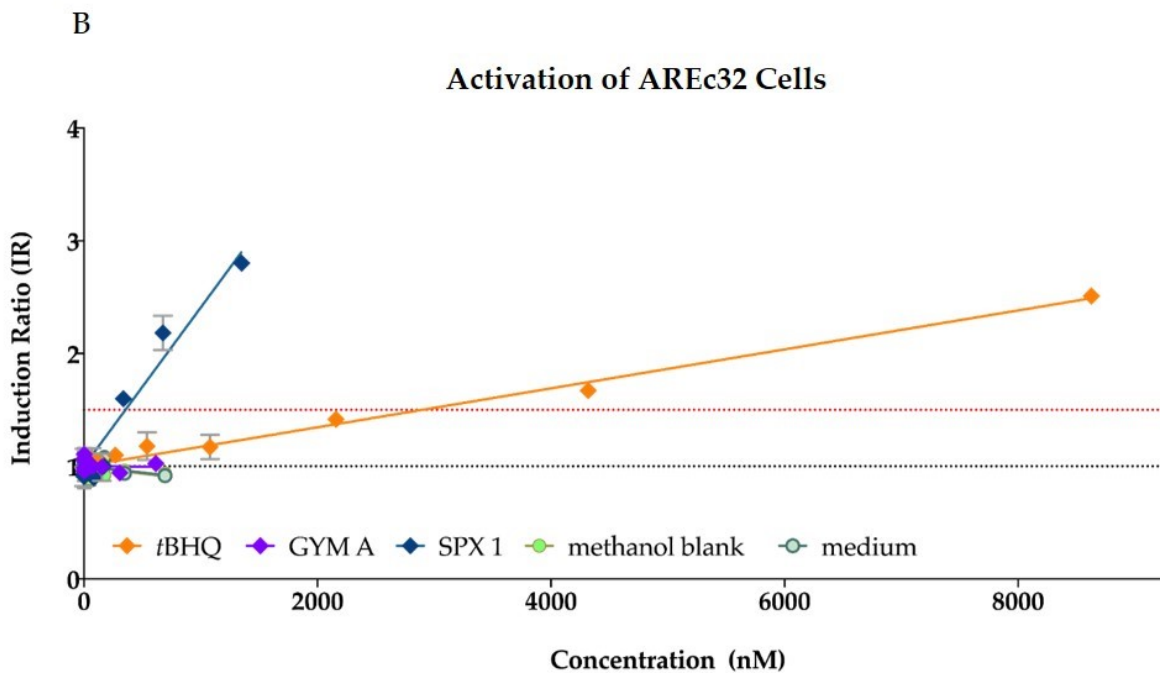
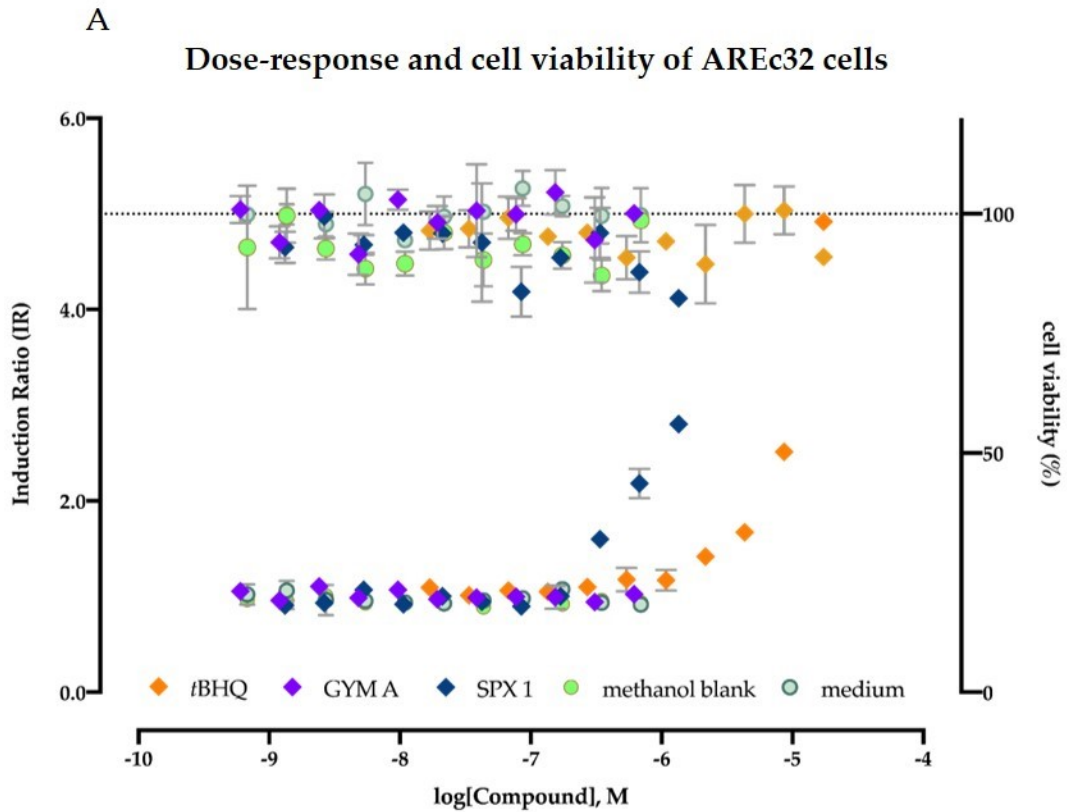


**Figure 6.4.** Activation experiments using AREc32 cell lines. (A) The induction of AREc32 cells treated with tBHQ (orange), GYM A (violet) and SPX 1 (blue) occurred when cells were still viable. No induction was observed in unstimulated treatments, which are methanol blank (green) and medium (light blue, in circle). (B) IR values that are less than 4 were used to measure the  $EC_{IR1.5}$ . Regression lines were fitted using GraphPad Prism (version 9) after y-intercept (IR) was set to 1 (IR=1 indicates control). Experiments were performed in duplicates ( $n=2$ ) and the standard error for each concentration was measured. \*For a more detailed distribution of  $EC_{IR1.5}$ , refer to Figure S11.

SPX 1 also differs in its bioactivity when compared to the antioxidant reference compound *t*BHQ. SPX 1 has a lower EC<sub>IR1.5</sub> than *t*BHQ (P-value < 0.0001, by t-test and at 95% confidence level), indicating that SPX 1 is more potent in inducing the oxidative stress response than the reference compound. The lack of activation of GYM A (at 1.85 μM) indicates that higher concentrations could be further tested to determine whether induction of oxidative stress response is possible. With respect to the tested concentrations used in this study, the order of potency is GYM A < *t*BHQ < SPX 1 for the activation of oxidative stress response in AREc32 cells.

### 6.3.2 CellSensor® *Nf-κB-bla* THP-1 assay for inflammation

#### 6.3.2.1 Reference compound tumor necrosis factor alpha (TNFα)

TNFα is a known activator of NfκB pathway that also acts as a proinflammatory protein (Bradley, 2008). No cytotoxicity was shown in the stimulated wells using TNFα. The inflammation response was observed at EC<sub>IR1.5</sub> = 659 ± 40 fM or 11.4 ± 0.7 ng L<sup>-1</sup> (Figure 6.6, in orange, Table 6.5). The result was comparable to previous studies that for TNFα had EC<sub>IR1.5</sub> = 20.0 ± 0.4 ng L<sup>-1</sup> (Neale *et al.*, 2015), EC<sub>IR1.5</sub> = 11.1 ± 0.21 ng L<sup>-1</sup> (König *et al.*, 2017) and EC<sub>IR1.5</sub> = 6.8 ± 0.2 ng L<sup>-1</sup> (Hebert *et al.*, 2018).

**Table 6.5.** Effective concentrations (EC<sub>IR1.5</sub>) for the Nf-κB assay. Experiments were performed in duplicates (*n*=2) and the standard error for each concentration was measured.

	TNFα (fM)	GYM A (nM)	SPX 1 (nM)	Methanol Blank (nM)	Medium
IC <sub>10</sub>	No cytotoxicity (up to 1.9 × 10 <sup>5</sup> μM)*	No cytotoxicity (up to 2.5 μM)*	No cytotoxicity (up to 1.8 μM)*	No cytotoxicity	No cytotoxicity
EC <sub>IR1.5</sub>	659** ± 40	586 ± 68	795 ± 127	1266 ± 325	No activation

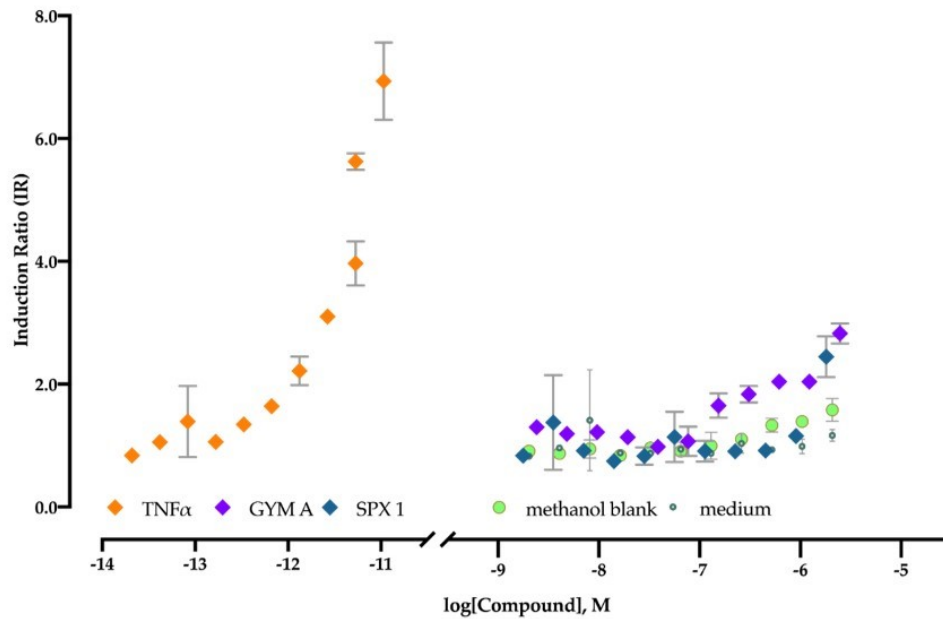
\*highest tested concentration

\*\* ng/L was converted to fM using the molecular weight of TNFα (17.3kDa)

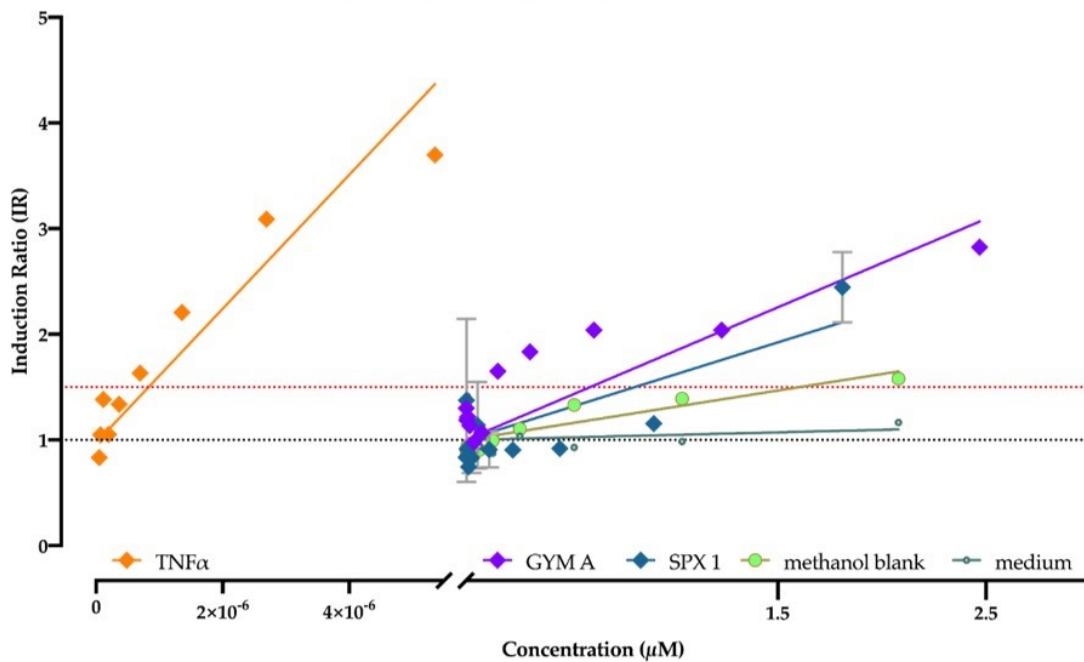
#### 6.3.2.2 Blanks

Methanol blank and medium showed no cytotoxicity in Nf-κB-*bla* THP-1 cells (Figure 6.5, in green and blue (in circle), Table 6.5). However, a response in inflammation was recorded at EC<sub>IR1.5</sub> = 1266 ± 325 nM (Figure 6.5B, in green, Table 6.5). No activation was observed in the medium blank samples.

A

Dose-response of NfκB-*bla* THP-1 cells

B

Activation of NfκB-*bla* THP-1 cells

**Figure 6.5.** Activation experiments using Nf-κB-*bla* THP-1 cell lines. (A) Nf-κB-*bla* THP-1 cells treated with TNFα (orange), GYM A (violet) and SPX 1 (blue) occurred when cells were still viable (Refer to Figure S12 for the cell viability of cells). An induction was observed in methanol blank (green) while no induction was observed in the medium blank (light blue, in circle). (B) IR values that are less than 4 were used to calculate the EC<sub>IR1.5</sub>. Regression lines were fitted using GraphPad Prism (version 9) after y-intercept (IR) was set to 1 (IR=1 indicates control). Experiments were performed in duplicates ( $n=2$ ) and the standard error for each concentration was measured.

### 6.3.2.3 GYM A and SPX 1

Nf- $\kappa$ B-*bla* THP-1 cells treated with either GYM A or SPX 1 showed a similar response on the inflammation pathway. No cytotoxicity could be recorded in cells treated with the toxins (Table 6.3, Figure 6.6) due to the large variability of the ToxBLAzer cell viability stain (see Figure S12). Large variability in the fluorescence reading might mean that during fluorescence measurement, cells with different viabilities were recorded. This account could also be attributed to the non-adherent nature of Nf- $\kappa$ B-*bla* THP-1 cells, wherein cells are not fixed to the cell plate. Nonetheless, it was still possible to measure the  $EC_{IR1.5}$  where cells were still viable (cell viability > 50%, Figure S12). Induction of Nf- $\kappa$ B was at  $EC_{IR1.5} = 586 \pm 68$  nM and  $795 \pm 127$  nM for GYM A and SPX 1, respectively. This shows that GYM A and SPX 1 can induce the Nf- $\kappa$ B signalling pathway and might activate the expression of proteins that participates in regulating inflammation. However, statistical support for  $EC_{IR1}$  values are rather low, especially for SPX 1. When compared to  $EC_{IR1}$  value of MeOH, P-values were greater than 0.0001 (by t-test and at 95% confidence level), indicating that the solvent residue and the toxins are not significantly different from one another. This observation could also mean that the solvent residue might have an effect to the activity of the toxin. Thus, further experiments (e.g., increasing the replicates) must be conducted to confirm the cell response to toxin addition.

In contrast to TNF $\alpha$ , the effective concentration needed to induce an inflammation response in GYM A and SPX 1 are in several orders of magnitude higher than the reference compound (P-value < 0.0001, by t-test and at 95% confidence level). The large difference could be accounted to the fact that TNF $\alpha$  is a large molecule (17.3 kDa or  $1.73 \times 10^4$  g mol<sup>-1</sup>) compared to GYM A (507 g mol<sup>-1</sup>) and SPX 1 (691 g mol<sup>-1</sup>). For better comparison with the reference compound, experiments where concentrations within the same range are used among the tested compounds and TNF $\alpha$  could be performed.

### 6.3.3 Implications of the oxidative stress and inflammation response of GYM A and SPX 1

Induction of any adaptive stress response pathway by either GYM A or SPX 1 has not been studied before. In this study, we describe the potential activity of the toxins to induce oxidative stress response (only for SPX 1) and inflammatory response. The production of antioxidant response elements (ARE) by SPX 1 could indicate the potential antioxidant activity of the toxin. The presence of excess oxidative-causing compounds (i.e., reactive oxygen species (ROS)) could probably be regulated by SPX 1 as it produces ARE to restore cell homeostasis. The induction of inflammatory response by GYM A and SPX 1 likely illustrates their capacity as pro-inflammatory compounds. Inflammation-stimulating compounds are important in staging cellular repair processes as a result

of infections (e.g., presence of pathogens) (Keane and Strieter, 2001). By understanding the response of GYM A and SPX 1 to oxidative stress response and inflammatory response, this study was able to provide preliminary insights that oxidative- and inflammation-mediated pathways might be the potential targets of the toxins. The targeted adaptive stress response pathway approach (visualized through reporter gene assays) also described the potential antioxidant (for SPX 1 only) and the pro-inflammatory activity of the toxins.

The effect of GYM A and SPX 1 on other cellular activities could be further explored by determining its relationship or complementarity to the previously known bioactivities of the toxin. Previous studies have also demonstrated that the toxins have different activities at the receptor and cellular levels. Receptor and inhibition binding assays showed that both toxins do not strongly interact with muscarinic acetylcholine receptors (mAChRs) but both are known antagonist to nicotinic acetylcholine receptors (nAChRs) (Kharrat *et al.*, 2008; Bourne *et al.*, 2010; Wandescheer *et al.*, 2010; Hauser *et al.*, 2012; Aráoz *et al.*, 2015, Cuesnon *et al.*, 2016). The AChRs as targets for GYM A and SPX 1 was also supported by the physiological studies using neuroendocrine PC12 cells. As described in **Chapter 5**, toxins have shown to dose-dependently interact with the nicotinic and muscarinic acetylcholine receptors. Further studies could focus on the effects of the toxin starting from the molecular up to the cellular level.

GYM A and SPX 1 have consistently shown diverse selectivity towards various types of cellular targets. The different structure of the toxins plays an active part on their observed bioactivities. The similarities of their effects or mechanism may be attributed to the cyclic imine moiety and butenolide ring that are shared between the toxins (Van Wagoner *et al.*, 2014), while the difference on their actions could be due to the triketal ring system that is only present in SPX 1. Thus, the structure-activity-relationship (SAR) of the toxins provide a good basis to evaluate which structural confirmation is responsible for a certain response. SAR may indicate which structural part of the toxins are able to activate the respective transcription factors of the adaptive stress response pathways.

In summary, this chapter has demonstrated that GYM A and SPX 1 might induce adaptive stress response pathways and can potentially initiate the expression of cryoprotective proteins to regulate oxidation and inflammation. Results of the adaptive stress response bioassay provided an indication that the toxins might have the capacity to introduce change or response at the molecular level.

## CHAPTER 7

### General Discussion

#### 7.1 Isolation of Gymnodimine A (GYM A) and 13-desmethyl spirolide C (SPX 1) from mass cultures of *Alexandrium ostenfeldii*

Studies on microalgal-associated toxins are less explored because of access to pure compounds is limited. This problem is confounded by challenges in obtaining toxins directly from microalgal source as limited amounts are produced per cell. Hence, there is a need to mass produce biomass of the target organism in culture. As described in **Chapter 3**, mass cultures of two *A. ostenfeldii* strains (OKNL 48 and X-LF-19-F10), which produce GYM A and SPX 1, have been successfully established. The gradual upscaling of *A. ostenfeldii* from small to 10-L culture volumes allowed for harvesting a total of 270 L of microalgal cultures. Determining the growth rate and toxin cell quota of the microalgae aided in providing the extent of mass culture required to obtain adequate amount of target compounds. For this study, large-scale *A. ostenfeldii* cultures was targeted not only to isolate GYM A and SPX 1 but also to obtain pure toxins to be used in subsequent bioassays. Toxin recovery after purification of the crude extract with HP-20 resin eluted with ACN and through HPLC was about 10%. The solid-phase extraction (SPE)-mediated purification steps carried out for obtaining pure toxins determine the final yield of the compound. As there are many ways to perform SPE, the most suitable method that presents high recovery and purity of the toxin should be applied. This study has shown that GYM A and SPX 1 vary in their affinities to SPE columns and desorbing solvents, as indicated by the differential recovery and purity from the four tested SPE conditions. Ideally, even at the SPE-mediated purification step, yield and purity should be high. The goal of high recovery of toxin was not fully met in this study. The low recovery of 10% could be improved by trying out other SPE methods that might enhance the toxin yield. SPE or any 'clean up' procedures are important steps in isolating and purifying compounds, ensuring that microalgal extracts are initially free from impurities (i.e., semi-purified) prior to subjecting them to a more sensitive chromatographic purification (i.e., HPLC). A total of 345 µg of GYM A and 559 µg of SPX 1 were purified (> 95% purity) from the mass cultivated *A. ostenfeldii*. Less than 10 µg of the purified toxins were further used in succeeding bioassays.

The process of obtaining sufficient amounts of pure toxins from large-scale microalgal cultures was laborious. While such constraint is commonly encountered in natural product isolation-based studies, this is amplified in microalgal strains that produce toxins that are not yet structurally identified. For such studies, adequate amount of pure toxin is required so that it can be subjected to



structural characterization studies (i.e., nuclear magnetic resonance (NMR) spectroscopy). Thus, it is important to assess which parameters (both for the culture conditions and extraction methods) could be further developed and enhanced to obtain a toxin that is both high in purity and recovery.

## 7.2 Structural variability of spirolides

*A. ostenfeldii* strains AON 24, NX-56-10, and MX-S-B11 produce structurally unknown spirolides, as indicated in **Chapter 4**. Isolation of the pure novel spirolides were not possible in quantities necessary for NMR structure elucidation work, but all unknown toxins were subjected to mass-spectral (MS)-based techniques for their preliminary structural information.

### 7.2.1 On MS-based structure elucidation techniques

The combined MS-based techniques proved to be very helpful in the discovery of a number of spirolide structural analogues. As with previous studies (Hu *et al.*, 2001; Sleno *et al.*, 2004a; Ciminiello *et al.*, 2010; Aasen *et al.*, 2005; Roach *et al.*, 2009; Tillmann *et al.*, 2014; Martens *et al.*, 2017; Gunder *et al.*, 2018), this study demonstrated the wide-ranging structural diversity of spirolides. The mass spectral information from previously identified structural types of SPX were utilized as references for the structural insights of unknown SPX. This was particularly demonstrated in compound **7**, where the resulting proposed structure is a combination of SPX **1** and 20-Me SPX **G**. Interestingly, compound **7** was proposed to be a new analogue of G-type SPX, suggesting that the structural variability of SPX is higher than currently known. The use of LC-HRMS/MS, the accurate masses obtained, and the resulting elemental formula were also important in differentiating novel SPX (i.e., Compound **5**) from the known ones (Table 7.1). For compounds that have similar (exact) mass and elemental formula, fragmentation patterns were compared to distinguish them from each other (e.g., Compound **4** and **6**). This work illustrates that different approaches can be used in MS-assisted structural characterization techniques.

**Table 7.1.** Examples of unknown SPX used in this study that have identical nominal masses with known SPX described in previous studies.

Unknown SPX in this study	Exact Mass	Elemental Formula	Known SPX from previous studies	Exact Mass	Elemental Formula
Compound <b>4</b> (696 > 164)	696.4471	C <sub>41</sub> H <sub>62</sub> NO <sub>8</sub> <sup>+</sup>	20-Hydroxy-13,19-didesMethyl D (696 > 164)*	696.4473	C <sub>41</sub> H <sub>62</sub> NO <sub>8</sub> <sup>+</sup>
Compound <b>5</b> (694 > 164)	694.4679	C <sub>42</sub> H <sub>64</sub> NO <sub>7</sub> <sup>+</sup>	20-Hydroxy-13,19-didesMethyl C (694 > 164)*	694.4307	C <sub>41</sub> H <sub>60</sub> NO <sub>8</sub> <sup>+</sup>
Compound <b>6</b> (708 > 164)	708.4836	C <sub>43</sub> H <sub>66</sub> NO <sub>7</sub> <sup>+</sup>	D (708 > 164)**	708.9865	C <sub>43</sub> H <sub>66</sub> NO <sub>7</sub> <sup>+</sup>

\*Zurhelle *et al.*, 2018; \*\* Hu *et al.*, 1995

This study also indicates that the variability of spirolides is higher than previously known and does not only include the presence or absence of certain functional groups but also involves new variants of the triketal ring system. The proposed new 6:5:6 triketal ring system of compound **5** was derived after its fragmentation pattern was cross-referenced to pinnatoxins, a potent cyclic imine produced by a dinoflagellate *Vulcanodinium rugosum*. The similarity of the triketal ring system shows that the fragmentation patterns from other closely-related toxins (i.e., pinnatoxins) belonging to the same class (i.e., cyclic imines) could also be explored for SPX characterization. In doing so, MS-based structural characterization efforts could be expanded to provide detailed structural insights of other novel spirolides.

### 7.2.2. Biosynthetic pathway of spirolides

The high structural diversity of spirolides results from modifying of the nascent polyketide chain (NPC), which is the fundamental structural backbone of the toxin. Once the NPC is assembled in a predetermined length, it undergoes modifications steps to produce different SPX structural analogues. For example, the absence of unsaturation (double carbon-carbon bonds) in Compound **3**, **6** and **8** at C2-C3 is a result of the deletion of the enoyl reduction (ER), which is the metabolic step that initiates unsaturation. Structural alteration is also observed in spirolide B (Hu *et al.*, 1995; 1996), D (Hu *et al.*, 1995) and its analogues (Sleno *et al.*, 2004a; Zurhelle *et al.*, 2018), suggesting that ER is a common occurrence in SPX. Post-NPC reactions also result to major structural modifications in SPX as demonstrated by the presence of the different triketal ring system. The expansion of a 5-membered ring B of C-type SPX to a 6-membered ring B in G-type SPX is a result of a deletion step (more specifically known as Favorskii rearrangement) combined with an addition of acetate unit. Meanwhile, the absence of ring A in dispiroketal ring SPX H/I is a product of the shortening of the NPC. The different mechanisms to which SPX analogues are formed suggest that the biosynthetic pathway of the toxin is flexible and is not constrained to one definite reaction mechanism. Van Wagoner *et al.* (2014) described that the NPC of SPX could cascade to different reaction mechanisms resulting to diverse substructures. The different reaction pathways suggested in SPX production could also be attributed to the fact that marine phycotoxins, including SPX, are naturally metabolized compounds. As such, several types of enzymatic systems (e.g., polyketide synthase) can produce NPC and induce post-NPC changes (Rossini and Hess, 2010).

Spirolides likely share a common biosynthetic pathway to its structurally-related toxins, gymnodimine (GYM) and pinnatoxin (PnTX) (Van Wagoner *et al.*, 2014). When the structures of the three cyclic imines were compared, SPX was observed to share similar and combined structures of

GYM and PnTX (Figure 7.1). This gives strong evidence that the pathway of SPX synthesis might diverge from the biosynthetic pathways of GYM and PnTX. Consequently, it is suggested that the toxin classes may also share some common biosynthetic genes (Van Wagoner *et al.*, 2014). The close association of SPX and GYM has been described when the toxins were simultaneously produced by *Alexandrium ostenfeldii* strains (Van Wagoner *et al.*, 2011; Van de Waal *et al.*, 2015; Harju *et al.*, 2016; Martens *et al.*, 2017; Zurhelle *et al.*, 2018). While there has been no evidence yet that SPX co-occur with PnTX in a single microalgal strain, this study provides initial information on how biosynthesis of SPX might be related to PnTX. The proposed novel 6:5:6 triketal ring system in compound **5**, which has only been identified in PnTX, strongly supports the assumption that SPX and PnTX may indeed share common biosynthetic genes. These genes may encode similar, if not the same, enzymes that drives the assembly of NPC, including the triketal ring system. The similarity of structural features among SPX and its closely related toxins (i.e., GYM or PnTX) are also observed in other marine phycotoxin groups. In fact, the ether ring system (e.g., triketal rings) is exclusively shared among toxins produced by dinoflagellates. Different ether ring systems, ranging from five- to nine-membered rings, may be joined together forming a ladder frame (e.g., brevetoxins) or may be fused in a spirocyclic rings (e.g., SPX, GYM and PnTX) or both (Van Wagoner *et al.*, 2014).

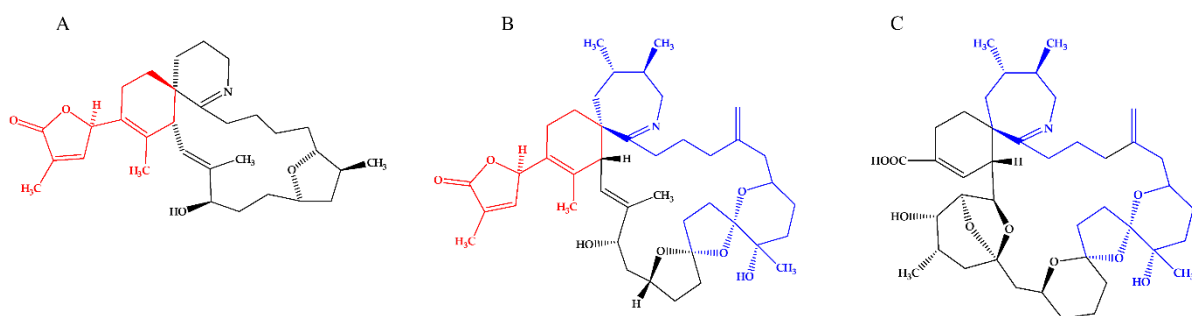


**Figure 7.1.** Structural configuration of **(A)** gymnodimine A (GYM A), **(B)** 13-desmethyl C (SPX 1) and **(C)** Pinnatoxin A (PnTX A) (modified from Van Wagoner *et al.*, 2014). Red color corresponds to the shared structure of GYM A and SPX 1. Blue color corresponds to the shared structure between SPX 1 and PnTX A.

### 7.3 Bioactivities of GYM A and SPX 1

The bioactivity of purified GYM A and SPX 1 was determined through their effects on intracellular calcium concentrations ( $[Ca]_i$ )- (**Chapter 5**) and adaptive stress response-mediated assays (**Chapter 6**).

### 7.3.1. Cellular effects of GYM A and SPX 1

GYM A and SPX 1 elicited differential effects at the cellular level as measured by intracellular calcium concentrations ( $[Ca]_i$ ) of mammalian neuroendocrine PC12 cells (**Chapter 5**). SPX 1 was more specific than GYM A in activating acetylcholine receptor (AChR) subtypes, indicating that the toxins have different binding profiles towards AChRs. Nonetheless, both act as stimulating compounds that could mimic the agonist acetylcholine (ACh). This observation means that toxins interact with AChR subtypes and, as a result, initiate a cascade of cellular reactions as indicated from the change of  $[Ca]_i$ . While previous inhibition and receptor binding assays identified the binding activity of the toxins to cell membrane receptors (Kharrat *et al.*, 2008; Bourne *et al.*, 2010; Hauser *et al.*, 2012; Wandscheer *et al.*, 2010; Aráoz *et al.*, 2015), it is also important to describe the cellular response of whole cells considering that cells comprised several types of receptors that are linked to different cell signaling pathways (Campbell and Reece, 2002).

Similar and yet different bioactivities were likewise observed in GYM A and SPX 1 as indicated by adaptive stress response pathways (**Chapter 6**). While both toxins are likely to induce inflammation, only SPX 1 was found to potentially counteract excess reactive oxygen species (ROS), suggesting that toxins might play a role in restoring cell homeostasis. As the induction of the adaptive stress response pathways were visualized through reporter gene assays, it was inferred that GYM A and SPX 1 have the potential to specifically target gene-regulations. Thus, the effect of the toxin at molecular level could also be explored in the future.

The mechanism of action of GYM A and SPX 1 at the cellular and molecular level are described in this study. Previous bioassay results provided information about the effects of toxins on mice (Munday *et al.*, 2012; Otero *et al.*, 2012) and on cell membrane receptors (Gill *et al.*, 2003; Munday *et al.*, 2004; Kharrat *et al.*, 2008; Bourne *et al.*, 2010; Wandscheer *et al.*, 2010; Hauser *et al.*, 2012; Aráoz *et al.*, 2015; Cuesnon *et al.*, 2016). The approaches used in this study shed light on the extensive capability of the toxins to initiate effects at the molecular level changing cellular signaling. Furthermore, the differential effects of the toxins observed in this study supports the selective interaction of GYM A and SPX 1 described in previous inhibition and receptor binding assays, illustrating how the structural difference of the two toxins play a role in their respective bioactivity.

### 7.3.2. Implications on the structure-activity relationship (SAR) of GYM A and SPX 1

As there is a strong relationship between the structure of GYM A and SPX 1, it can be assumed that there is also a similar underlying mode of action. This assumption has been inferred from the

inhibition and receptor binding assays, where the differential effects of GYM A and SPX 1 to the AChR subtypes has been reported (Gill *et al.*, 2003; Munday *et al.*, 2004; Kharrat *et al.*, 2008; Bourne *et al.*, 2010; Wandscheer *et al.*, 2010; Hauser *et al.*, 2012; Aráoz *et al.*, 2015; Cuesnon *et al.*, 2016). This study further supports the SAR of the toxins as demonstrated by the diverse effects in both molecular and cellular level. The common structural features, which are the cyclic imine moiety and the butenolide side chain (in red, Figure 6.1), might explain the shared bioactivity of the two toxins. The similar effect on nAChRs and the induction of the inflammation response pathway might be due to the shared structural motifs in GYM A and SPX 1. Likewise, the triketal ring system that is found in SPX 1 but not in GYM A, could be the reason for the different effects observed between the two toxins. The constitutive effect on mAChRs (**Chapter 5**) and the induction of the oxidative stress response pathway (**Chapter 6**) were distinctly observed in SPX 1-treated cell, suggesting the role of the triketal ring system for this specific bioactivity.

The role of the cyclic imine moiety and the triketal ring system have been intensively described in previous studies particularly those that focused on spiroptides. The difference in toxicity between the intact cyclic imines and their hydrolyzed forms, in which the imine group is hydrolyzed to a primary amine, indicates the importance of the cyclic imine in inducing biological effects (Hu *et al.*, 1996). The fundamental role of the triketal ring system was demonstrated when dispiroketal ring system SPX H and I were found inactive in mouse bioassays despite having an intact cyclic imine (Roach *et al.*, 2009). While the bioactivity of the two distinct chemical features have been clearly described, the potential role of the butenolide side chain as a pharmacophore (or the structural part of the compound that induces an effect) could also be investigated. There is an indication that butenolide side chain might be a pharmacophore as described by the molecular and cellular effects from this study as well as the receptor-binding assay from previous reports. In particular, the reason behind the activation of mAChRs by GYM A (but not in SPX 1) described in this study and its reversible effects in nAChRs (Kharrat *et al.*, 2008) might be attributed to the butenolide side chain that is not linked to a triketal ring system. Taking into account all the bioassays conducted for GYM A and SPX 1, it implies that the pharmacophores responsible for the extended bioactivity of the toxins include the cyclic imine moiety, triketal ring system and probably the butenolide side chain.

#### 7.4 Outlook of the study

The study of phycotoxins is an interplay of the biology and ecology of toxin-producing organism and the structure and mechanism of the toxin they produce. The role of the toxin-producing microalgae (i.e., *A. ostenfeldii*) is significant in cyclic imine isolation studies as it limits the

amount of toxins produced, isolated, purified; consequently, controlling for factors that are needed to mass propagate them are essential. To further improve the growth and culture conditions on a large-scale setting, microalgal cultures could be grown in a controlled environment where both the physical (e.g., mixing) and chemical parameters (e.g., pH of the bulk cultures are continuously regulated (Medhioub *et al.*, 2011; Beunzenberg *et al.*, 2012). While the use of sophisticated photobioreactors provides an excellent option, these requires high input and can be costly and it is suggested to consider other simpler and cost-effective mass culture procedures. Gymnodimine or spirolide extraction and purification must also be optimized to reduce losses during each purification step and/or keeping them at the minimum. Optimization could include selecting the most suitable pre-HPLC purification conditions that removes impurities as well as provides high-yielding fractions that are also pure.

The availability of pure phycotoxins, especially new and structurally unknown GYM and SPX, would be advantageous to structural characterization and mode of action studies. While the structural proposals through MS-based techniques provide detailed insights into novel toxins, there is a need to confirm the full structural profile of the compounds through NMR. This will clarify the uncertainties posed by MS-based structural characterization and the absolute configuration including the spatial arrangement of each functional group can be determined.

With the structure at hand, SAR-targeted approach could be applied to pinpoint the pharmacophore of the spiroimines. This could be achieved by performing bioassays on the different structural types of GYM or SPX. Through SAR studies, the functional group responsible for a specific toxicity could be identified. It is suggested to initially explore *in silico* analysis (e.g., quantitative structure–activity relationship models (QSARS), Polishchuk, 2017) in order to provide insights in the toxin activity without compromising the pure extracts. Information from both *in silico* analysis and current bioactivity of the cyclic imines could be used as a baseline to determine the additional assays that could be performed on the toxins. Using wide array of different bioassays could provide the much-needed evidence to evaluate which structural motif is responsible for the mechanism of action of GYM or SPX.

Pharmacophores, especially those that are naturally produced, are noteworthy because they could offer mechanism of action that are novel or similar to known therapeutic or medicinal drugs. Identifying pharmacophores in cyclic imines could benchmark its potential application in pharmaceuticals. Considering that these toxins affect AChRs and has the potential to activate

inflammatory response pathways, it is interesting to test their capability as neuromuscular and pro-inflammatory drugs. As cyclic imines can potentially threaten humans, identifying of the pharmacophore/s could hasten the development of treatment methods caused by the possible spiroimine poisoning.

While the possibilities for further studies on cyclic imines are endless, studies that will focus on elucidating potential ecological role(s) should seriously be considered. Once adequate pure toxins are available, ecologically relevant investigations should be performed in order to determine the effect of toxins at the population, if not ecosystem, level. The knowledge and understanding of the mechanisms of action of cyclic imines could hopefully direct us to determine its ecological function.

## REFERENCES

- Aasen, J.; MacKinnon, S.L.; LeBlanc, P.; Walter, J.A.; Hovgaard, P.; Aune, T.; Quilliam, M.A. Detection and Identification of Spirolides in Norwegian Shellfish and Plankton. *Chem. Res. Toxicol.* **2005**, *18*, 509–515.
- Abe, M.; Inoue, D.; Matsunaga, K.; Ohizumi, Y.; Ueda, H.; Asano, T.; Murakami, M.; Sato, Y. Goniiodomin A, an Antifungal Polyether Macrolide, Exhibits Antiangiogenic Activities Via Inhibition of Actin Reorganization In Endothelial Cells. *J. Cell. Physiol.* **2002**, *190*, 109–116
- Albuquerque, E.X.; Pereira, E.F.R.; Alkondon, M.; Rogers, S.W. Mammalian Nicotinic Acetylcholine Receptors: From Structure to Function. *Physiol. Rev.* **2008**, *89*, 73-120.
- Almandoz, G.O.; Montoya, N.G.; Hernando, M.P.; Benavides, H.R.; Carignan, M.O.; Ferrario, M.E. Toxic Strains of the *Alexandrium ostenfeldii* Complex in Southern South America (Beagle Channel, Argentina). *Harmful Algae.* **2014**, *37*, 100–109.
- Álvarez G, Uribe E, Ávalos P, Mariño C, Blanco J. First Identification of Azaspiracid and Spirolides in *Mesodesma donacium* and *Mulinia edulis* from Northern Chile. *Toxicon.* **2010**, *55*:638–641.
- Anderson, D.M., Glibert, P.M.; Burkholder, J.M. Harmful Algal Blooms and Eutrophication: Nutrient Sources, Composition, and Consequences. *Estuaries.* **2002**, *25*, 704–726.
- Anderson, D.M.; Hoagland, P.; Kaoru, Y.; White, A.W. Estimated Annual Economic Impacts from Harmful Algal Blooms (HABs) in the United States. National Oceanic and Atmospheric Administration. **2000**
- AOAC. Official methods of analysis (15th ed.). Association of Official Analytical Chemists, Washington DC, USA. **1990**
- Aráoz, R.; Ouanounou, G.; Iorga, B.I.; Goudet, A.; Alili, D.; Amar, M.; Benoit, E.; Molgó, J.; Servent, D.; The Neurotoxic Effect of 13,19-Didesmethyl and 13-Desmethyl Spirolide C Phycotoxins Is Mainly Mediated by Nicotinic Rather Than Muscarinic Acetylcholine Receptors. *Tox. Sci.* **2015**, *147*, 156–157.
- Assmy, P., Lochte, K. and Smetacek, V. Plankton productivity and the role of iron in Southern Ocean, Biological studies in polar oceans: exploration of life in icy waters ; 35 research reports and reviews / Gotthilf and Irmtraut Hempel (ed.) Bremerhaven : Wirtschaftsverl. NW, Verl. für neue Wissenschaft, ISBN: 978-3-86509-865-8. **2009**
- Bacchiocchi S.; Siracusa M.; Campacci D.; Ciriaci M.; Dubbini A.; Tavoloni T.; Stramenga A.; Gorbi S.; Piersanti A. Cyclic Imines (CIs) in Mussels from North-Central Adriatic Sea: First Evidence of Gymnodimine A in Italy. *Toxins.* **2020**, *12*(6), 370.
- Balech, E.; Tangen, K. Morphology and Taxonomy of Toxic Species in the Tamarensis group (Dinophyceae): *Alexandrium excavatum* (Braarud) comb. nov. and *Alexandrium ostenfeldii* (Paulsen) comb. nov. *Sarsia* **1985**, *70* (4), 333–343.
- Berdalet, E.; Fleming, L.; Gowen, R.; Davidson, K.; Hess, P.; Backer, L.; Enevoldsen, H. Marine Harmful Algal Blooms, Human Health and Wellbeing: Challenges and Opportunities in the 21st Century. *J. Mar. Biol.* **2016**, *96*(1), 61-91.
- Berridge, M.J.; Lipp, P.; Bootman, M.D. The Versatility of Calcium Signaling. *Nat. Rev. Mol. Cell Biol.* **2000**, *1*, 11-21.
- Beuzenberg, V., Mountfort, D., Holland, P. *et al.* Optimization of growth and production of toxins by three dinoflagellates in photobioreactor cultures. *J. Appl. Phycol.* **2012**, *24*, 1023–1033



- Bickmeyer, U.; Grube, A.; Klings, K.W., Pawlick, J.R.; Köck, M. Siphonodictyal B1 from a Marine Spong Increases Intracellular Calcium Levels Comparable to Ca<sup>2+</sup>-ATPase (SERCA) Inhibitor Thapsigargin. *Mar. Biotechnol.* **2010**, *12*, 267-272.
- Binzer, S.B.; Svenssen, D.K.; Daugbjerg, N.; Alves-de-Souza, C.; Pinto, E.; Hansen, P.J.; Larsen, T.O.; Varga, E. A-, B- and C-type Prymnesins are Clade Specific Compounds and Chemotaxonomic Markers in *Prymnesium parvum*. *Harmful Algae.* **2019**, *81*, 10-17.
- Biré, R.; Krysz, S.; Frémy, J.-M.; Dragacci, S.; Stirling, D.; Kharrat, R. First Evidence on Occurrence of Gymnodimine in Clams from Tunisia. *J. Nat. Toxins.* **2002**, *11*, 269–275.
- Blanco, S.L.; Rodríguez, L.P.; Lago, J.; Vieites, J.M.; Cabado, A.G. Potential Uses and Medical Management of Neurotoxic Phycotoxins. In: Kim, S-W, ed. *Encyclopedia of Marine Biotechnology.* **2020**, pp. 1581-1617
- Bourne, Y.; Radić, Z.; Aráoz, R.; Talley, T.T.; Benoit, E.; Servent, D.; Taylor, P.; Molgó, J.; Marchot, P. Structural Determinants in Phycotoxins an AChBP Conferring High Affinity Binding and Nicotinic AChR Antagonism. *PNAS.* **2010**, *107* (13), 6076-6081.
- Brann, M.R.; Ellis, J.; Jørgensen, H.; Hill-Eubanks, D.; Jones, S.V.P. Chapter 12: Muscarinic Acetylcholine Receptor Subtypes: Localization and Structure/Function. *Prog. Brain Res.* **1993**, *98*, 121-127.
- Cardenas, M.E.; Sanfridson, A.; Cutler, N.S.; Heitman, J. Signal-transduction Cascades as Targets for Therapeutic Intervention by Natural Products. *Trend Biotechnol.* **1998**, *16*(10), 427-433
- Catterall, W.A. Structure and Function of Voltage-gated Ion Channels. *Annu. Rev. Biochem.* **1995**, *64*, 493-531.
- Cembella, A.D. Chemical Ecology of Eukaryotic Microalgae in Marine Ecosystem. *Phycologia.* **2003**, *42*(4), 420-447.
- Cembella, A.D., Bauder, A.G., Lewis, N.I., Quilliam, M.A. Association of the Gonyaulacoid Dinoflagellate *Alexandrium ostenfeldii* with Spirolide Toxins in Size-fractionated Plankton. *J. Plankton Res.* **2001**, *23* (12), 1413–1419.
- Cembella, A.D.; Bauder, A.G.; Lewis, N.I.; Quilliam, M.A.; Hancock, S. **1999**. Planktonic Origin and Spatio-temporal Distribution of Spirolides at Nova Scotian Aquaculture Sites. In: Martin, J.L., Haya, K. (Eds.), Sixth Canadian Workshop ARTICLE IN PRESS K.E. Gribble et al. / Deep-Sea Research II 52 (2005) 2745–2763 2761 on Harmful Marine Algae. Canadian Technical Report of Fisheries and Aquatic Sciences, pp. 99–101.
- Cembella, A.D.; Lewis, N.I.; Quilliam, M.A. The marine dinoflagellate *Alexandrium ostenfeldii* (Dinophyceae) as the Causative Organism of Spirolide Shellfish Toxins. *Phycologia.* **2000**, *39*, 67–74.
- Cho, K.; Heo, J.; Han, J.; Hong, H.D.; Jeon, H.; Hwang, H.-J.; Hong, C.-Y.; Kim, D.; Han, J.W.; Baek, K. Industrial Applications of Dinoflagellate Phycotoxins Based on Their Modes of Action: A Review. *Toxins.* **2020**, *12*(12), 805.
- Christian, B.; Below, A.; Dreßler, N.; Scheibner, O.; Luckas, B.; Gerdt, G. Are Spirolides Converted in Biological Systems? - A study. *Toxicon.* **2008**, *51*(5), 934-940.
- Ciminiello, P.; Dell’Aversano, C.; Fattorusso, E.; Forino, M.; Grauso, L.; Tartaglione, L.; Guerrini, F.; Pistocchi, R. Spirolide Toxin Profile of Adriatic *Alexandrium ostenfeldii* Cultures and Structure Elucidation of 27-Hydroxy-13,19-Didesmethyl Spirolide C. *J. Nat. Prod.* **2007**, *70*, 1878–1883.
- Ciminiello, P.; Dell’Aversano, C.; Iacovo, E.D.; Fattorusso, E.; Forino, M.; Grauso, L.; Tartaglione, L.; Guerrini, F.; Pezzolesi, L.; Pistocchi, R. Characterization of 27-hydroxy-13-desmethyl spirolide C and 27-oxo-13,19-didesmethyl spirolide C. Further insights into the complex Adriatic *Alexandrium ostenfeldii* toxin profile. *Toxicon.* **2010**, *56*, 1327–1333.

- Colin, S.P.; Dam, H.G. Effects of the Toxic Dinoflagellate *Alexandrium fundyense* on the Copepod *Acartia hudsonica*: A Test of the Mechanisms That Reduce Ingestion Rates. *Mar. Ecol. Prog. Ser.* **2003**, *248*, 55-65
- Couesnon, A.; Aráoz, R.; Iorga, B.I.; Benoit, E.; Reynaud, M.; Servent, D.; Molgó, J. The Dinoflagellate Toxin 20-Methyl Spirolide-G Potently Blocks Skeletal Muscle and Neuronal Nicotinic Acetylcholine Receptors. *Toxins.* **2016**, *8*, 249.
- Dell'Aversano, C.; Tartaglione, L. Recent Advances in the Analysis of Marine Toxins. In: Diogène, J.; Campàs, M., eds. *Comprehensive Analytical Chemistry*. Volume 78. **2017**, 1-466
- Dragunow, M.; Trzoss, M.; Brimble, M.A.; Cameron, R.; Beuzenberg, V.; Holland, P.; Mountfort, D. Investigations into the Cellular Actions of the Shellfish Toxin Gymnodimine and Analogues. *Environ. Toxicol. Pharmacol.* **2005**, *20* (2), 305-312
- Efremov, Yu.M.; Dokrunova, A.A.; Bagrov, D.V.; Kudryashova, K.S.; Sokolova, O.S.; Shaitan, K.V. The Effects of Confluency on Cell Mechanical Properties. *J. Biomech.* **2013**, *46* (6), 1081-1087
- EFSA Panel on Contaminants in the Food Chain (CONTAM). Scientific Opinion on marine biotoxins in shellfish – Cyclic imines (spirolides, gymnodimines, pinnatoxins and pteriatoxins). *EFSA J.* **2010**, *8*, 1628–1667.
- Eglen, R.M. Muscarinic Receptor Subtype Pharmacology and Physiology. *Prog. Med. Chem.* **2005**, *43*, 105-136.
- Escher, B.I.; Henneberger, L.; König, M.; Schlichting, R.; Fischer, F.C. Cytotoxicity Burst? Differentiating Specific from Nonspecific Effects in Tox21 *in Vitro* Reporter Gene Assays. *Environ. Health Perspect.* **2020**, *128*(7), 77007.
- Escher, B.I.; Dutt, M.; Maylin, E.; Tang, J.Y.M.; Toze, S.; Wolf, C.R.; Lang, M. Water Quality Assessment Using the AREC32 Reporter Gene Assay Indicative of the Oxidative Stress Response Pathway. *J. Environ. Monit.* **2012**, *14*, 2877–2885.
- Escher, B.I.; Leusch, F. Bioanalytical Tools in Water Quality Assessment. IWA, London, UK. **2012**.
- Escher, B.I.; Neale, P.A.; Villeneuve, D. The Advantages of Linear Concentration–Response Curves for *In Vitro* Bioassays with Environmental Samples. *Environ. Toxicol. Chem.* **2018**, *37*(9), 2273–2280,
- Escher, B.I.; van Daele, C.; Dutt, M.; Tang, J.Y.M.; Altenburger, R. Most Oxidative Stress Response In Water Samples Comes from Unknown Chemicals: The Need for Effect-Based Water Quality Trigger Values. *Environ. Sci. Technol.* **2013**, *47*, 7002–7011.
- Farabegoli F.; Blanco L.; Rodríguez L.P.; Vieites J.M.; Cabado A.G. Phycotoxins in Marine Shellfish: Origin, Occurrence and Effects on Humans. *Mar Drugs.* **2018**, *16*(6), 188.
- Fraga, S.; Sánchez, F. Toxic and Potentially Toxic Dinoflagellates Found in Galacian Rias (NW Spain). In: Anderson, D.M.; White, A.; Baden, D., eds. *Toxic Dinoflagellates. Elsevier Science Publishing Co., Inc., New York*, **1985**, pp. 51–54
- Friis, S.; Mathes, C.; Sunesen, M.; Bowlby, M.R.; Dunlop, J. Characterization of compounds on nicotinic acetylcholine receptor alpha7 channels using high throughput electrophysiology. *J. Neurosci. Methods.* **2009**, *177* (1), 142-148.
- García Camacho, F.; Gallardo Rodríguez, J.; Sánchez Mirón, A.; Cerón García, M.C.; Belarbi, E.H.; Chisti, Y.; Molina Grima, E. Biotechnological Significance of Toxic Marine Dinoflagellates. *Biotechnol. Adv.* **2007**, *25* (2), 176-194

- Gill, S.; Murphy, M.; Clausen, J.; Richard, D.; Quilliam, M.; MacKinnon, S.; LaBlanc, P.; Mueller, R.; Pulido, O. Neural Injury Biomarkers of Novel Shellfish Toxins, Spirolides: A Pilot Study Using Immunochemical and Transcriptional Analysis. *Neurotoxicology*. **2003**, *24*, 593-604.
- Glibert, P.M.; Anderson, D.M.; Gentien, P.; Granéli, E.; Sellner, K.G. The Global, Complex Phenomena of Harmful Algal Blooms. *Oceanography*. **2005**, *18*, 136-147.
- Glibert, P.M.; Icarus Allen, J.; Bouwman, A.F.; Brown, C.W.; Flynn, K.J.; Lewitus, A.J.; Madden, C.J. Modeling of HABs and Eutrophication: Status, Advances, Challenges. *J. Mar. Syst.* **2010**, *83* (3-4), 262-275
- Gobler, C. J. Climate Change and Harmful Algal Blooms: Insights and Perspective. *Harmful Algae*. **2020**, *91*.
- Gotti, C.; Zoli, M.; Clementi, F. Brain Nicotinic Acetylcholine Receptors: Native Subtypes and Their Relevance. *Trends Pharmacol. Sci.* **2006**, *27*, 482-491.
- Grattan, L.M.; Holobaugh, S.; Morris, J.G. Harmful Algal Blooms and Public Health. *Harmful Algae*. **2016**, *57*, 2-8.
- Gribble, K.E.; Keafer, B.A.; Quilliam, M.A.; Cembella, A.D.; Kulis, D.M.; Manahan, A.; Anderson, D.M. Distribution and toxicity of *Alexandrium ostenfeldii* (Dinophyceae) in the Gulf of Maine, USA. *Deep-Sea Res. II*. **2005**, *52*, 2745-2763.
- Guéret, S.M.; Brimble, M.A. Synthetic Studies Toward the Spiroimine Unit of the Spirolides. *Pure Appl. Chem.* **2011**, *83*(3), 425-433.
- Guinder, V.A.; Tillmann, U.; Krock, B.; Delgado, A.L.; Krohn, T.; Garzón Cardona, J.E.; Metfies, K.; Abbate, C.L.; Silva, R.; Lara, R. Plankton Multiproxy Analyses in the Northern Patagonian Shelf, Argentina: Community Structure, Phycotoxins, and Characterization of Toxic *Alexandrium* Strains. *Front. Mar. Sci.* **2018**, *5*, 394.
- Hallegraeff, G.M. 2014. Harmful Algae and Their toxins: Progress, Paradoxes and Paradigm shifts. In: Rossini, G.P. (ed.). *Toxins and Biologically Active Compounds from Microalgae*. CRC Press. **2014**, pp. 3-20.
- Hallegraeff, G.M. Algal blooms and Their Apparent Global Increase. *Phycologica*. **1993**, *32*(2), 79-99.
- Harju, K.; Koskela, H.; Kremp, A.; Suikkanen, S.; La Iglesia, P. de; Miles, C.O.; Krock, B.; Vanninen, P. Identification of Gymnodimine D and Presence of Gymnodimine Variants in the Dinoflagellate *Alexandrium ostenfeldii* from the Baltic Sea. *Toxicon*. **2016**, *112*, 68-76.
- Hauser, T.A.; Hepler, C.D.; Kombo, D.C.; Grinevich, V.P.; Kiser, M.N.; Hooker, D.N.; Zhang, J.; Mountfort, D.; Selwood, A.; Akireddy, S.R.; Letchworth, S.R.; Yohanne, D. Comparison of Acetylcholine Receptor Interactions of the Marine Toxins, 13-desMethylspirolide C and Gymnodimine. *Neuropharmacology*. **2012**, *62*(7), 2239-2250.
- Hess, P. Requirements for Screening and Confirmatory Methods for the Detection and Quantification of Marine Biotoxins in End-Product and Official Control. *Anal. Bioanal. Chem.* **2010**, *397*, 1683-1694.
- Hoagland, P.; Scatasta, S. The Economic Effects of Harmful Algal Blooms. In: Granéli, E.; Turner, J., eds., *Ecology of Harmful Algae*. Ecology Studies Series. Dordrecht: Springer Verlag. **2006**
- Hu, T.; Burton, I.W.; Cembella, A.D.; Curtis, J.M.; Quilliam, M.A.; Walter, J.A.; Wright, J.L.C. Characterization of Spirolides A, C, and 13-desmethyl C, New Marine Toxins Isolated from Toxic Plankton and Contaminated shellfish. *J. Nat. Prod.* **2001**, *64*, 308-312.
- Hu, T.; Curtis, J.M.; Oshima, Y.; Quilliam, M.A.; Walter, J.A.; Watson-Wright, W.M.; Wright, J.L.C. Spirolides B and D, Two novel Macrocycles Isolated from the Digestive Glands of Shellfish. *J. Chem. Soc. Chem. Commun.* **1995**, 2159-2161.

- Hu, T.; Curtis, J.M.; Walter, J.A.; Wright, J.L.C. Characterization of Biologically Inactive Spirolides E and F: Identification of the Spirolide Pharmacophore. *Tetrahedron Lett.* **1996**, *37*, 7671–7674.
- Hummert, C.; Rühl, A.; Reinhardt, K.; Gerdt, G.; Luckas, B. Simultaneous Analysis of Different Algal Toxins by LC-MS. *Chromatographia.* **2002**, *55*, 673–680.
- Hurst, R.; Rollema, H.; Bertrand, D. Nicotinic Acetylcholine Receptors: From Basic Science to Therapeutics. *Pharmacol. Therapeut.* **2013**, *1*, 22–54.
- Ianora, A.; Bentley, M.G.; Caldwell, G.S.; *et al.* The Relevance of Marine Chemical Ecology to Plankton and Ecosystem Function: An Emerging Field. *Mar. Drugs.* **2011**, *9*(9), 1625–1648.
- Jacobson, D.M.; Anderson, D.M. Widespread Phagocytosis of Ciliates and Other Protists by Marine Mixotrophic and Heterotrophic Thecate Dinoflagellates. *J. Phycol.* **1996**, *32* (2), 279–285.
- John, U.; Cembella, A.; Hummert, C.; Elbrächter, M.; Groben, R.; Medlin, L. Discrimination of the Toxicogenic Dinoflagellates *Alexandrium tamarense* and *A. ostenfeldii* in Co-occurring Natural Populations from Scottish Coastal Waters. *Eur. J. Phycol.* **2003**, *38*, 25–40.
- Katikou, P.; Aligizaki, K.; Zacharaki, T.; Iossifidis, D.; Nikolaidis, G. First report of spirolides in Greek shellfish associated with causative *Alexandrium* species. Proceedings of the 14<sup>th</sup> International Conference on Harmful Algae. Crete Island, Greece, November 1-5, 2010; Pagou, P.; Hallegraeff, G., Eds.; International Society for the Study of Harmful Algae and Intergovernmental Oceanographic Commission of UNESCO 2013
- Keane, M.P.; Strieter, R.M. The Importance of Balanced Pro-inflammatory and Anti-inflammatory Mechanisms in Diffuse Lung disease. *Respir. Res.* **2001**, *3*, 5.
- Kharrat, R.; Servent, D.; Girard, E.; Ouanounou, G.; Amar, M.; Marrouchi, R.; Benoit, E.; Molgo, J. The Marine Phycotoxin Gymnodimin Targets Muscular and Neuronal Nicotinic Acetylcholine Receptor Subtypes with High Affinity. *J. Neurochem.* **2008**, *107* (4), 952–963.
- König, M.; Escher, B.I.; Neale, P.A.; Krauss, M.; Hilscherova, K.; Novak, J.; Teodorovic, I.; Schulze, T.; Seidensticker, S.; Kamal Hashmi, M.A.; Ahlheim, J.; Brack, W. Impact of Untreated Wastewater on a Major European River Evaluated With a Combination of In Vitro Bioassays and Chemical Analysis. *Environ. Pollut.* **2017**, *220*, 1220–1230.
- Krock, B., Tillmann, U., John, U. *et al.* LC-MS-MS Aboard Ship: Tandem Mass Spectrometry in the Search for Phycotoxins and Novel Toxicogenic Plankton from the North Sea. *Anal. Bioanal. Chem.* **2008**, *392*, 797–803
- Krock, B.; Pitcher, G.C.; Ntuli, J.; Cembella, A.D. Confirmed Identification of Gymnodimine in Oysters from the West Coast of South Africa by Liquid Chromatography–Tandem Mass Spectrometry. *Afr. J. Mar. Sci.* **2009**, *31*(1), 113–118
- Levasseur, M.; Berard-Therriault, L.; Bonneau, E.; Roy, S.; **1997**. Distribution of the Toxic Dinoflagellate *Alexandrium ostenfeldii* in the Gulf of St. Lawrence, Canada. In: Reguera, B., Blanco, J., Fernández, M.L., Wyatt, T. (Eds.), VIII International Conference on Harmful Algae. Xunta de Galicia, Intergovernmental Oceanographic Commission of UNESCO, Vigo, Spain, pp. 54–57.
- Liu, R.; Liang, Y.; Wu, X.; Xu, D.; Liu, Y.; Liu, L. First Report on the Detection of Pectenotoxin Groups in Chinese Shellfish by LC–MS/MS. *Toxicon.* **2011**, *57*, 1000–1007.
- Mackenzie, L. Importance of taxonomic data of marine flora and fauna. In Ballast Water a Marine Cocktail on the Move. *J. R. Soc. N. Z.* **1995**, *30*, 91
- MacKinnon, S.L.; Walter, J.A.; Quilliam, M.A.; Cembella, A.D.; LeBlanc, P.; Burton, I.W.; Hardstaff, W.R.; Lewis, N.I. Spirolides Isolated from Danish Strains of Toxicogenic Dinoflagellate *Alexandrium ostenfeldii*. *J. Nat. Prod.* **2006**, *69*, 983–987.

- Martens, H.; Tillmann, U.; Harju, K.; Dell'Aversano, C.; Tartaglione, L.; Krock, B. Toxin Variability Estimations of 68 *Alexandrium ostenfeldii* (Dinophyceae) Strains from The Netherlands Reveal a Novel Abundant Gymnodimine. *Microorganisms*. **2017**, *5*,29.
- McLafferty, F.W.; Tureček, F. Interpretation of Mass Spectra. 4th ed.; University Science Books: California, USA, **1993**; pp. 12-13
- Michel, A.D.; Stefanich, E.; Whiting, R.L. PC12 Phaeochromocytoma Cells Contain an Atypical Muscarinic Receptor Binding Site. *Br. J. Pharmacol.* **1989**, *97*(3), 914–920.
- Miles, C. O.; Wilkins, A. L.; Stirling, D. J.; MacKenzie, A. L. New Analogue of Gymnodimine From a Gymnodinium Species. *J. Agric. Food Chem.* **2000**, *48*, 1373-1376.
- Miles, C.O.; Samdal, I.A.; Aasen, J.A.G.; Jensen, D.J.; Quilliam, M. A.; Petersen, D.; Briggs, L. M.; Wilkins, A. L.; Rise, F.; Cooney, J. M.; MacKenzie, A. L. Evidence for Numerous Analogs of Yessotoxin in *Protoceratium reticulatum*. *Harmful Algae*. **2005**, *4*(6), 1075-1091.
- Miles, C.O.; Wilkins, A.L.; Stirling, D.J.; MacKenzie, A. L. Gymnodimine C, an Isomer of Gymnodimine B, from *Karenia selliformis*. *J. Agric. Food Chem.* **2003** *51* (16), 4838-4840
- Milisav, I.; Poljsak, B.; Suput, D. Adaptive Response, Evidence of Cross-Resistance and Its Potential Clinical use. *Int. J. Mol. Sci.* **2012**, *13*(9), 10771-10806.
- Miller, S.C.; Huang, R.; Sakamuru, S.; Shukla, S.J.; Attene-Ramos, M.S.; Shinn, P.; Van Leer, D.; Leister, W.; Austin, C.P.; Xia, M. Identification of Known Drugs That Act as Inhibitors of NF- $\kappa$ B Signaling and Their Mechanism of Action. *Biochem. Pharmacol.* **2010**, *79* (9), 1272-1280
- Moestrup, Ø.; Hansen, P.J. On the Occurrence of the Potentially Toxic Dinoflagellates *Alexandrium tamarense* (*Gonyaulax excavata*) and *A. ostenfeldii* in Danish and Faroese Waters. *Ophelia*. **1988**, *28* (3), 195–213.
- Moore, S.K.; Trainer, V.L.; Mantua, N.J. *et al.* Impacts of Climate Variability and Future Climate Change on harmful algal blooms and human health. *Environ. Health*. **2008**, *7*, S4.
- Munday, R.; Quilliam, M.A.; Leblanc, P.; Lewis, N.; Gallant, P.; Sperker, S.A.; Ewart, H.S.; MacKinnon, S.L. Investigation into the Toxicology of Spirolides, a Group of Marine Phycotoxins. *Toxins*. **2012**, *4*, 1–14.
- Munday, R.; Towers, N.R.; Mackenzie, L.; Beuzenberg, V.; Holland, P.T.; Miles, C.O. Acute Toxicity of Gymnodimine to Mice. *Toxicon*. **2004**, *44* (2), 173-178.
- Murakami, M.; Makabe, K.; Yamaguchi, K.; Konosu, S.; Wälchli, M.R. Goniiodomin a, A novel Polyether Macrolide from the Dinoflagellate *Goniiodoma pseudogoniaulax*. *Tetrahedron Lett.* **1988**, *29*(10), 1149-1152
- Nagai, S.; Yasuike, M.; Nakamura, Y.; Tahvanainen, P.; Kremp, A. Development of Ten Microsatellite Markers for *Alexandrium ostenfeldii*, A Bloom-forming Dinoflagellate Producing Diverse Phycotoxins. *J. Appl. Phycol.* **2015**, *27*, 2333–2339.
- Naila, I.B.; Hamza, A.; Gdoura, R.; Diogène, J.; de la Iglesia, P. Prevalence and Persistence of Gymnodimines in Clams from the Gulf of Gabes (Tunisia) Studied by Mouse Bioassay and LC–MS/MS. *Harmful Algae*. **2012**, *18*, 56-64
- Neale P.A.; Brack, W.; Ait-Aissa, S.; Busch, W.; Hollender, J.; Krauss, M.; MaillotMarechal, E.; Munz, N.A.; Schlichting, R.; Schulze, T.; Vogler, B.; Escher, B.I. Solid-Phase extraction as Sample Preparation of Water Samples for Cell-based and Other In Vitro Bioassays. *Environ. Sci. Process Impacts*. **2018**, *20*, 493–504.
- Nielsen, L.T.; Krock, B.; Hansen, P.J. Production and excretion of okadaic acid, pectenotoxin-2 and a novel dinophysistoxin from the DSP-causing marine dinoflagellate *Dinophysis acuta*—Effects of light, food availability and growth phase. *Harmful Algae*. **2013**, *23*, 34–45

- Nivala, J.; Neale, P.A.; Haasis, T.; Kahl, S.; König, M.; Müller, R.; Reemtsma, T.; Schlichting, R.; Escher, B.I. Application of Cell-based Bioassays to Evaluate Treatment Efficacy of Conventional and Intensified Treatment Wetlands. *Environ. Sci.: Water Res. Technol.* **2018**, *4*, 206–217.
- Okolodkov, Y.B., Dodge, J.D., 1996. Biodiversity and Biogeography of Planktonic Dinoflagellates in the Arctic Ocean. *J. Exp. Mar. Biol. Ecol.* **1996**, *202* (1), 19–27
- Otero, P.; Alfonso, A.; Rodríguez, P.; Rubiolo, J.A.; Cifuentes, J.M.; Bermúdez, R.; Vieytes, M.R.; Botana, L.M. Pharmacokinetic and Toxicological Data of Spirolides After Oral and Intraperitoneal Administration. *Food Chem. Toxicol.* **2012**, *50*, 232–237.
- Parker, J.C.; Sarkar, D.; Quick, M.W.; Lester, R.A.J. Interactions of Atropine with Heterogously Expressed and Native  $\alpha 3$  Subunit-containing Nicotine Acetylcholine Receptors. *Br. J. Pharmacol.* **2003**, *138*, 801–810.
- Parker, N.; Negri, A.; Frampton, D. *et al.* Growth of the Toxic Dinoflagellate *Alexandrium minutum* (Dinophyceae) Using High Biomass Culture Systems. *J. Appl. Phycol.* **2002**, *14*, 313–324
- Paulsen O. Plankton-Investigations in the Waters Around Iceland in 1903. *Medd. Kommn. Havunders. København. Ser. Plankt.* **1904**, *1*, 1–40.
- Peperzak, L. Future Increase in Harmful Algal Blooms in the North Sea Due to Climate Change. *Water Sci. Technol.* **2005**, *51* (5), 31–36.
- Polishchuk, P. Interpretation of Quantitative Structure–Activity Relationship Models: Past, Present, and Future. *J. Chem. Inf. Model.* **2017**, *57* (11), 2618–2639.
- Quilliam, M.A. Phycotoxins, *J. AOAC Int.* **1997**, *80* (1), 131–136
- Quilliam, M.A.; Gilcan, M.W.; Pleasance, S.; de Freitas, A.S.W.; Douglas, D.; Fritz, L.; Hu, T.; Marr, J.C.; Smyth, C.; Wight, J.L.C. Confirmation of an incident of diarrhetic shellfish poisoning in eastern Canada. In: Toxic Phytoplankton Blooms in the Sea, Smayda, T.J.; Shimizu, Y., Eds.; Elsevier: New York, USA, **1993**; pp. 547–552
- Rhodes, L.; Smith, K.; Selwood, A.; McNabb, P.; Munday, R.; Suda, S.; Molenaar, S.; Hallegraef, G. Dinoflagellate *Vulcanodinium rugosum* Identified as the Causative Organism of Pinnatoxins in Australia, New Zealand and Japan. *Phycologia.* **2011**, *50*, 624–628.
- Rhodes, L.; McNabb, P.; de Salas, M.; Briggs, L.; Beuzenberg, V.; Gladstone, M. Yessotoxin Production by *Gonyaulax spinifera*. *Harmful Algae.* **2006**, *5* (2), 148–155,
- Richard, D.; Arsenault, E.; Cembella, A.D.; Quilliam, M. Investigations into the Toxicology and Pharmacology of Spirolides, a Novel Group of Shellfish Toxins, In: Hallegraef, G.M.; Blackburn, S.I.; Bolch, C.J.; Lewis, R.J., eds. Harmful Algal Blooms 2000. Intergovernmental Oceanographic Commission of UNESCO, **2001**, pp. 383–386.
- Roach, J.S.; LeBlanc, P.; Lewis, N.I.; Munday, R.; Quilliam, M.A.; MacKinnon, S.L. Characterization of a Dispiroketal Spirolide Subclass from *Alexandrium ostenfeldii*. *J. Nat. Prod.* **2009**, *72*, 1237–1240.
- Rodríguez, L.P.; Vilariño, N.; Molgó, J.; Aráoz, R.; Antelo, A.; Vieytes, M.R.; Botana, L.M. Solid-Phase Receptor-Based Assay for the Detection of Cyclic Imines by Chemiluminescence, Fluorescence, or Colorimetry. *Anal. Chem.* **2011**, *83* (15), 5857–5863
- Rossini, G.P.; Hess, P. Phycotoxins: Chemistry, Mechanisms of Action and Shellfish Poisoning. In: Luch, A., ed. *Molecular, Clinical and Environmental Toxicology. Volume 2: Clinical Toxicology.* Birkhäuser Verlag: Switzerland, **2010**; pp. 65–122

- Rundberget, T.; Sandvik, M.; Hovgaard, P.; Nguyen, L.; Aasen, J.A.B.; Castberg, T.; Gustad, E.; Miles, C. O., Use of SPATT disks in Norway: Detection of AZAs & DTXs and Comparison with Algal Cell Counts and Toxin Profiles in Shellfish. *Marine Biotoxin Science Workshop* **2006**, *23*, 35-38.
- Salgado, P.; Riobó, P.; Rodríguez, F.; Franco, J.M.; Bravo, I. Differences in the Toxin Profiles of *Alexandrium ostenfeldii* (Dinophyceae) Strains Isolated From Different Geographic Origins: Evidence of Paralytic toxin, Spirolide, and Gymnodimine. *Toxicon*. **2015**, *103*, 85-98,
- Schmidt, K.N.; Traenckner, E.B.; Meier, B.; Baeuerle, P.A. Induction of Oxidative Stress by Okadaic Acid is Required for Activation of Transcription Factor NF-kappa B. *J Biol Chem*. **1995**, *270(45)*, 27136-42.
- Seki, T.; Satake, M.; MacKenzie, L.; Kaspar, H.F.; Yasumoto, T. Gymnodimine, A New Marine Toxin of Unprecedented Structure Isolated from New Zealand Oysters and the Dinoflagellate, *Gymnodinium* sp. *Tetrahedron Lett*. **1995**, *36*, 7093–7096.
- Sellner, K.G., Doucette, G.J.; Kirkpatrick, G.J. Harmful Algal blooms: Causes, Impacts and detection. *J. Ind. Microbiol. Biotechnol*. **2003**, *30*, 383–406.
- Selwood, A.I., Miles, C.O.; Wilkinson, A.L.; Van Ginkel, R.; Munday, R.; Rise, F.; McNabb, P. Isolation, Structural Determination and Acute Toxicity of Pinnatoxins E, F and G. *J. Agric. Food Chem*. **2010**, *58*, 6532–6542.
- Sequeira, E.; Pierce, M.; Gomez, D.; Murray, T. Investigation of the Potential Therapeutic Use of Brevetoxin to Promote Ischemic Stroke Recovery. *The FASEB Journal*. **2019**, *33*, 500.
- Seta, K.; Kim, H.W.; Ferguson, T.; Kim, R.; Pathrose, P.; Yuan, Y.; Lu, G.; Spicer, Z.; Millhorn, D.E. Genomic and Physiological Analysis of Oxygen Sensitivity and Hypoxia Tolerance in PC12 Cells. *Ann. N.Y. Acad. Sci*. **2002**, *971*, 379-388.
- Shafer, T.J.; Atchison W.D. Transmitter, Ion Channel and Receptor Properties of Pheochromocytoma (PC12) cells: A Model for Neurotoxicological Studies. *Neurotoxicology*. **1991**, *12(3)*, 473-492.
- Simmons, S. O.; Fan, C. Y.; Ramabhadran, R. Cellular Stress Response Pathway System as a Sentinel Ensemble in Toxicological Screening. *Toxicol. Sci*. **2009**, *111*, 202–225.
- Sleno, L.; Windust, A.J.; Volmer, D.A. Structural Study of Spirolide Marine Toxins by Mass Spectrometry Part II. Mass spectrometric Characterization of Unknown Spirolides and Related Compounds in a Cultured Phytoplankton Extract. *Anal. Bioanal. Chem*. **2004a**, *378*, 977–986.
- Sleno, L.; Windust, A.J.; Volmer, D.A. Structural Study of Spirolide Marine Toxins by Mass Spectrometry Part I. Fragmentation Pathways of 13-desmethyl spirolide C by Collision-Induced Dissociation and Infrared Multiphoton Dissociation Mass Spectrometry. *Anal. Bioanal. Chem*. **2004b**, *378*, 969–976.
- Smayda, T.J. Complexity in the Eutrophication–Harmful Algal Bloom Relationship, With Comment on the Importance of Grazing. *Harmful Algae*. **2008**, *8 (1)*, 140-151
- Sommer, U.; Adrian,R.; De Senerpont Domis,L.; Elser, J.J; Gaedke, U.; Ibelings, B.; Jeppesen, E.; Lürling, M.; Molinero, J.C.; Mooij, W.M.; van Donk,E.; Winder, M. Beyond the Plankton Ecology Group (PEG) Model: Mechanisms Driving Plankton Succession. *Annu. Rev. Ecol. Evol. Syst*. **2012**, *43(1)*, 429-448.
- Spalding, T.A.; Burstein, E.S. Constitutive Activity of Muscarinic Acetylcholine Receptors. *J. Recept. Sig. Transd*. **2006**, *26*, 61-65.
- Takahashi, E.; Yu, Q.; Eaglesham, G.; Connell, D.W.; McBroom, J.; Costanzo, S.; Shaw, G.R. Occurrence and Seasonal Variations of Algal toxins in Water, Phytoplankton and Shellfish from North Stradbroke Island, Queensland, Australia. *Mar. Environ. Res*. **2007**, *64(4)*, 429-442

- Takahashi, T.; Yamashita, H.; Nakamura, S.; Ishiguro, H.; Nagatsu, T.; Kawakami, H. Effects of Nerve Growth Factor and Nicotine on the Expression of Nicotinic Acetylcholine Receptor Subunits in PC12 cells. *J. Neurosci. Sci.* **1999**, *35*(3), 175-181.
- Takeshi, Yasumoto, T.; Murata, M. Marine Toxins. *Chem. Rev.* **1993**, *93* (5), 1897-1909
- Tillmann, U.; Kremp, A.; Tahvanainen, P.; Krock, B. Characterization of Spirolide Producing *Alexandrium ostenfeldii* (Dinophyceae) from the Western Arctic. *Harmful Algae.* **2014**, *39*, 259–270.
- Touzet, N.; Franco, J.M.; Raine, R. Morphogenetic Diversity and Biotxin Composition of *Alexandrium* (Dinophyceae) in Irish Coastal Waters. *Harmful Algae* **2008**, *7*, 782–797.
- Trautmann, T. Intraspecific Trait Diversity in the Marine Dinoflagellate *Alexandrium ostenfeldii* and Resulting Effects on the Community Composition. Master thesis, University of Bremen, Bremen, Germany, 2017. [hdl:10013/epic.ef108fe5-76f8-4f47-97c5-a74e9eb8265d](https://hdl.handle.net/10013/epic.ef108fe5-76f8-4f47-97c5-a74e9eb8265d)
- Van de Waal, D.B.; Tillmann, U.; Martens, H.; Krock, B.; van Scheppingen, Y.; John, U. Characterization of Multiple Isolates from an *Alexandrium ostenfeldii* Bloom in The Netherlands. *Harmful Algae.* **2015**, *49*, 94–104.
- Van Dolah FM. Marine algal toxins: origins, health effects, and their increased occurrence. *Environ. Health Perspect.* **2000**, *108*, 133-141.
- Van Wagoner, R.M.; Misner, I.; Tomas, C.R.; Wright J.L.C. Occurrence of 12-Methylgymnodimine in a Spirolide-producing Dinoflagellate *Alexandrium peruvianum* and the Biogenetic Implications. *Tetrahedron Lett.* **2011**, *52*, 4243–4246.
- Van Wagoner, R.M.; Satake, M.; Wright, J.L.C. Polyketide Biosynthesis in Dinoflagellate: What Makes It Different? *Nat. Prod. Rep.* **2014**, *31*, 1101.
- Verma, A.; Kohli, G.S.; Harwood, D.T.; Ralph, P.J.; Murray, S.A. Transcriptomic investigation into polyketide toxin synthesis in *Ostreopsis* (Dinophyceae) species. *Environ. Microbiol.* **2019**, *21*, 4196-4211.
- Vijlder, T.; Valkenburg, D.; Lemièrre, F.; Romijn, E.P.; Laukens, K.; Cuyckens, F. A Tutorial in Small Molecule Identification via Electrospray Ionization-mass Spectrometry: The Practical Art of Structural Elucidation. *Mass Spec. Rev.* **2018**, *37*, 607–629.
- Vilariño, N.; Fonfría, E.S.; Molgó, J.; Aráoz, R.; Botana, L.M. Detection of Gymnodimine-A and 13-Desmethyl C Spirolide Phycotoxins by Fluorescence Polarization. *Anal. Chem.* **2009**, *81* (7), 2708-2714
- Villar González, A.; Rodríguez-Velasco, L.M.; Ben-Gigirey, B.; Botana, L.M. First Evidence of Spirolides in Spanish Shellfish. *Toxicon.* **2006**, *48*, 1068–1075.
- Visciano; P.; Schirone, M.; Berti, M.; Milandri, A.; Tofalo, R.; Suzzi, G. Marine Biotoxins: Occurrence, Toxicity, Regulatory Limits and Reference Methods. *Front. Microbiol.* **2016**, *7*, 1051.
- Wandscheer, C.B.; Vilariño, N.; Espiña, B.; Louzao M.C.; Botana, L.M. Human Muscarinic Acetylcholine Receptors Are a Target of the Marine Toxin 13-desMethyl C Spirolide. *Chem. Res. Toxicol.* **2010**, *11*, 1753-1761.
- Wang, C.; Lan, C.Q. Effects of Shear Stress on Microalgae – A Review. *Biotechnol. Adv.* **2018**, *36* (4), 986-1002
- Wang, X. J.; Hayes, J. D.; Wolf, C. R. Generation of a Stable Antioxidant Response Element-Driven Reporter Gene Cell Line and Its Use to Show Redox-Dependent Activation of Nrf2 by Cancer Chemotherapeutic Agents. *Cancer Res.* **2006**, *66* (22), 10983–10994.
- Wiese, M.; D’Agostino, P.M.; Mihali, T.K.; Moffitt, M.C.; Neilan, B.A. Neurotoxic Alkaloids: Saxitoxin and Its Analogs. *Mar. Drugs.* **2010**, *8*, 2185-2211.



Wright, J.L.C.; Cembella, A.D. Ecophysiology and Biosynthesis of Polyether Marine Biotoxins. In: D. M. Anderson, A. D. Cembella & G. M. Hallegraeff (eds.). *Physiological Ecology of Harmful Algal Bloom*. NATO ASI Ser., **1998**, 41: 427-451.

Yasumoto, O.; Oshima, Y.; Yamaguchi, M. Occurrence of New Type of Shellfish Poisoning in Tohoku District. *Bull. Jpn. Soc. Sci. Fish.* **1978**, 44, 1249-1255

Zurhelle, C.; Nieva, J.; Tillmann, U.; Harder, T.; Krock, B.; Tebben, J. Identification of Novel Gymnodimines and Spirolides from the Marine Dinoflagellate *Alexandrium ostenfeldii*. *Mar. Drugs.* **2018**, 16, 446.

Zwart, R.; Vijverberg, H. P.M. Potentiation and Inhibition of Neuronal Nicotinic Receptors by Atropine: Competitive and Non-Competitive Effects. *Mol. Pharmacol.* **1997**, 52 (5), 886-895.

## SUPPORTING INFORMATION

Figure S1. HRMS/MS spectrum of compound 1 (670>164) from AON 24.	115
Figure S2. HRMS/MS spectrum of compound 2 (666>164) from NX-56-10.	116
Figure S3. HRMS/MS spectrum of compound 3 (696>164) from NX-56-10.	116
Figure S4. HRMS/MS spectrum of compound 4 (678>150) from MX-S-B11.	117
Figure S5. HRMS/MS spectrum of compound 5 (694>164) from MX-S-B11.	117
Figure S6. HRMS/MS spectrum of compound 6 (708>164) from MX-S-B11.	118
Figure S7. HRMS/MS spectrum of compound 7 (720>164) from MX-S-B11.	118
Figure S8. HRMS/MS spectrum of compound 8 (722>164) from MX-S-B11.	119
Figure S9. HRMS/MS spectrum of compound 9 (738>180) from MX-S-B11.	119
Figure S10. Proposed fragmentation pattern of $m/z$ 592 from compound 1 (670>164).	120
Figure S11. EC <sub>IR1.5</sub> in AREc32 cells.	121
Figure S12. Induction of NfκB- <i>bla</i> THP-1 cell lines.	121
Table S1. Extended fragment list from known spiroptides.	122
Table S2. Extended HRMS/MS fragment list of compounds 1 from AON 24.	123
Table S3. Extended HRMS/MS fragment list of compounds 2 and 3 from NX-56-10.	124
Table S4. Extended HRMS/MS fragment list of compounds 4-9 from MX-S-B11.	125

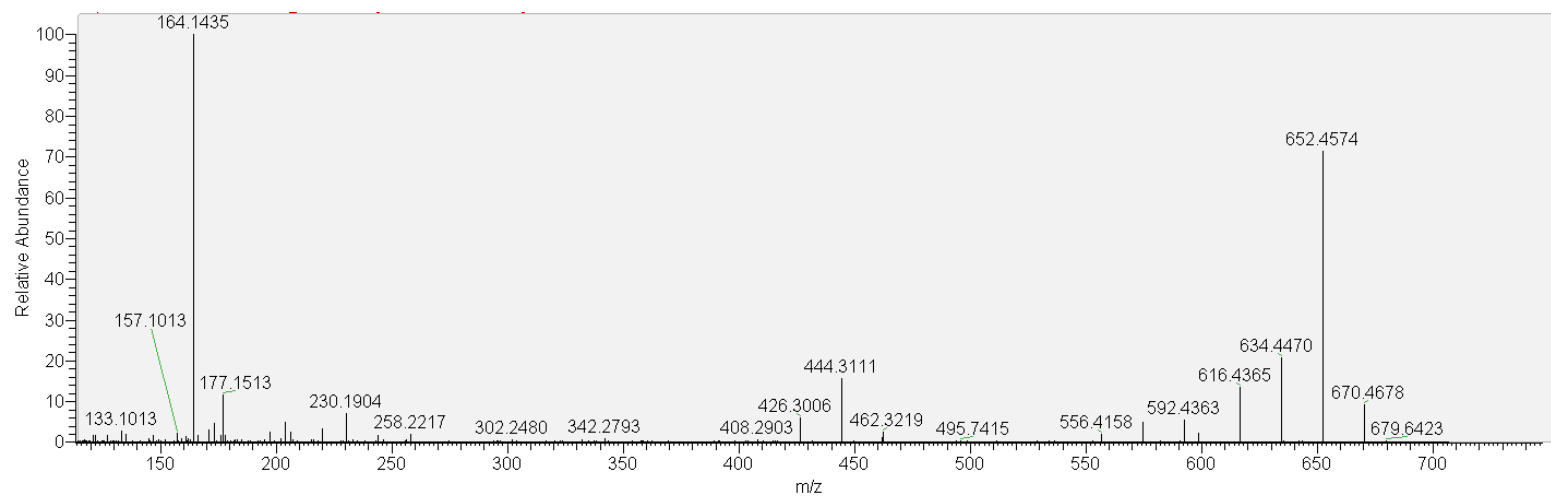


**Figure S1.** HRMS/MS spectrum of compound **1** (670>164) from AON 24.

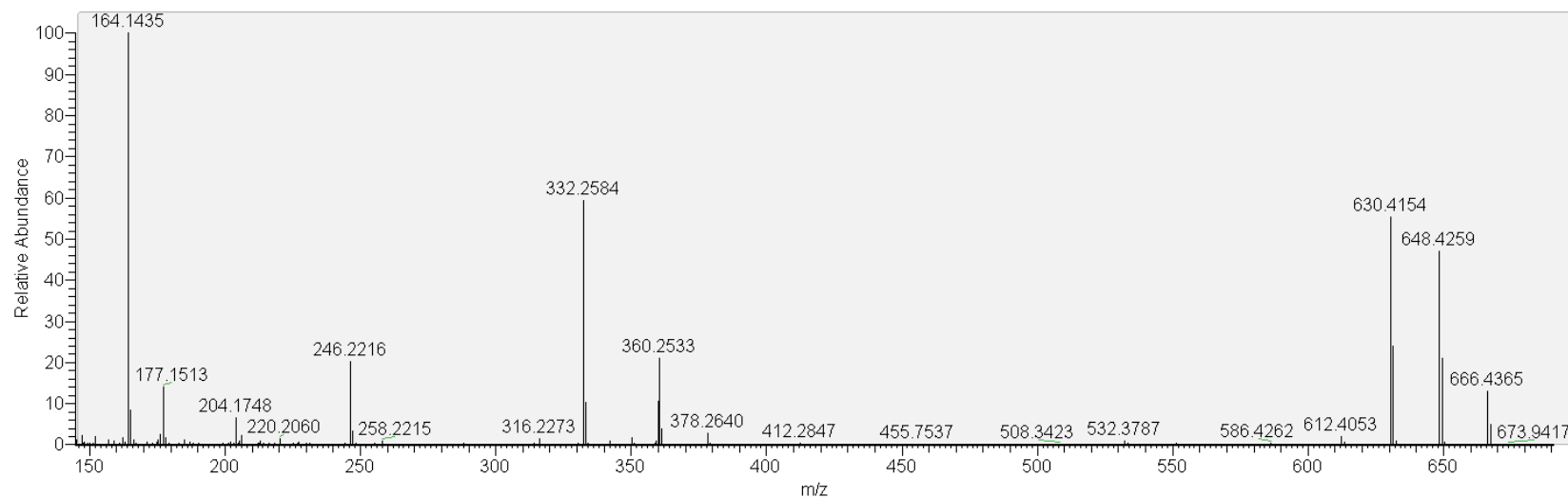


**Figure S2.** HRMS/MS spectrum of compound 2 (666>164) from NX-56-10.

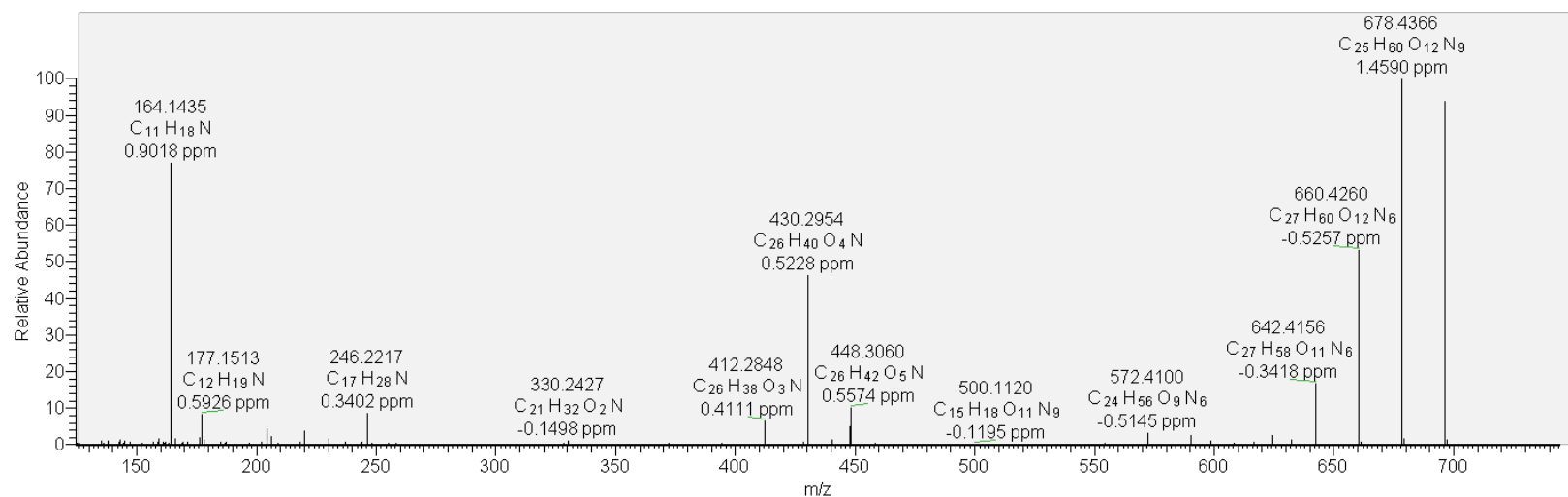


**Figure S3.** HRMS/MS of compound 3 (696>164) from NX-56-10.

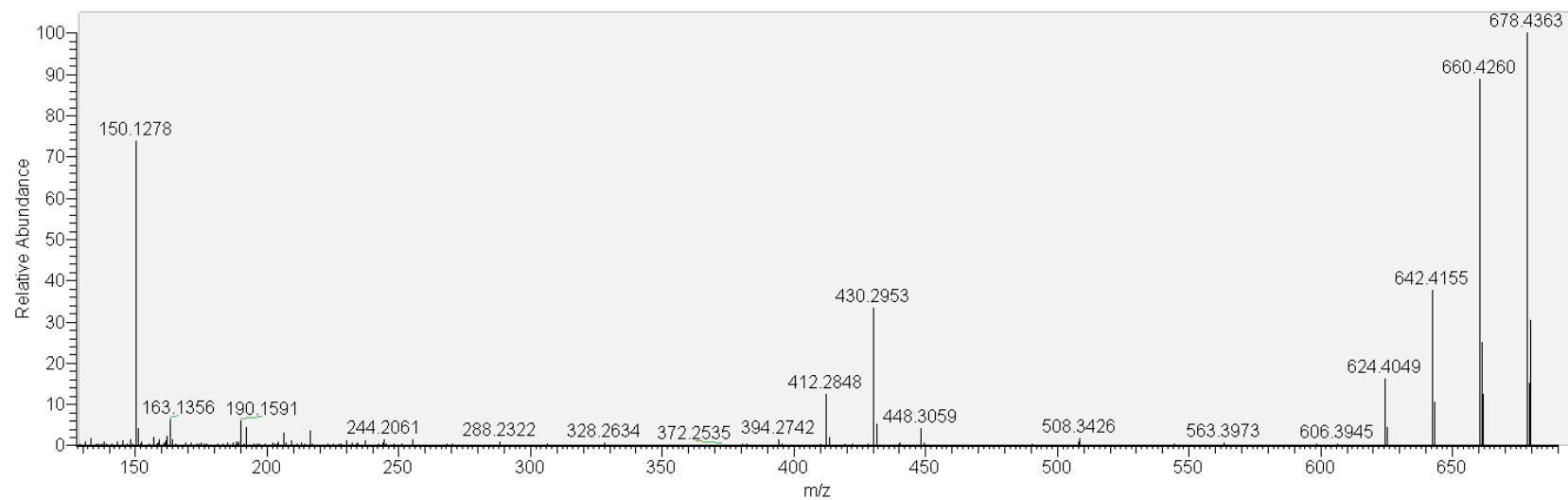


**Figure S4.** HRMS/MS spectrum of compound 4 (678>150) from MX-S-B11.

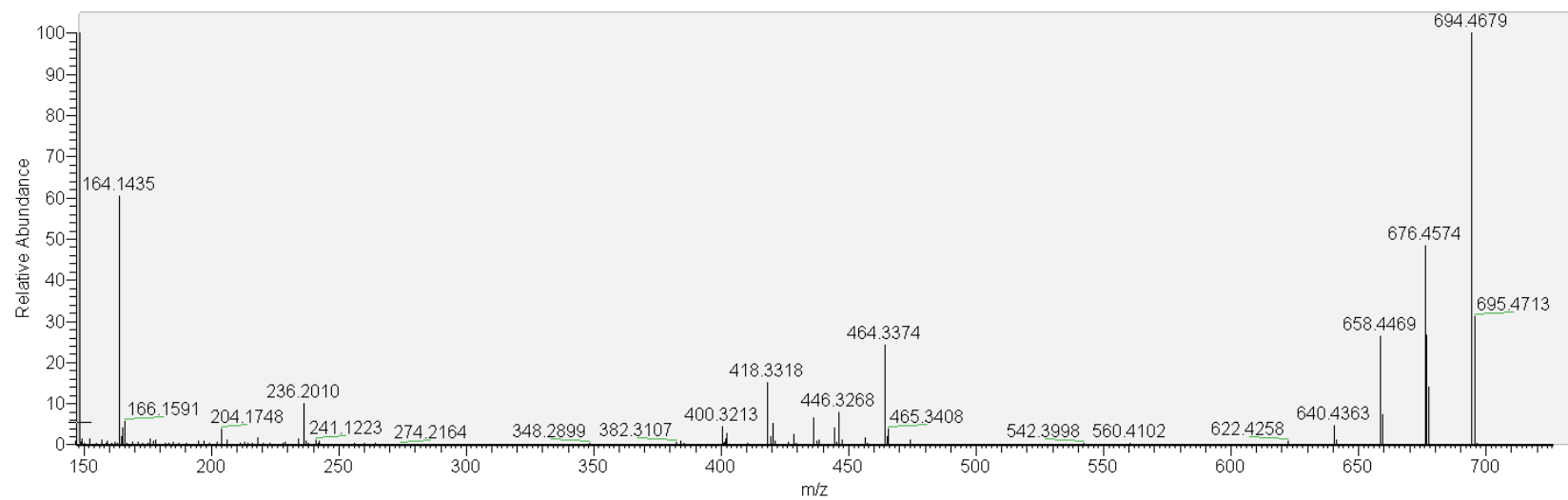


**Figure S5.** HRMS/MS spectrum of compound 5 (694>164) from MX-S-B11.

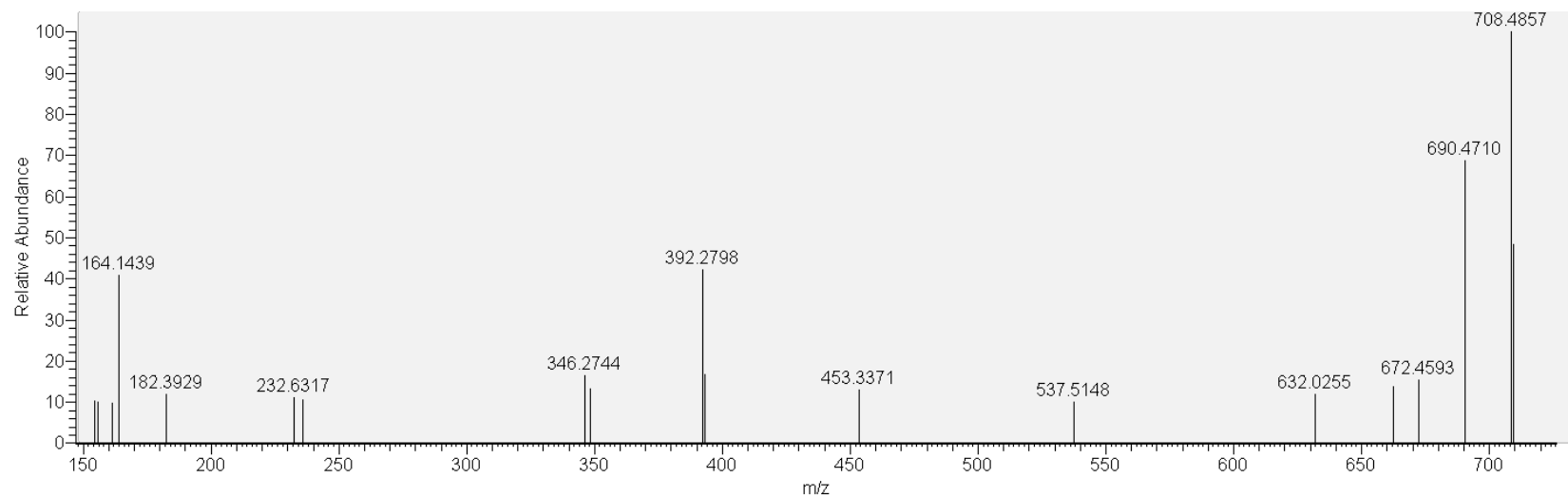


**Figure S6.** HRMS/MS spectrum of compound 6 (708>164) from MX-S-B11.

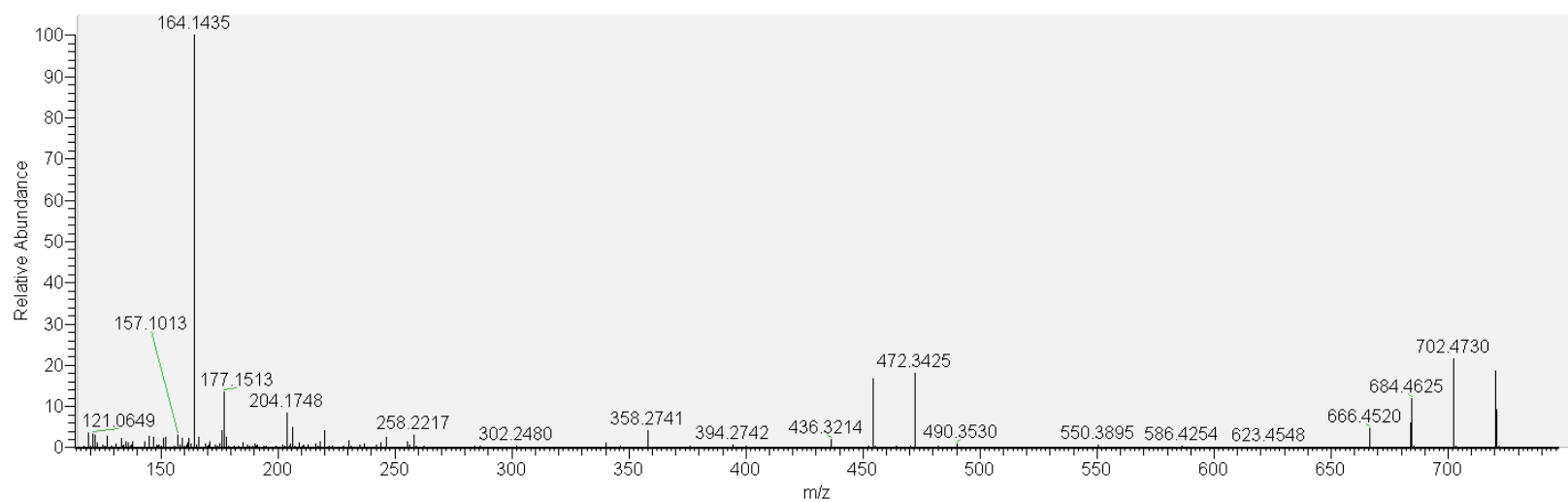


**Figure S7.** HRMS/MS spectrum of compound 7 (720>164) from MX-S-B11.

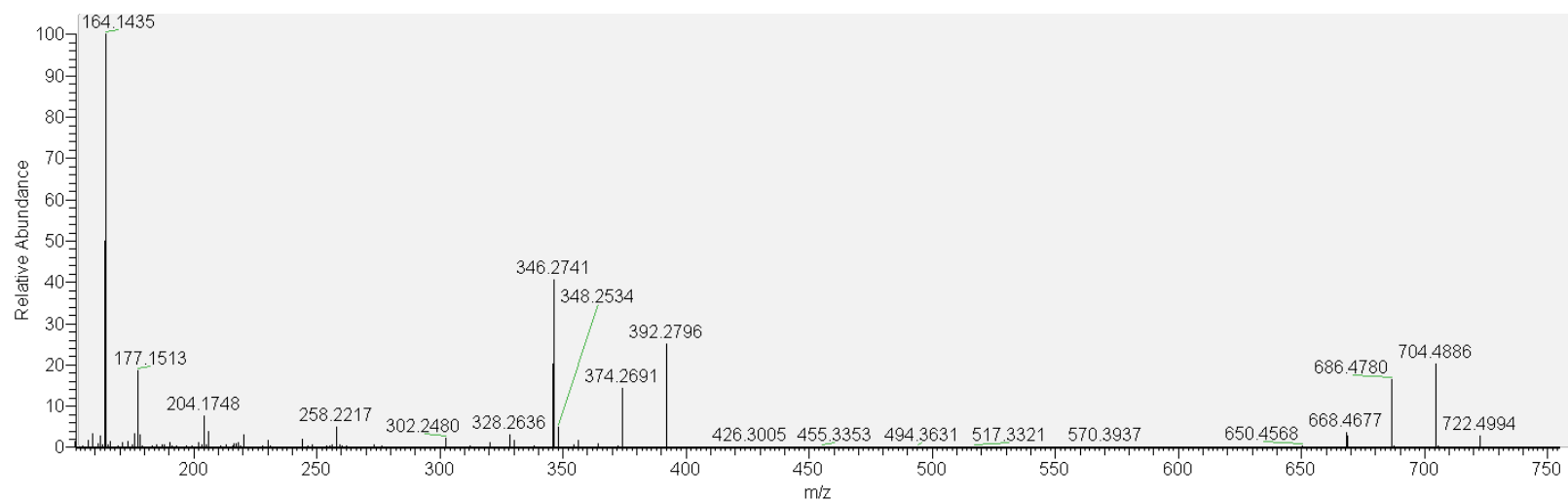


**Figure S8.** HRMS/MS spectrum compound 8 (678>164) from MX-S-B11.

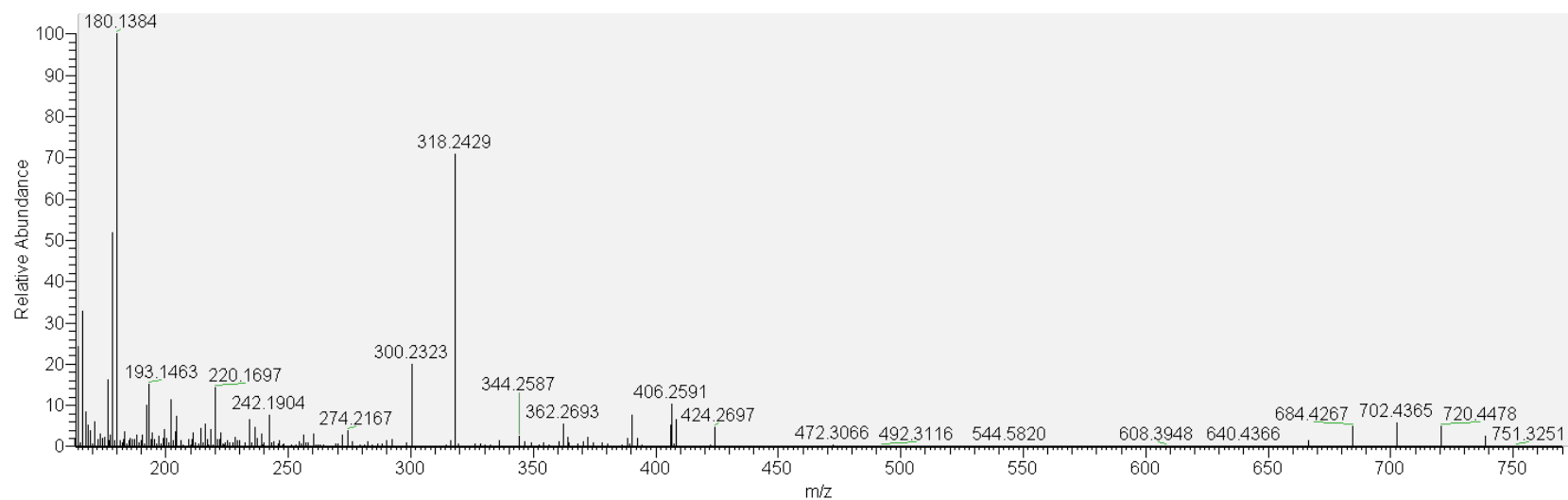


**Figure S9.** HRMS/MS spectrum compound 9 (738>180) from MX-S-B11.

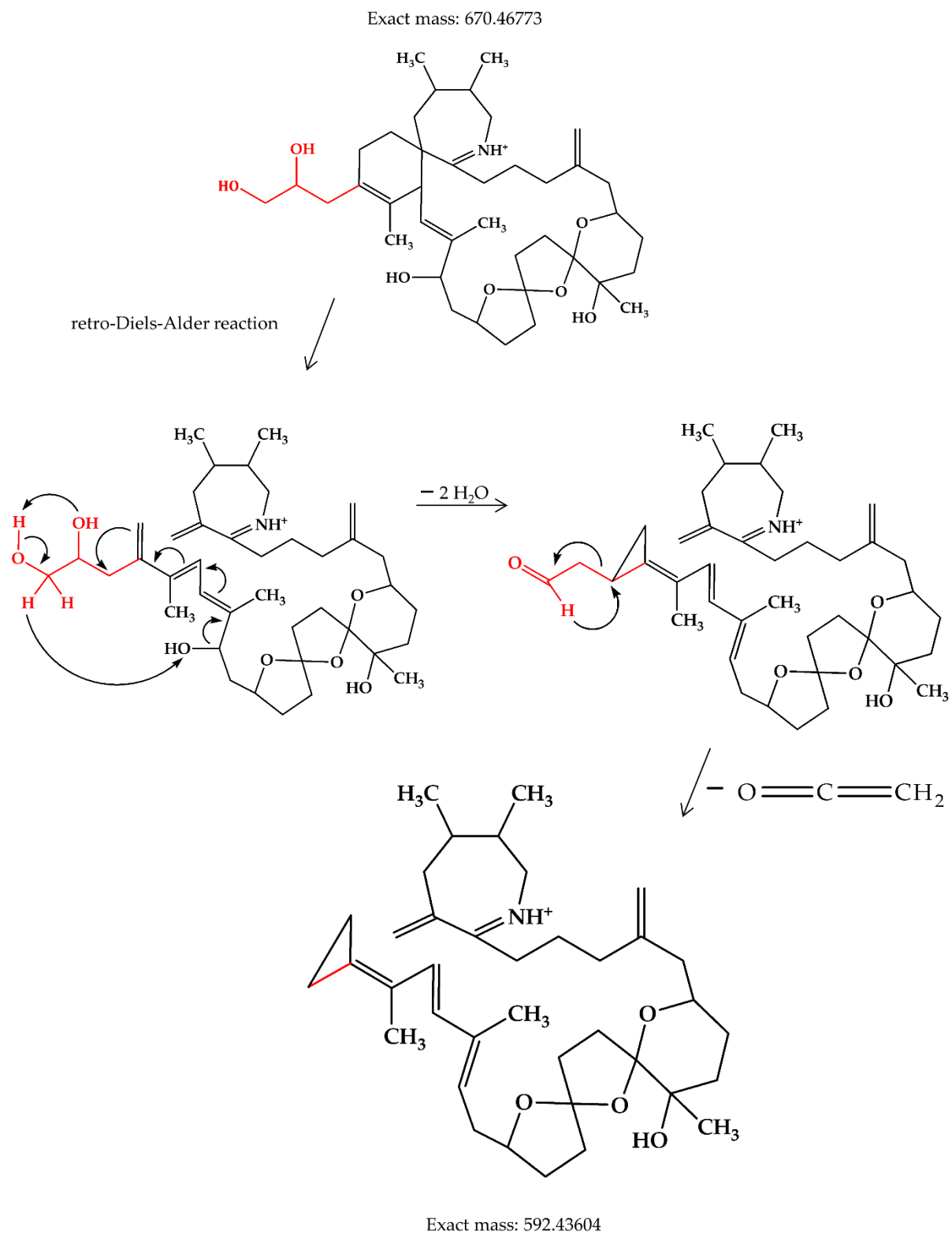
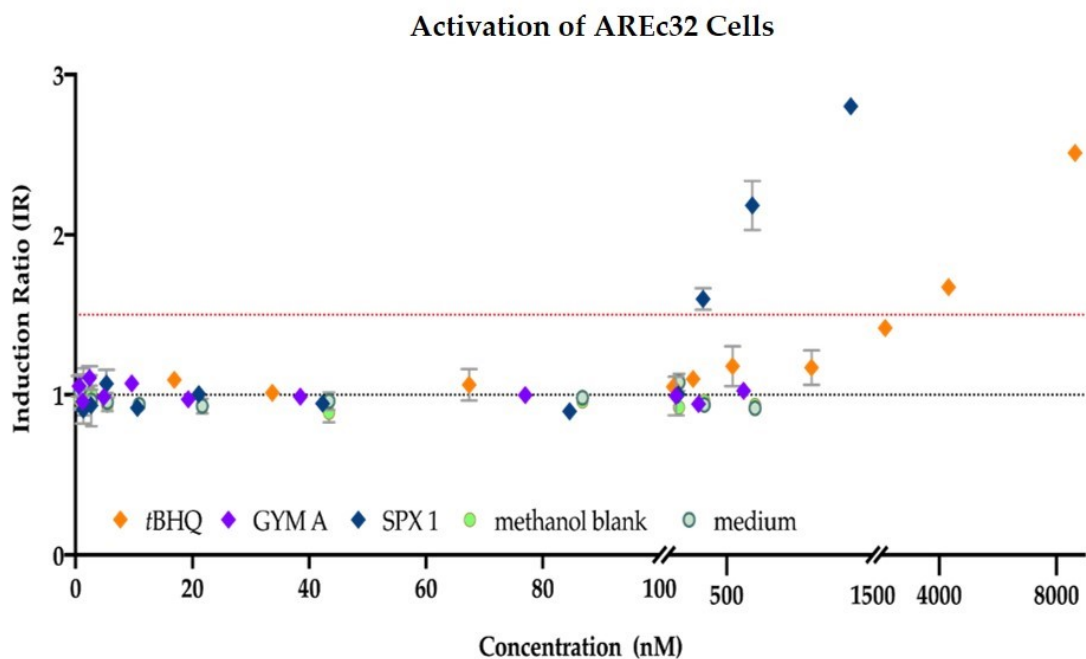
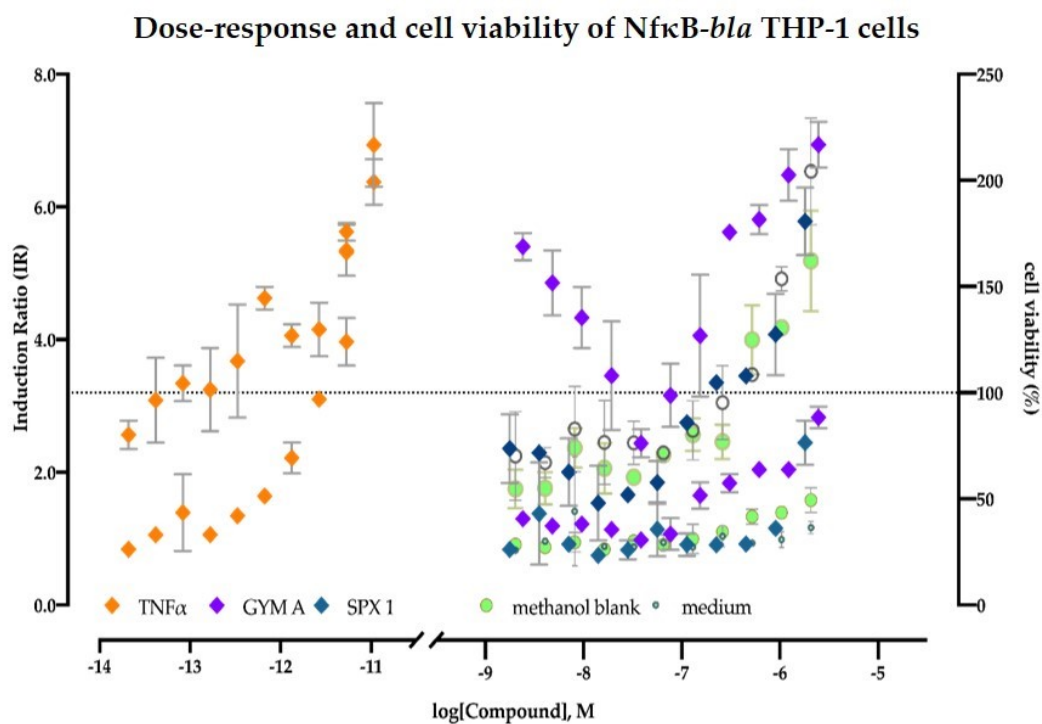


Figure S10. Proposed fragmentation pattern of  $m/z$  592 from compound 1 (670>164).





**Figure S11.** Detailed distribution of  $EC_{IR1.5}$  in AREc32 cells treated with tBHQ (orange), GYM A (violet) and SPX 1 (blue), methanol blank (green) and medium (light blue, in circle).



**Figure S12.** The induction of *NfκB-bla* THP-1 cell lines treated with  $TNF\alpha$  (orange), GYM A (violet) and SPX 1 (blue) occurred when cells were still viable. Although cells remained viable at more than 50%, cell toxicity cannot be derived due to variability of cell viability.

**Table S1.** Extended fragment list from known spiroptides.

Spiroptide	Mass transition ( <i>m/z</i> )	Fragments ( <i>m/z</i> )				Reference
		Group 1	Group 2	Group 3	Group 4	
A	692 > 150	692/674/624	444/390	190	150	Hu <i>et al.</i> , 2001
B	694 > 150	694/676/658/640	462/444/426		150	Hu <i>et al.</i> , 1995; 1996
C	706 > 164	706/688/638	458/404	204	164	Hu <i>et al.</i> , 2001
13-desMethyl C	692 > 164	692/674/656/638	462/444/426	230	164	Hu <i>et al.</i> , 2001
13,19-didesMethyl C	678 > 164	678/660/642/624	448/430/412/394		164	Ciminiello <i>et al.</i> , 2007
20-Hydroxy-13,19-didesMethyl C	694 > 164	694/676/658/640	446/428/410/392	292/274/248/230	164	Zurhelle <i>et al.</i> , 2018
27-Hydroxy-13-desMethyl C	708 > 180	708/690/672/654/636	478/460/442/424		180	Ciminiello <i>et al.</i> , 2010
27-Hydroxy-13,19-didesMethyl C	694 > 180	694/676/658/640	464/446/428/410		180	Ciminiello <i>et al.</i> , 2010
27-Oxo-13,19-didesMethyl C	692 > 178	692/674/624	444		178	Ciminiello <i>et al.</i> , 2010
D	708 > 164	708/690/672/654	458/440	230/206/204/177	164	Hu <i>et al.</i> , 1995
13-desMethyl D	694 > 164	694/676/658/640	444/426	230/204/177	164	Sleno <i>et al.</i> , 2004
20-Hydroxy-13,19-didesMethyl D	696 > 164	696/678/660/642	446/428/410/392	292/274/248/230	164	Zurhelle <i>et al.</i> , 2018
G	692 > 164	692/674/656/638	378/360/332	258	164	Aasen <i>et al.</i> , 2005
20-Methyl G	706 > 164	706/688/670/652	392/374/346	258	164	Aasen <i>et al.</i> , 2005
H	650 > 164	650/632/614	402/384	206	164	Roach <i>et al.</i> , 2009
I	652 > 164	652/634/616	402/384	206	164	Roach <i>et al.</i> , 2009

**Table S2.** Extended HRMS/MS fragment list of compounds **1** from AON 24.

<b>Compound 1 (670&gt;164)</b>					
<i>m/z</i>	Intensity	Relative	Theoretical Mass	$\Delta$ (ppm)	Elemental Composition
670.4678	631	9.48	670.4677	0.04	C <sub>40</sub> H <sub>64</sub> NO <sub>7</sub> <sup>+</sup>
652.4574	4794	72.00	652.4572	0.23	C <sub>40</sub> H <sub>62</sub> NO <sub>6</sub> <sup>+</sup>
634.4470	1451	21.80	634.4466	0.36	C <sub>40</sub> H <sub>60</sub> NO <sub>5</sub> <sup>+</sup>
616.4365	890	13.36	616.436	0.49	C <sub>40</sub> H <sub>58</sub> NO <sub>4</sub> <sup>+</sup>
592.4363	373	5.60	592.436	0.30	C <sub>38</sub> H <sub>58</sub> NO <sub>4</sub> <sup>+</sup>
574.4258	344	5.16	574.4255	0.31	C <sub>38</sub> H <sub>56</sub> NO <sub>3</sub> <sup>+</sup>
462.3219	175	2.62	462.3214	0.47	C <sub>27</sub> H <sub>44</sub> NO <sub>5</sub> <sup>+</sup>
444.3111	1087	16.33	444.3108	0.29	C <sub>27</sub> H <sub>42</sub> NO <sub>4</sub> <sup>+</sup>
426.3006	416	6.25	426.3003	0.30	C <sub>27</sub> H <sub>40</sub> NO <sub>3</sub> <sup>+</sup>
230.1904	477	7.17	230.1903	0.07	C <sub>16</sub> H <sub>24</sub> N <sup>+</sup>
177.1513	804	12.07	177.1512	0.06	C <sub>12</sub> H <sub>19</sub> N <sup>+</sup>
164.1435	6659	100.00	164.1434	0.13	C <sub>11</sub> H <sub>18</sub> N <sup>+</sup>

**Table S3.** Extended HRMS/MS fragment list of compounds **2** and **3** from NX-56-10.

<b>Compound 2 (666&gt;164)</b>					
<i>m/z</i>	Intensity	Relative	Theoretical Mass	$\Delta$ (ppm)	Elemental Composition
666.4365	4596	12.69	666.4364	0.09	C <sub>40</sub> H <sub>60</sub> NO <sub>7</sub> <sup>+</sup>
648.4259	17328	47.83	648.4259	0.04	C <sub>40</sub> H <sub>58</sub> NO <sub>6</sub> <sup>+</sup>
630.4154	20498	56.58	630.4153	0.10	C <sub>40</sub> H <sub>56</sub> NO <sub>5</sub> <sup>+</sup>
550.3898	25	/	550.3891	1.36	C <sub>35</sub> H <sub>52</sub> NO <sub>4</sub> <sup>+</sup>
532.3787	326	/	532.3785	0.38	C <sub>35</sub> H <sub>50</sub> NO <sub>3</sub> <sup>+</sup>
378.2640	966	2.67	378.2639	0.12	C <sub>22</sub> H <sub>36</sub> NO <sub>4</sub> <sup>+</sup>
360.2533	7620	21.03	360.2533	-0.02	C <sub>22</sub> H <sub>34</sub> NO <sub>3</sub> <sup>+</sup>
332.2584	21586	59.59	332.2584	-0.04	C <sub>21</sub> H <sub>34</sub> NO <sub>2</sub> <sup>+</sup>
246.2216	7500	20.70	246.2216	0.02	C <sub>17</sub> H <sub>28</sub> N <sup>+</sup>
177.1513	4933	13.62	177.1512	0.07	C <sub>12</sub> H <sub>19</sub> N <sup>+</sup>
164.1435	36225	100.00	164.1434	0.10	C <sub>11</sub> H <sub>18</sub> N <sup>+</sup>
<b>Compound 3 (696&gt;164)</b>					
<i>m/z</i>	Intensity	Relative	Theoretical Mass	$\Delta$ (ppm)	Elemental Composition
696.4471	18674	90.33	696.4470	0.09	C <sub>41</sub> H <sub>62</sub> NO <sub>8</sub> <sup>+</sup>
678.4366	20673	100.00	678.4364	0.15	C <sub>41</sub> H <sub>60</sub> NO <sub>7</sub> <sup>+</sup>
660.426	10407	50.34	660.4259	0.16	C <sub>41</sub> H <sub>58</sub> NO <sub>6</sub> <sup>+</sup>
642.4156	3308	16.00	642.4153	0.29	C <sub>41</sub> H <sub>56</sub> NO <sub>5</sub> <sup>+</sup>
624.4048	514	2.49	624.4047	0.05	C <sub>41</sub> H <sub>54</sub> NO <sub>4</sub> <sup>+</sup>
608.4315	70.3	/	608.43146	0.83	C <sub>38</sub> H <sub>58</sub> NO <sub>5</sub> <sup>+</sup>
590.4208	491	2.37	590.4204	0.45	C <sub>38</sub> H <sub>56</sub> NO <sub>4</sub> <sup>+</sup>
572.4100	664	3.21	572.4098	0.21	C <sub>38</sub> H <sub>54</sub> NO <sub>3</sub> <sup>+</sup>
554.3998	127	0.62	554.3993	0.52	C <sub>38</sub> H <sub>52</sub> NO <sub>2</sub> <sup>+</sup>
500.1120	40	0.19	500.1129	-0.89	C <sub>31</sub> H <sub>18</sub> NO <sub>6</sub> <sup>+</sup>
448.3060	1961	9.49	448.3057	0.25	C <sub>26</sub> H <sub>42</sub> NO <sub>5</sub> <sup>+</sup>
432.3114	43	0.21	432.3108	0.60	C <sub>26</sub> H <sub>42</sub> NO <sub>4</sub> <sup>+</sup>
430.2954	9046	43.76	430.2952	0.22	C <sub>26</sub> H <sub>40</sub> NO <sub>4</sub> <sup>+</sup>
412.2848	1342	6.49	412.2846	0.17	C <sub>26</sub> H <sub>38</sub> NO <sub>3</sub> <sup>+</sup>
394.2742	69	0.34	394.2741	0.18	C <sub>26</sub> H <sub>36</sub> NO <sub>2</sub> <sup>+</sup>
248.2009	63	0.31	248.2009	0.05	C <sub>16</sub> H <sub>26</sub> NO <sup>+</sup>
246.2217	1776	8.59	246.2216	0.08	C <sub>17</sub> H <sub>28</sub> N <sup>+</sup>
177.1513	1612	7.80	177.1512	0.10	C <sub>12</sub> H <sub>19</sub> N <sup>+</sup>
164.1435	15352	74.26	164.1434	0.15	C <sub>11</sub> H <sub>18</sub> N <sup>+</sup>

**Table S4.** Extended HRMS/MS fragment list of compounds **4-9** from MX-S-B11.

<b>Compound 4 (678&gt;150)</b>					
<i>m/z</i>	Intensity	Relative	Theoretical Mass	$\Delta$ (ppm)	Elemental Composition
678.4363	107716	100.00	678.4364	-0.15	C <sub>41</sub> H <sub>60</sub> NO <sub>7</sub> <sup>+</sup>
660.4260	93076	86.41	660.4259	0.10	C <sub>41</sub> H <sub>58</sub> NO <sub>6</sub> <sup>+</sup>
642.4155	39210	36.40	642.4153	0.17	C <sub>41</sub> H <sub>56</sub> NO <sub>5</sub> <sup>+</sup>
624.4049	17080	15.86	624.4047	0.17	C <sub>41</sub> H <sub>54</sub> NO <sub>4</sub> <sup>+</sup>
508.3426	1867	1.73	508.3421	0.45	C <sub>32</sub> H <sub>46</sub> NO <sub>4</sub> <sup>+</sup>
490.3318	576	0.53	490.3316	0.25	C <sub>32</sub> H <sub>44</sub> NO <sub>3</sub> <sup>+</sup>
448.3059	4390	4.08	448.3057	0.19	C <sub>26</sub> H <sub>42</sub> NO <sub>5</sub> <sup>+</sup>
430.2953	35422	32.88	430.2952	0.16	C <sub>26</sub> H <sub>40</sub> NO <sub>4</sub> <sup>+</sup>
412.2848	13180	12.24	412.2846	0.14	C <sub>26</sub> H <sub>38</sub> NO <sub>3</sub> <sup>+</sup>
394.2742	1535	1.43	394.2741	0.14	C <sub>26</sub> H <sub>36</sub> NO <sub>2</sub> <sup>+</sup>
380.2584	467	0.43	380.2584	-0.01	C <sub>25</sub> H <sub>34</sub> NO <sub>2</sub> <sup>+</sup>
244.2061	1573	1.46	244.2060	0.08	C <sub>17</sub> H <sub>26</sub> N <sup>+</sup>
230.1904	1180	1.10	230.1903	0.09	C <sub>16</sub> H <sub>24</sub> N <sup>+</sup>
216.1747	3648	3.39	216.1747	0.07	C <sub>15</sub> H <sub>22</sub> N <sup>+</sup>
206.1904	3209	2.98	206.1903	0.09	C <sub>14</sub> H <sub>24</sub> N <sup>+</sup>
192.1748	4859	4.51	192.1747	0.11	C <sub>13</sub> H <sub>22</sub> N <sup>+</sup>
190.1591	6194	5.75	190.1590	0.06	C <sub>13</sub> H <sub>20</sub> N <sup>+</sup>
150.1278	77982	72.40	150.1277	0.10	C <sub>10</sub> H <sub>16</sub> N <sup>+</sup>
<b>Compound 5 (694&gt;164)</b>					
<i>m/z</i>	Intensity	Relative	Theoretical Mass	$\Delta$ (ppm)	Elemental Composition
694.4679	439976	100.00	694.4677	0.24	C <sub>42</sub> H <sub>64</sub> NO <sub>7</sub> <sup>+</sup>
676.4574	215774	49.04	676.4572	0.34	C <sub>42</sub> H <sub>62</sub> NO <sub>6</sub> <sup>+</sup>
658.4469	113275	25.75	658.4466	0.45	C <sub>42</sub> H <sub>60</sub> NO <sub>5</sub> <sup>+</sup>
640.4363	20366	4.63	640.436	0.48	C <sub>42</sub> H <sub>58</sub> NO <sub>4</sub> <sup>+</sup>
622.4258	3963	0.90	622.4255	0.60	C <sub>42</sub> H <sub>56</sub> NO <sub>3</sub> <sup>+</sup>
614.4571	1110	0.25	614.4568	0.52	C <sub>41</sub> H <sub>60</sub> NO <sub>3</sub> <sup>+</sup>
560.4102	1784	0.41	560.4098	0.71	C <sub>37</sub> H <sub>54</sub> NO <sub>3</sub> <sup>+</sup>
474.3581	5138	1.17	474.3578	0.65	C <sub>29</sub> H <sub>48</sub> NO <sub>4</sub> <sup>+</sup>
464.3374	107168	24.36	464.337	0.76	C <sub>27</sub> H <sub>46</sub> NO <sub>5</sub> <sup>+</sup>
456.3476	7674	1.74	456.3472	0.82	C <sub>29</sub> H <sub>46</sub> NO <sub>3</sub> <sup>+</sup>
446.3268	33845	7.69	446.3265	0.73	C <sub>27</sub> H <sub>44</sub> NO <sub>4</sub> <sup>+</sup>
444.3476	18160	4.13	444.3472	0.77	C <sub>28</sub> H <sub>46</sub> NO <sub>3</sub> <sup>+</sup>
436.3425	28540	6.49	436.3421	0.76	C <sub>26</sub> H <sub>46</sub> NO <sub>4</sub> <sup>+</sup>
428.3163	10930	2.48	428.3159	0.85	C <sub>27</sub> H <sub>42</sub> NO <sub>3</sub> <sup>+</sup>
420.3111	22489	5.11	420.3108	0.55	C <sub>25</sub> H <sub>42</sub> NO <sub>4</sub> <sup>+</sup>

418.3318	64135	14.58	418.3316	0.59	C <sub>26</sub> H <sub>44</sub> NO <sub>3</sub> <sup>+</sup>
410.3057	1978	0.45	410.3054	0.83	C <sub>27</sub> H <sub>40</sub> NO <sub>2</sub> <sup>+</sup>
402.3006	12085	2.75	402.3003	0.74	C <sub>25</sub> H <sub>40</sub> NO <sub>3</sub> <sup>+</sup>
400.3213	19423	4.41	400.321	0.63	C <sub>26</sub> H <sub>42</sub> NO <sub>2</sub> <sup>+</sup>
382.3107	3077	0.70	382.3104	0.75	C <sub>26</sub> H <sub>40</sub> NO <sup>+</sup>
236.2010	44657	10.15	236.2009	0.35	C <sub>15</sub> H <sub>26</sub> NO <sup>+</sup>
204.1748	16971	3.86	204.1747	0.78	C <sub>14</sub> H <sub>22</sub> N <sup>+</sup>
177.1513	4197	0.95	177.1512	0.76	C <sub>12</sub> H <sub>19</sub> N <sup>+</sup>
164.1435	269143	61.17	164.1434	0.90	C <sub>11</sub> H <sub>18</sub> N <sup>+</sup>
<b>Compound 6 (708&gt;164)</b>					
<i>m/z</i>	Intensity	Relative	Theoretical Mass	Δ (ppm)	Elemental Composition
708.4857	119695	100.00	708.4834	1.06	C <sub>43</sub> H <sub>66</sub> NO <sub>7</sub> <sup>+</sup>
690.4710	82644	69.05	690.4728	-2.62	C <sub>43</sub> H <sub>64</sub> NO <sub>6</sub> <sup>+</sup>
672.4593	18347	15.33	672.4623	-2.96	C <sub>43</sub> H <sub>63</sub> NO <sub>5</sub> <sup>+</sup>
392.2798	49950	41.73	392.2795	0.56	C <sub>23</sub> H <sub>38</sub> NO <sub>4</sub> <sup>+</sup>
346.2744	18766	15.68	346.2741	0.86	C <sub>22</sub> H <sub>36</sub> NO <sub>2</sub> <sup>+</sup>
164.1439	47095	39.35	164.1434	3.30	C <sub>11</sub> H <sub>18</sub> N <sup>+</sup>
<b>Compound 7 (720&gt;164)</b>					
<i>m/z</i>	Intensity	Relative	Theoretical Mass	Δ (ppm)	Elemental Composition
720.4836	838216	18.34	720.4834	0.36	C <sub>44</sub> H <sub>66</sub> NO <sub>7</sub> <sup>+</sup>
702.4730	1006502	22.02	702.4728	0.30	C <sub>44</sub> H <sub>64</sub> NO <sub>6</sub> <sup>+</sup>
684.4625	524711	11.48	684.4623	0.31	C <sub>44</sub> H <sub>62</sub> NO <sub>5</sub> <sup>+</sup>
666.4520	219421	4.80	666.4517	0.42	C <sub>44</sub> H <sub>60</sub> NO <sub>4</sub> <sup>+</sup>
586.4254	16660	0.36	586.4255	-0.20	C <sub>39</sub> H <sub>56</sub> NO <sub>3</sub> <sup>+</sup>
490.3530	43167	0.94	490.3527	0.61	C <sub>29</sub> H <sub>48</sub> NO <sub>5</sub> <sup>+</sup>
472.3425	809589	17.71	472.3421	0.70	C <sub>29</sub> H <sub>46</sub> NO <sub>4</sub> <sup>+</sup>
454.3318	778851	17.04	454.3316	0.61	C <sub>29</sub> H <sub>44</sub> NO <sub>3</sub> <sup>+</sup>
436.3214	91264	2.00	436.3210	0.86	C <sub>29</sub> H <sub>42</sub> NO <sub>2</sub> <sup>+</sup>
376.2849	14601	0.32	376.2846	0.77	C <sub>23</sub> H <sub>38</sub> NO <sub>3</sub> <sup>+</sup>
358.2741	181103	3.96	358.2741	0.15	C <sub>23</sub> H <sub>36</sub> NO <sub>2</sub> <sup>+</sup>
346.2743	14120	0.31	346.2741	0.59	C <sub>22</sub> H <sub>36</sub> NO <sub>2</sub> <sup>+</sup>
340.2637	47557	1.04	340.2635	0.71	C <sub>23</sub> H <sub>34</sub> NO <sup>+</sup>
302.2480	17381	0.38	302.2478	0.58	C <sub>20</sub> H <sub>32</sub> NO <sup>+</sup>
246.2217	115447	2.53	246.2216	0.22	C <sub>17</sub> H <sub>28</sub> N <sup>+</sup>
230.1905	76776	1.68	230.1903	0.58	C <sub>16</sub> H <sub>24</sub> N <sup>+</sup>
177.1513	623947	13.65	177.1512	0.59	C <sub>12</sub> H <sub>19</sub> N <sup>+</sup>
164.1435	4570111	100.00	164.1434	0.72	C <sub>11</sub> H <sub>18</sub> N <sup>+</sup>

<b>Compound 8 (722&gt;164)</b>					
<i>m/z</i>	Intensity	Relative	Theoretical Mass	$\Delta$ (ppm)	Elemental Composition
722.4994	3498	2.98	722.4990	0.50	C <sub>44</sub> H <sub>68</sub> NO <sub>7</sub> <sup>+</sup>
704.4886	24066	20.48	704.4885	0.26	C <sub>44</sub> H <sub>66</sub> NO <sub>6</sub> <sup>+</sup>
686.4780	20248	17.23	686.4779	0.18	C <sub>44</sub> H <sub>64</sub> NO <sub>5</sub> <sup>+</sup>
686.4420	1734	1.48	686.4415	0.73	C <sub>43</sub> H <sub>60</sub> NO <sub>6</sub> <sup>+</sup>
668.4677	4385	3.73	668.4673	0.56	C <sub>44</sub> H <sub>62</sub> NO <sub>4</sub> <sup>+</sup>
668.4315	1014	0.86	668.4310	0.76	C <sub>43</sub> H <sub>58</sub> NO <sub>5</sub> <sup>+</sup>
650.4568	371	0.32	650.4568	0.12	C <sub>44</sub> H <sub>60</sub> NO <sub>3</sub> <sup>+</sup>
392.2796	31295	26.63	392.2795	0.17	C <sub>23</sub> H <sub>38</sub> NO <sub>4</sub> <sup>+</sup>
374.2691	16917	14.39	374.2690	0.28	C <sub>23</sub> H <sub>36</sub> NO <sub>3</sub> <sup>+</sup>
372.2897	660	0.56	372.2897	-0.09	C <sub>24</sub> H <sub>38</sub> NO <sub>2</sub> <sup>+</sup>
364.2846	1170	1.00	364.2846	-0.12	C <sub>22</sub> H <sub>38</sub> NO <sub>3</sub> <sup>+</sup>
356.2585	2172	1.85	356.2584	0.22	C <sub>23</sub> H <sub>34</sub> NO <sub>2</sub> <sup>+</sup>
354.2794	701	0.60	354.2791	0.87	C <sub>24</sub> H <sub>36</sub> NO <sup>+</sup>
348.2534	5914	5.03	348.2533	0.37	C <sub>21</sub> H <sub>34</sub> NO <sub>3</sub> <sup>+</sup>
346.2741	47722	40.60	346.2741	0.24	C <sub>22</sub> H <sub>36</sub> NO <sub>2</sub> <sup>+</sup>
302.2480	2632	2.24	302.2478	0.48	C <sub>20</sub> H <sub>32</sub> NO <sup>+</sup>
258.2217	6122	5.21	258.2216	0.32	C <sub>18</sub> H <sub>28</sub> N <sup>+</sup>
230.1904	2108	1.79	230.1903	0.45	C <sub>16</sub> H <sub>24</sub> N <sup>+</sup>
177.1513	22196	18.89	177.1512	0.51	C <sub>12</sub> H <sub>19</sub> N <sup>+</sup>
164.1435	117532	100.00	164.1434	0.72	C <sub>11</sub> H <sub>18</sub> N <sup>+</sup>
<b>Compound 9 (738&gt;180)</b>					
<i>m/z</i>	Intensity	Relative	Theoretical Mass	$\Delta$ (ppm)	Elemental Composition
738.4579	5015	2.43	738.4576	0.44	C <sub>43</sub> H <sub>64</sub> NO <sub>9</sub> <sup>+</sup>
720.4478	10345	5.01	720.4470	1.14	C <sub>43</sub> H <sub>62</sub> NO <sub>8</sub> <sup>+</sup>
702.4365	12580	6.09	702.4364	0.13	C <sub>43</sub> H <sub>60</sub> NO <sub>7</sub> <sup>+</sup>
684.4267	10002	4.85	684.4259	1.22	C <sub>43</sub> H <sub>58</sub> NO <sub>6</sub> <sup>+</sup>
666.4155	2887	1.40	666.4153	0.34	C <sub>43</sub> H <sub>56</sub> NO <sub>5</sub> <sup>+</sup>
424.2697	10171	4.93	424.2694	0.68	C <sub>23</sub> H <sub>38</sub> NO <sub>6</sub> <sup>+</sup>
406.2591	21182	10.26	406.2588	0.80	C <sub>23</sub> H <sub>36</sub> NO <sub>5</sub> <sup>+</sup>
362.2693	11554	5.60	362.2690	0.79	C <sub>22</sub> H <sub>36</sub> NO <sub>3</sub> <sup>+</sup>
336.2537	3168	1.53	336.2533	1.11	C <sub>20</sub> H <sub>34</sub> NO <sub>3</sub> <sup>+</sup>
318.2429	147628	71.51	318.2428	0.42	C <sub>20</sub> H <sub>32</sub> NO <sub>2</sub> <sup>+</sup>
258.1852	2081	1.01	258.1852	0.00	C <sub>17</sub> H <sub>24</sub> NO <sup>+</sup>
242.1904	16377	7.93	242.1903	0.43	C <sub>17</sub> H <sub>24</sub> N <sup>+</sup>
236.2010	9959	4.82	236.2009	0.67	C <sub>15</sub> H <sub>26</sub> NO <sup>+</sup>
234.1854	13794	6.68	234.1852	0.72	C <sub>15</sub> H <sub>24</sub> NO <sup>+</sup>

230.1905	2085	1.01	230.1903	0.91	$C_{16}H_{24}N^+$
230.1540	2970	1.44	230.1539	0.42	$C_{15}H_{20}NO^+$
180.1384	206431	100.00	180.1383	0.59	$C_{11}H_{18}NO^+$



## AFTERWORD

Beyond this bound piece of work are narratives that include every individual that helped, supported and encouraged me as I rally past all the difficulties and challenges in this PhD journey. Herein, I take the opportunity to express my gratitude to all of them.

To Dr. Bernd Krock, thank you for your guidance and persistent support. Thank you for the opportunity to be one of your students. Thank you for being a mentor who is always present every step of the way, especially during the most crucial times.

To Dr. Ulf Bickmeyer, thank you for the encouragement and support throughout my thesis. Thank you for being readily available whenever I need your suggestions and advice.

To Dr. Urban Tillmann, thank you for the timely and insightful inputs and corrections that greatly improved the manuscripts in this thesis. Thank you for always extending your help in every way possible. Thank you to Dr. Jan Tebben for the help and assistance not just in the experiments and manuscript writing but also for coordinating the groundwork of my thesis committee and university requirements.

To Prof. Dr. Maarten Boersma and Prof. Dr. Boris Koch, thank you for your advice and encouragement that goes beyond this thesis. Thank you both for listening to me and for making sure that I will see the end of all this.

To Prof. Dr. Beate Escher and the Cell Toxicology Laboratory, thank you for introducing me to adaptive stress response assays and for accommodating me in my visits to Leipzig.

To Alfred Wegener Institute, thank for funding my research stay at the Institute.

To Frau Gesa Koberg and Herr Jan Bensien, thank you for your prompt assistance in my inquiries and the Christian-Albrecht University of Kiel for the financial help during my thesis writing stage.

To Annegret Müller, Thomas Max and Nancy Kühne, thank you for the continuous help and assistance. Thank you for ensuring that I have everything I need before every experiment and for allotting your time and effort whenever I need a hand.

To Dr. Stephan Wietkamp, thank you for being the best PhD partner. Thank you for constant encouragement, help in navigating local German offices, and for always listening to everything. Thank you also for treating me and Lena with our much-needed dose of sweets and treats.

To Marianne Camoying, thank you for our unique friendship. Thank you for always being there and for allowing me to see the different perspective in every situation. To Daphnie Galvez, thank you for sharing your energetic and fighting spirit. Thank you both for the fun times together!

To Simone Andresen, thank you for constantly cheering for me. Thank you for the long walks and encouraging talks in either Bremen or Bremerhaven.

To Dr. Christian Zurhelle, thank you for the practical help both in and out of AWI.

To Andrea Bleyer, thank you for your help from the very beginning up to this day. Thank you for introducing me to ins and outs of German culture.

To Dr. Susanne Gatti, thank you for the advice and kind assistance in my AWI endeavors and for inspiring me in every way.

To the DokTeam, thank you for the piña coladas and for making my stay in AWI bearable.

To the entire Ecological Chemistry Group for your help throughout the PhD. Thank you to Gesa Duhme for all the help in my paper works and administrative requirements.

To POLMAR (Claudias and Dörte), thank you for all the help and support.

To the AWI Helpdesk, thank you always for the kind and prompt assistance especially during my PhD Committee Meetings and presentations.

To my long-distance and long-time friends, thank you for the friendship through all these years. To Dr. Wilfred John Santiañez, thank you for the honest criticisms, corrections in my manuscripts and random calls. To Dr. Karen Bondoc-Naumovitz, thank you for rallying for and with me in this journey and for sharing ate Aryan Bondoc to me. To Iris Bea Ramiro, thank you for the late night GraphPad sessions and for being my go-to person whom I can sort my anxious thoughts. To Iris Orizar, thank you for supporting me in everything and for accompanying me to random places.

To Dr. Joemark Narsico and Norchel Gomez, thank you for sharing with me your cheerfulness. To Dr. Deo Florence Onda, Dr. Joshua Torres, Alper James Alacaraz and Peter Paolo Rivera, thank you for making time to listen and talk to me.

To Milky Baugbog and Kathleen Peret, thank you for your love and support. To Kristie Joy Montes, Ivy Intano and Julius Galamiton, thank you for the good laughs over anything.

Thank you to Louise and Dr. Leilani Mapa for welcoming me to your home whenever I need a time off from Bremerhaven

Thank you to COF, Friday Club and Mandaragat for the epic sanity breaks. Thank you for all the fun moments that we've shared together.

To Tina Steiger and Kathy Prütz, thank you for sharing your stories with me and for being my family here in Bremerhaven.

To my IBC Bremen family, especially to the YAM, thank you always for the love, support and prayers. Thank you to Marge Hintze for being my mom, sister, friend and confidante. Thank you for all the little and big things that you do for me. Thank you to Grace Kim for being my eonni (older

sister) and for treating me with road trips, good food and cheerful stories. Thank you to Wendi Penggu for being my adik (younger sister) and for the sleep-overs in Bremen.

To Tina Steiger and Kathy Prütz, thank you for sharing your stories with me and for being my family here in Bremerhaven.

To my family, thank you for everything. I am so grateful to have each and every one of you. I would not have done it without your unwavering love, support and prayers. For Papa and Mama, thank you always for inspiring me to persevere. To my siblings (Kuya Jason, Kuya Jezer and Julie), their loved ones (Ate Gracele, Yam, Francis), and to the new additions of our family (Scarlette, Phoenix and Peregreene) thank you all for the wonderful memories and meaningful conversations.

And finally, my utmost praise and gratitude to El-Roi, who carried me through every single moment of this journey with His grace, strength and love.

*So that well was named Beer-lahai-roi (which means "well of the Living One who sees me").*  
– Gen 16:14a

**Daghang Salamat!**